



THE HONG KONG  
POLYTECHNIC UNIVERSITY

香港理工大學

Pao Yue-kong Library

包玉剛圖書館

---

## Copyright Undertaking

This thesis is protected by copyright, with all rights reserved.

**By reading and using the thesis, the reader understands and agrees to the following terms:**

1. The reader will abide by the rules and legal ordinances governing copyright regarding the use of the thesis.
2. The reader will use the thesis for the purpose of research or private study only and not for distribution or further reproduction or any other purpose.
3. The reader agrees to indemnify and hold the University harmless from and against any loss, damage, cost, liability or expenses arising from copyright infringement or unauthorized usage.

### IMPORTANT

If you have reasons to believe that any materials in this thesis are deemed not suitable to be distributed in this form, or a copyright owner having difficulty with the material being included in our database, please contact [lbsys@polyu.edu.hk](mailto:lbsys@polyu.edu.hk) providing details. The Library will look into your claim and consider taking remedial action upon receipt of the written requests.

MODELLING VULNERABILITY AND  
RESILIENCE OF URBAN COMPLEX  
SYSTEMS IN RESPONSE TO  
RECURRING COVID-19 WAVES

NINGYEZI PENG

PhD

The Hong Kong Polytechnic University

2025

The Hong Kong Polytechnic University

Department of Land Surveying and Geo-Informatics

Modelling Vulnerability and Resilience  
of Urban Complex Systems in Response  
to Recurring COVID-19 Waves

Ningyezi PENG

A thesis submitted in partial fulfilment of the requirements for  
the degree of Doctor of Philosophy

August 2024

## CERTIFICATE OF ORIGINALITY

I hereby declare that this thesis is my own work and that, to the best of my knowledge and belief, it reproduces no material previously published or written, nor material that has been accepted for the award of any other degree or diploma, except where due acknowledgement has been made in the text.

\_\_\_\_\_ (Signed)

Ningyezi PENG (Name of student)

# **Dedication**

To my parents.

To all the people I love.

To all people who are fully engaged in life.

# **Acknowledgements**

Gratitude to all the people I have encountered along the way, it is because of you that I am who I am today. Appreciation to my parents for being my pillars of strength. Appreciation to my supervisor Dr. Liu Xintao for creating a relaxed learning environment during my doctoral studies. Thanks to my dear friends, to the teachers and peers I met at PolyU LSGI, as well as to teachers and students I encountered at CPGIS and AAG. Fate brought us together, allowing us to feel the warmth of connection.

# Publications

**Ningyezi Peng**, Xintao Liu. The Impact of Urban Scaling Structure on the Local-Scale Transmission of COVID-19: A Case Study of the Omicron Wave in Hong Kong Using Agent-Based Modeling. *Annals of the American Association of Geographers* (2024): 1-19.

Chun Yin\*, **Ningyezi Peng**\*, Yuchen Li\*, Yuanyuan Shi, Shujuan Yang, and Peng Jia. (2023). A Review on Street View Observations in Support of the Sustainable Development Goals. *International Journal of Applied Earth Observation and Geoinformation* 117. Elsevier:103205. doi:10.1016/j.jag.2023.103205.

Yiming Zhang\*, **Ningyezi Peng**\*, Shujuan Yang, and Peng Jia. 2022. Associations between Nighttime Light and COVID-19 Incidence and Mortality in the United States. *International Journal of Applied Earth Observation and Geoinformation* 112. Elsevier:102855. doi:10.1016/j.jag.2022.102855.

**Ningyezi Peng**, Xintao Liu. Path Dependency of Urban Resilience to Recurring COVID-19 Waves: The Role of Initial Invasion Contexts and Urban Scaling Structure. Submitted to *Cities*.

\* The co-first authors

# Table of Contents

Dedication.....	i
Acknowledgements.....	ii
Publications.....	iii
Table of Contents.....	iv
List of Tables.....	vii
List of Figures.....	viii
List of Abbreviations.....	ix
Abstract.....	x
Chapter 1 Introduction.....	1
1.1 Local spread dynamics from urban structure perspective.....	2
1.2 Vulnerability and resilience of urban complex systems.....	3
1.3 Conceptual framework and objectives.....	4
1.3.1 Conceptual framework.....	4
1.3.2 Research objectives and questions.....	6
1.3.3 Theoretical and practical significance.....	7
1.3.4 Outline.....	8
Chapter 2 Literature Review.....	9
2.1 Disease dynamic modeling.....	9
2.1.1 Statistical or machine learning methods.....	9
2.1.2 Mathematical models.....	10
2.1.3 Agent-based models.....	12
2.2 Geographical views of complex spread processes.....	14
2.2.1 Spatial diffusion theory.....	15
2.2.2 The scaling of human mobility.....	16
2.2.3 Urban complex systems.....	17
2.3 Disaster vulnerability and resilience.....	18
2.3.1 COVID-19 research on disaster vulnerability and resilience.....	20
2.4 Summary.....	22
Chapter 3 Methodology.....	25
3.1 Study events and datasets.....	26
3.1.1 Case data.....	27
3.1.2 Demographic data.....	28
3.1.3 Mobility data.....	29
3.1.4 Vaccine data.....	29
3.2 Simulating individuals.....	30
3.2.1 Demographic and household characteristics.....	30
3.2.2 Urban scaling structure, the scaling index, and mobility behaviors.....	33
3.2.3 Contact behaviors.....	38
3.2.4 Infection attributes.....	39
3.3 Coping responses.....	40

3.3.1 Protection behaviors.....	40
3.3.2 Vaccine- and infection-acquired immunity.....	41
3.3.3 Reporting behaviours.....	42
3.4 Model initialization, calibration and validation.....	43
3.4.1 Model initialization.....	43
3.4.2 Model calibration.....	43
3.4.3 Model validation.....	46
Chapter 4 Local spread dynamics influenced by urban scaling structure.....	48
4.1 Model Results.....	49
4.1.1 Model fitting.....	49
4.1.2 The superspreading subTPUs.....	51
4.1.3 The effects of urban scaling structure on local transmission risks.....	53
4.1.4 The effects of urban scaling structure on individual's probability of becoming a superspreader.....	54
4.1.5 The unevenly distributed strain on local hospitals.....	54
4.2 Discussion.....	56
4.2.1 How urban scaling structure influences local transmission risks.....	57
4.2.2 How urban scaling structure contributes to superspreaders.....	58
4.2.3 Practical suggestions on hospital emergency preparedness.....	59
4.3 Summary.....	60
Chapter 5 Vulnerability and resilience to different virus characteristics.....	62
5.1 Analyzing vulnerability and resilience under individual infectiousness heterogeneity scenarios.....	63
5.1.1 Vulnerability under individual infectiousness heterogeneity scenarios.....	63
5.1.2 Resilience to new virus invasions under individual infectiousness heterogeneity scenarios.....	64
5.1.3 The counterfactual simulation of the lockdown scenario.....	64
5.2 Model results.....	65
5.2.1 Model fitting.....	65
5.2.2 The effects of individual infectiousness heterogeneity on community vulnerability.....	66
5.2.3 The effects of individual infectiousness heterogeneity on resilience to new virus invasions.....	69
5.2.4 The counterfactual outcomes of the lockdown scenario.....	70
5.3 Discussion.....	72
5.3.1 The opposing effects of individual infectiousness heterogeneity on two community vulnerability patterns.....	73
5.3.2 The critical role of early SSEs in the resilience to new virus invasions.....	75
5.3.3 Long-term implications of the lockdown policy.....	75
5.4 Summary.....	76
Chapter 6 Resilience to different invasion contexts.....	78

6.1 Modelling the high and low scenarios of invasion contexts .....	79
6.1.1 The high and low scenarios.....	79
6.1.2 Analyzing spatial characteristics of spread .....	79
6.2 Model results.....	80
6.2.1 Success probability of new invasions in the high and low scenarios .	80
6.2.2 Early spread characteristics critical for successful invasions .....	82
6.2.3 Spatiotemporal spread characteristics for successful invasions.....	86
6.2.4 Local spread dynamics for successful invasions .....	87
6.3 Discussions .....	91
6.3.1 The influence of invasion places on the success probability of new invasions .....	92
6.3.2 The underlying reasons for the shifting spread advantage between the low and high scenarios.....	93
6.3.3 The significance and challenges of early detection in proactive policy design .....	95
6.4 Summary .....	96
Chapter 7 Sensitivity analysis.....	98
7.1 Comparison of 2011 travel survey data with 2020 mobility data .....	98
7.2 Sensitivity analyses on report rates.....	99
7.3 Sensitivity analyses on partially-fixed contactees .....	101
7.4 Sensitivity analyses on the effect of heterogeneous infectiousness on superspreader results .....	103
Chapter 8 Conclusion.....	106
8.1 Contributions.....	107
8.1.1 Theoretical implications.....	107
8.1.2 Methodological implications .....	109
8.1.3 Practical implications for policymaking .....	110
8.2 Limitations .....	110
8.3 Future directions .....	112
8.3.1 Building a scalable network of health systems to enhance urban resilience .....	112
8.3.2 The role of cyberspace in spatial diffusion phenomena.....	113
Reference .....	115
Appendices.....	129

# List of Tables

Table 3-1 Individual attributes, values, and sources .....	32
Table 4-1 The effect of the scaling index on the average transmission risk for subTPUs through multivariate linear regression. ....	53
Table 4-2 The average effects of the scaling index on individual’s probability of becoming a superspreader through logistic regressions across 30 runs with the best-fit parameters. ....	53
Table 5-1 The effect of individual infectiousness heterogeneity on local SSE risks through multivariate linear regression, including the interaction term with the scaling index.....	68
Table 6-1 Comparison of the first seven-day spread characteristics of the high and low scenarios.....	83
Table 7-1 Scenarios of report rates .....	99
Table 7-2 The comparison of the city-level and TPU-level RMSE of the best-fit models across scenarios.....	100
Table 7-3 For partially-fixed contactee scenario, the effect of the scaling index on the average transmission risk for subTPUs through multivariate linear regression. ....	102
Table 7-4 For partially-fixed contactee scenario, the average effects of the scaling index on individual’s probability of becoming a superspreader through logistic regressions across 30 runs with best-fit parameters.....	103
Table 7-5 When the infection probabilities are heterogeneously distributed among agents, the average effects of the scaling index on individual’s risk of becoming superspreaders through logistic regressions across 30 simulations. ....	105

# List of Figures

Figure 1-1 The conceptual framework of vulnerability and resilience of urban complex systems under the pandemic context.....	6
Figure 2-1 The agent-based modeling framework.....	13
Figure 3-1 The spatially explicit agent-based model and simulation scenarios..	26
Figure 3-2 The workflow for simulating synthetic mobility behaviors across 4,863 subTPUs utilizing the subTPU network. ....	37
Figure 4-1 Model fitting results..	50
Figure 4-2 The simulated superspreading subTPUs and the observed high-risk subTPUs .....	52
Figure 4-3 Simulated hospital strain on the Emergency Department services and hospital beds.....	56
Figure 5-1 Model fitting of the city-level epidemic curves for the fifth and sixth waves. ....	66
Figure 5-2 The individual infectiousness heterogeneity and community vulnerability in local infection risks. ....	67
Figure 5-3 Individual infectiousness heterogeneity and resilience to new virus invasions. ....	70
Figure 5-4 Counterfactual simulation of the lockdown scenario. ....	72
Figure 6-1 Daily infections of successful invasions across high and low scenarios. ..	82
Figure 6-2 The spatial characteristics of the first month spread among successful and failed runs in the high and low scenarios. ....	85
Figure 6-3 The monthly changes in spread characteristics for successful runs in the high and low scenarios. ....	87
Figure 6-4 Correlation between monthly mean of local infections and log-transformed scaling index for successful runs in the high and low scenarios across subTPUs. ....	89
Figure 6-5 Correlation between monthly coefficient of variation of local infections and log-transformed scaling index for successful runs in the high and low scenarios across subTPUs. ....	91
Figure 7-1 The comparison of the mobility structure of 2011 travel survey data and 2020 MTR card data. ....	98
Figure 7-2 Model fittings under different report rate settings..	101
Figure 7-3 The log-normal distribution for sampling the infection probability.....	104

# List of Abbreviations

Agent-based model	ABM
Coefficient of variation	CV
Cumulative distribution functions	CDF
Disaster resilience of place model	DROP
Emergency Department	ED
Iterative proportional fitting	IPF
Non-pharmacological Interventions	NPI
Points of Interest	POI
Rapid Antigen Tests	RAT
Root Mean Square Error	RMSE
Superspreading event	SSE
Susceptible-Infectious-Recovery	SIR
Susceptible-Exposed-Infectious-Recovery	SEIR
Subunit of tertiary planning unit	subTPU
Tertiary planning unit	TPU

# Abstract

Superspreading events (SSEs) underscore the uneven spreading patterns of COVID-19 across individuals and places. These heterogeneous spread dynamics may stem from human mobility, yet the underlying mechanisms are still not fully understood. While existing research has predominantly emphasized the significance of local mobility intensity, it has often overlooked other critical aspects, such as the spatial structure of human mobility. Therefore, this thesis aims to investigate how the spatial structure of human mobility influences on local spread dynamics. Specifically, within urban areas, human mobility patterns follow a widely found power-law scaling distribution, referred to as the urban scaling structure afterwards. Our first objective is to explore the impact of the urban scaling structure on local spread dynamics.

The scaling property of the urban scaling structure indicates that cities are urban complex systems composed of hierarchically ordered subsystems. After exploring how COVID-19 spreads within urban complex systems, the subsequent objective is to examine how coronavirus variants with different characteristics interact with urban complex systems, influencing local spread dynamics and ultimately contributing to heterogeneous vulnerability patterns. Finally, this thesis aims to compare different scenarios of new variant invasions and their influence on urban resilience.

To achieve these goals, this thesis employs a spatially-explicit agent-based model that incorporates the urban scaling structure to simulate fine-grained human mobility patterns and individual-to-individual spread processes. The simulation results fit

reasonably well with empirical data from the fifth and the sixth waves of the Omicron variants at various spatial scales in Hong Kong.

The validated model is firstly used to explore the impact of urban scaling structure on local spread dynamics. The results reveal a positive association between the scaling index and local spread risks among places, as well as the likelihood for local visitors to become superspreaders. The scaling index represents a place's importance within the urban scaling structure. The findings implies that the urban scaling structure may offer the first-mover advantage to a minority of places and their local visitors to infect earlier and thus infect more. Further simulations on hospital stress reveal large variations among local hospitals and over time concerning Emergency Department services and hospital beds.

Secondly, the model is employed to examine local vulnerability patterns considering different variant characteristics. Different variants may lead to differing degrees of individual heterogeneity in infectiousness. Simulations show that while different degrees of individual heterogeneity alone exert small effects on local SSE risks, it amplifies the effects of the urban scaling structure on local SSE risks. The findings imply that individual characteristics may not play as decisive a role in SSEs as expected. Instead, places could play a dominant role by constraining individuals' ability to fully realize their spread potential. Additionally, a counterfactual simulation of the lockdown scenario demonstrated that implementing lockdown measures, despite the significant cost, would not yield substantial long-term benefits and could potentially exacerbate spatial inequalities.

Thirdly, the model is utilized to compare new variant invasion scenarios involving the introduction of new variant into origin places with high or low scaling indices, which signify places' importance within the urban scaling structure. Our analysis reveals differences in initial places of invasion have path-dependent effects on urban resilience. While high scenarios exhibit a greater chance of successfully initiating new waves, low scenarios surprisingly show more explosive early spread.

This study brings important insights into local spread dynamics of COVID-19 and similar diseases. Firstly, it highlights the crucial role of urban scaling structure in shaping local spread risks and local SSEs. Secondly, it demonstrates how variant invasion contexts interact with urban complex systems, leading to diverse vulnerability and resilience outcomes. These findings could inform policymaking at finer spatial scales and over relatively longer temporal scales. The research framework presented here holds potential for broader applications in wider spatial contexts (e.g., Great Bay Areas) and various disaster contexts.

# Chapter 1 Introduction

Since the end of 2019, the world has experienced recurring waves of COVID-19, with new variant to be more infectious than its predecessor, leading to numerous infections and fatalities (Keni et al., 2020; A. T. Levin et al., 2022; Paul et al., 2020). The impact of COVID-19 has been unevenly distributed across social groups and urban areas (Ahmed et al., 2020; Blundell et al., 2022; Damme et al., 2020). Evidence suggests that disadvantaged groups and individuals residing in densely populated areas often experience a higher burden of infection (Chang et al., 2021; Chowkwanyun & Reed, 2020; Yancy, 2020).

The diverse incidence patterns indicate that the underlying spread processes are also varied. Many studies have highlighted the significance of superspreading events (SSEs) during the pandemic, demonstrating that a minority of individuals and places contributes to the majority of transmission (Adam et al., 2020; Lau et al., 2020; Lewis, 2021; Majra et al., 2021). Understanding the key factors influencing these heterogeneous spread processes is critical for anticipating and managing of pandemic risks (Koks et al., 2020; Lewis, 2021; Rasmussen et al., 2020). However, the underlying mechanisms driving these processes are still not fully understood (Alessandretti, 2022).

Existing research has identified mobility as a critical influencing factor of local spread dynamics, suggesting that higher mobility volumes results in more intensive contacts and thus an increased risk of spread (Badr et al., 2020; Hong et al., 2021a;

Kogan et al., 2021; R. Levin et al., 2021; Nouvellet et al., 2021). However, this explanation may not provide a comprehensive understanding, as it primarily focuses on the magnitude of local mobility while overlooking other crucial aspects, such as the spatial structure of mobility.

Consequently, this thesis aims to reexamine local spread dynamics from an urban structure perspective, followed by a systematic analysis of how urban systems respond to waves with different characteristics.

## **1.1 Local spread dynamics from urban structure perspective**

Mobility volumes within urban areas follows a widely-found power-law scaling distribution (Batty, 2008; Bettencourt, 2013; Brockmann et al., 2006; Jiang et al., 2009).

Evidence has shown that a higher degree of scaling can facilitate the overall spread across entire cities or countries (Aguilar et al., 2022; Lima & Atman, 2021; Schläpfer et al., 2014; Tizzoni et al., 2015). However, how the scaling might influence on local spread processes remains unclear.

The scaling patterns suggest cities are urban complex systems comprising hierarchically ordered subsystems (Batty, 2008, 2013; Jiang, 2023). The underlying structure could play a crucial role in shaping the scaling property of human mobility. (Jiang et al., 2009; Jiang & Jia, 2010; Jiang & Liu, 2012). The structure, referred as urban scaling structure afterwards, characterizes how urban areas with heterogenous mobility volumes are spatially distributed and how they adapt to and differentiate from each other (Jiang, 2018). Understanding how this structure may impact local spread

processes is a key question for this research.

Within the framework of the urban scaling structure, local spread dynamics exhibits complexity. The origin place of initial cases transports the virus to interconnected places. Throughout the processes, individual-to-individual spread gradually alter the landscape, and the landscape further influences subsequent spread dynamics. Initially, places abundant in susceptible individuals will experience an accelerated rate of spread. Once saturation is reached, a lack of new contacts significantly reduces the rate of transmission in that place (R. Morrill et al., 1988). The dynamic interplays among multiple places give rise to local spread dynamics.

## **1.2 Vulnerability and resilience of urban complex systems**

*Section 1.1* describes how a single wave would spread throughout urban complex systems. Considering multiple waves with different characteristics, the vulnerability and resilience of urban complex systems are intrinsically intertwined with a combination of socio-physical drivers and dynamic processes (Adger, 2000; Folke, 2006; Yabe et al., 2022). Disaster vulnerability and resilience aim to measure potential losses (Adger, 2006; Cutter, 1996, 2003) and recovery and adaptive capacity (Cutter et al., 2008; Folke, 2006; Tang et al., 2024), respectively. However, current research often relies on static measurements that may not effectively capture the cumulative impact of disasters, the dynamic interplay of social and physical systems, and regime transitions (Yabe et al., 2022).

This thesis adopts a dynamic view to understand the vulnerability and resilience of

urban complex systems in response to different waves of the COVID-19 pandemic. Urban complex systems, influenced by various variant invasion events, will undergo distinct space-time processes that shape vulnerability and resilience outcomes. Two significant pathways of influence are likely to emerge:

Firstly, variants may have heterogenous impacts on individual infectiousness. Evidence suggests that some individuals exhale significantly higher viral loads than others (Sidik, 2023), indicating a strong potential for large heterogeneity in individual infectiousness. Therefore, exploring how different degrees of individual heterogeneity affect local vulnerability is an essential area of exploration. Secondly, the initial invasion contexts may have significant implications for urban resilience outcomes due to the path dependency of complex systems (Holland, 2014). Particularly, exploring how the initial invasion place may affect urban resilience is a question to be explored.

## **1.3 Conceptual framework and objectives**

### **1.3.1 Conceptual framework**

The conceptual framework of this research is presented in Figure 1-1. This framework draws inspiration from the Cutter's vulnerability of places model and the disaster resilience of place (DROP) model (Cutter, 1996; Cutter et al., 2008). However, we reorganize key elements within the pandemic context, as the previous versions have primarily targeted on natural disasters.

Our framework is rooted in urban complex system, simulating the intricate processes that influence disaster impact. This is because pandemics, distinct from natural disasters, involve people who can both be victims and pose a threat, leading to more complex dynamics. Each element in this framework changes over time. In the context of recurring waves, the spread patterns from prior waves can influence the dynamics of subsequent waves.

Within this study, vulnerability is defined as the potential of individuals to be infected across places, and resilience is defined as the adaptive capacity of urban complex systems in response to the invasion of new variants. Vulnerability and resilience are the combined outcome of the interaction among urban complex systems, virus invasion event, and coping responses (Figure 1-1). Urban complex system serves as both antecedent conditions preceding disaster events and as constantly evolving contexts of vulnerability and resilience. It comprises interconnected social and physical systems.

Virus invasion events and coping responses are other important components that shapes disaster impact, interacting with urban complex systems. For virus invasion events, virus characteristics (e.g., individual infectiousness heterogeneity) and importing contexts of new variants (e.g., importing date, invasion place, or initial case number) could lead to diverse outcomes of vulnerability and resilience. Regarding coping responses, various human interventions, aimed at reducing contacts or the probability of infection, can mitigate spread in the short term. However, they may

inadvertently shift current risks to future situations, or transfer risks from one population to the another.

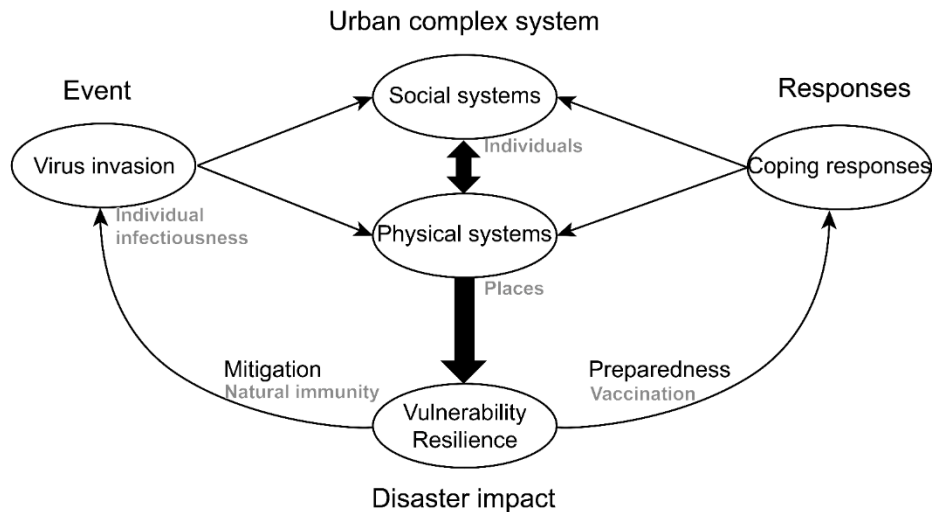


Figure 1-1 The conceptual framework of vulnerability and resilience of urban complex systems under the pandemic context

### 1.3.2 Research objectives and questions

This study aims to provide a comprehensive understanding of the interplay between urban scaling structure, local spread dynamics, and urban resilience in the face of evolving challenges. Our first research question centers on exploring how the urban scaling structure influences local spread dynamics, particularly leading to heterogeneous spread patterns across different places and individuals.

Building upon this, the second research question focuses on how variant characteristics, which lead to differing degrees of individual heterogeneity in infectiousness, contribute to local vulnerability patterns within urban complex systems. The third question delves into how urban resilience varies in response to invasion events

originating from diverse origin places.

### **1.3.3 Theoretical and practical significance**

The research questions posed in this study are significant both theoretically and practically. Firstly, the urban scaling structure provides a mesoscopic view to sheds new light into intricate spread processes. Existing research have primarily focused on the microscale individual interactions that leads to the emergence of macroscopic patterns. By integrating the structural relations between places, this study has potential to offer mid-range explanatory mechanism underlying local spread processes. The scaling property of human mobility is widely-found, and the ubiquity suggests that the urban scaling structure and its implications may have broad applicability to other regions.

Moreover, the research framework of this study can be applied to many other spatial diffusion phenomena, such as the adoption of innovations, ideas, or behaviours, may gain insights from our research. Theses phenomena depend on human mobility and interactions for dissemination but with distinct spread mechanisms and different contextual factors.

Secondly, this study expands the current static measurements in disaster research to study the dynamic processes underlying vulnerability and resilience. Different disaster events will interact with urban complex systems, contributing to the evolving characteristics of vulnerability and resilience. This research framework can be applied to more general disaster contexts. Although natural disasters are different from the

COVID-19 pandemic, they all involve information flow, adoption of protective behaviours, and the dissemination of panic all entail interpersonal spread.

Thirdly, this research can inform policymaking at finer spatial scales and over relatively longer temporal scales. In an uncertain future, this research considers the context of urban complex systems, which may offer a more reliable approach to providing policy recommendations that can help avoid disastrous outcomes as much as possible.

### **1.3.4 Outline**

This thesis consists of the following sections: Chapter 2 provides a brief review of the literature related to disease spread modelling in non-geographic and geographic fields, urban complex systems, and disaster vulnerability and resilience. Chapter 3 introduces the methodology of this study, ranging from the introduction of study events and datasets to the construction and validation of a spatially explicit agent-based model (ABM).

Chapter 4 to 6 are the core parts of this thesis. Chapter 4 investigates the impact of urban scaling structure on local spread dynamics. Chapter 5 examines the influence of individual infectiousness heterogeneity on local vulnerability. Chapter 6 analyzes the path-dependent effects of initial invasion places on urban resilience. Chapter 7 conducts sensitivity analysis of the model to explore alternative assumptions on local spread dynamics. Chapter 8 summarizes the contributions, limitations, and future directions of this research.

# Chapter 2 Literature Review

## 2.1 Disease dynamic modeling

### 2.1.1 Statistical or machine learning methods

For forecasting purpose, statistical approaches are utilized for short-term predictions, typically spanning a week or a few weeks ahead (Holmdahl & Buckee, 2020). They primarily involve fitting historical case data, making them more suited them well-suited for such short-term projections. However, statistical methods play a pivotal role in deriving critical epidemiological information directly from data. For instance, they are instrumental in assessing risks associated with diverse transmission pathways or environmental factors (Heesterbeek et al., 2015).

Geo-spatial statistical techniques delve deeper into the geographic dimensions to unravel intricate disease patterns and dynamics. Much research has delved into the impact of a broad range of risk factors on the heterogeneous disease patterns, and these factors include but are not limited to socioeconomic factors (e.g., income levels), geographical factors (e.g., distinctions between urban and rural areas), demographic factors (e.g., age and race), environmental factors (e.g., air quality) (Yao et al., 2023).

While statistical methods are valuable in identifying potential risk factors and their associations with disease patterns, understanding how these risk factors interact and potentially multiply the effects needs further investigation (Yao et al., 2023). In contrast to statistical methodologies, mechanistic modelling tools such as mathematical

models and agent-based models could be more suitable for long-term projections. These models incorporate intricate nonlinear feedback mechanisms, where the proliferation of infections accelerates the spread of disease.

### **2.1.2 Mathematical models**

Mathematical models employ mathematical concepts and language to depict the dynamics of disease spread and propagation, serving as a valuable tool for quantitatively representing and predicting infection dynamics at the population level (Heesterbeek et al., 2015). These models offer a means to delve into the intricate complexity of infectious disease dynamics, a complexity stemming from a web of interconnected temporal, organizational, and spatial scales.

However, traditional mathematical models often overlook individual heterogeneity, which can wield a significant impact on disease transmission, particularly in the context of respiratory infections such as SARS and COVID-19, where superspreaders play a defining role in disease dissemination.

Among the most widely used mathematical models are compartmental models, which conceptualize a host population as divided into discrete units. These models group individuals into compartments where each shares similar average characteristics and typically interacts with every other individual. One of the simplest forms is the Susceptible-Infectious-Recovery (SIR) model (Kermack & McKendrick, 1927). Originally designed to elucidate the rapid rise and decline of infected cases during epidemics, this model embodies our intuitive grasp of how simple communicable

diseases propagate in reality. It segregates individuals into three categories: susceptible individuals at risk of infection, infectious individuals capable of transmitting the disease to the susceptible, and recovered individuals immune to reinfection and incapable of transmitting the disease further.

Some studies integrated the compartment models with complex network models to account for movement between population (Pastor-Satorras et al., 2015). The concept of an individual's number of connections serves as a fundamental metric for delineating the network's topology. When combined with infection rates, an individual's connectivity plays a crucial role in shaping how diseases propagate within a network. These network models can be categorized as either population-based or individual-based, contingent on the type of networks employed and the accessibility of relevant data.

A notable instance of network-based epidemic modelling is the global epidemic and mobility model, which integrates census and mobility data within a fully stochastic metapopulation network framework. This model facilitates detailed simulations of the dissemination of influenza-like illnesses on a global scale (Chinazzi et al., 2020; Van den Broeck et al., 2011). The world population is segmented into geographic census areas centred around transportation hubs and interconnected via mobility flows. Disease transmission occurs within each subpopulation, with individuals traversing between subpopulations along the mobility network based on high-quality transportation data, thereby mimicking the global trajectory of epidemic outbreaks.

At the more granular level of urban settings, synthetic population constructions offer even greater precision by incorporating diverse location types such as residences, schools, and workplaces. Movements and durations spent in each location contribute to the generation of individual-location bipartite networks, whose unipartite projection delineates the synthetic interaction network at the individual level, governing the dynamics of epidemic propagation.

### **2.1.3 Agent-based models**

ABM are designed to simulate the diverse agents and the interactions between agents and their environment (Railsback, 2019) (Figure 2-1). These agents can encompass individuals, households, governmental bodies, or any other entities of interest. At its core, ABM enables the emergence of population-level phenomena that transcend or deviate from the summation of individual behaviours. As such, ABM adopts a bottom-up methodology, where micro-level behaviours give rise to macro-level dynamics. Given the shared characteristics with complex systems, ABM becomes a promising tool to explore complex systems.

ABMs exhibit key attributes such as heterogeneity, interaction, and autonomy. Heterogeneity implies that agents typically possess distinct characteristics. Interaction denotes that agents commonly engage with their neighbours either spatially or through a network. Autonomy signifies that agents operate independently and pursue individual objectives. Owing to these traits, ABM proves to be an ideal tool for investigating a broader spectrum of research queries compared to conventional methodologies.

Furthermore, ABMs align naturally with modelling infectious disease transmission, as interactions among individuals and between individuals and local environments frequently underpin population-level patterns of disease incidence and perpetuation (Tracy et al., 2018).

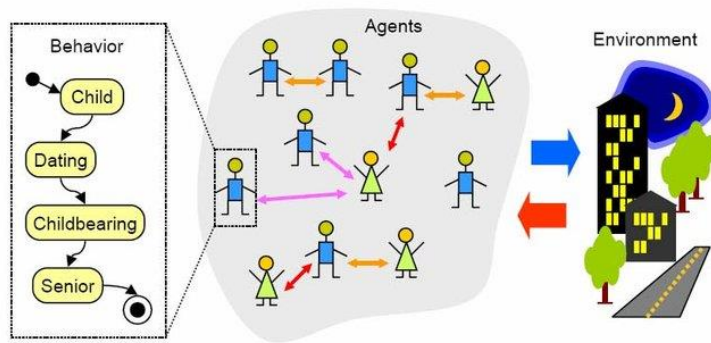


Figure 2-1 The agent-based modeling framework (Metcalf, 2007)

In this section, we delve into the existing ABMs tailored for modelling infectious diseases, with a specific focus on COVID-19. Different from SIR or SEIR models discussed in *Section 2.1.2*, these ABM models introduce individual heterogeneity and intricate network interactions, both spatially and temporally, providing deeper insights into the transmission processes within real-world scenarios (Tracy et al., 2018). To replicate the spread dynamics on an urban scale, ABMs operate under certain assumptions (Bian & Liebner, 2007): (a) Individuals exhibit diversity in characteristics like age, race, occupation, and infection status; (b) Individuals engage with a finite number of others within specific timeframes; (c) Interaction frequencies vary among individuals; (d) Individuals are geographically dispersed; and (e) Individuals are mobile.

Building upon these foundational heterogeneity assumptions, the majority of ABMs in infectious disease modelling are tailored to simulate transmission dynamics and control measures within populations (Lorig et al., 2021; Tracy et al., 2018; N. Zhang, Jack Chan, et al., 2021). Existing ABMs for COVID-19 leverage big data and heuristic rules to depict human mobility behaviours and social contact patterns. Human mobility and social interactions are pivotal components in the propagation of infectious diseases (Chen et al., 2014). Given the challenge of precisely determining individual physical contacts, human mobility serves as the closest proxy for social interactions. Consequently, human mobility alone can effectively forecast shifts in real case numbers and highlight elevated infection rates within vulnerable populations, even amidst substantial alterations in human behaviours (Chang et al., 2021; Nouvellet et al., 2021).

Although there are many different types of epidemic models, most focus on the temporal dimension. To spatialize epidemic modelling, M. Li et al. (2019) proposed a framework for the epidemic forest approach. This method involves the use of epidemic trees, where each tree uses the tree structure to represent an epidemic starting from a primary case. By structuring the model in this way, it becomes possible to integrate spatiotemporal, structural, and epidemiological information.

## **2.2 Geographical views of complex spread processes**

In *Section 2.1*, the majority of models focus primarily on individuals, with space serving a supplementary role for analysis. However, from a geographical perspective, shifting the analytical focus from individuals to space may offer a fresh perspective and

potentially shed new light in local spread dynamics.

### **2.2.1 Spatial diffusion theory**

The classic spatial diffusion theory introduced by Torsten Hägerstrand in his dissertation (Hägerstrand, 1973) provides a geographic framework for explaining diffusion phenomena. Diffusion entails the gradual spread of phenomena over space and time, with disease spread, innovation diffusion, and information dissemination representing typical examples. Hägerstrand revolutionarily viewed diffusion phenomena as predictable space-time processes that could be modelled as person-to-person spread. His theory emphasized diffusion as a fundamental geographical process influenced by both human and physical landscapes, which, in turn, shape and transform the landscape (R. Morrill et al., 1988).

In line with these principles, Hägerstrand pioneeringly created the Monte Carlo simulation, which enabled the modelling of individual behaviours to generate collective patterns, laying the foundation for current agent-based modelling methods. While the original Hägerstrand model is now seldom used, the geographical thinking behind Hägerstrand's theory still holds the potential to offer fresh insights into the local spread dynamics of COVID-19. From a geographical perspective, diffusion acts as an equalizing force that diminishes disparities between locations to facilitate the spread of phenomena (R. Morrill et al., 1988). This process persists until the forces maintaining differences align with those eliminating them.

Furthermore, Morrill's wave theory may also aid in understanding the local spread process of COVID-19. This theory portrays diffusion as dynamic waves progressing over space and time, changing in shape as they move (R. Morrill et al., 1988; R. L. Morrill, 1968, 1970). The dynamic wave is shaped by the interaction between initial adopters and subsequent contacts, as evidenced in various datasets (Cliff et al., 1983; R. Morrill et al., 1988; R. L. Morrill, 1970).

## **2.2.2 The scaling of human mobility**

As emphasized in *Section 2.2.1*, the landscape plays a crucial role in influencing diffusion processes. In the context of COVID-19 spread, the spatial heterogeneity and structure of human mobility patterns emerge as key factors shaping transmission dynamics.

Previous research has established that mobility volumes within urban areas follows a power-law scaling distribution (Batty, 2008; Bettencourt, 2013; Brockmann et al., 2006; Jiang et al., 2009). In simple terms, only a minority of urban areas exhibit large mobility volumes, while the majority have lower mobility volumes. The scaling property of human mobility could be mainly shaped by the underlying scaling structure of urban space (Jiang et al., 2009; Jiang & Jia, 2010; Jiang & Liu, 2012). Jiang created complex networks that capture the urban scaling structure, which successfully reproduced heterogeneous human mobility patterns across local places (Jiang, 2015, 2018; D. Ma et al., 2020).

Urban scaling structure characterizes how urban areas with heterogenous mobility

volumes are spatially distributed and how they adapt to and differentiate from each other (Jiang, 2018). This structure may influence the evolution of local spread patterns, but most existing COVID-19 studies have primarily focused on examining its effects on overall spread trends of entire counties, cities or countries, with limited exploration of its impact on the local scale within cities (Aguilar et al., 2022; Lima & Atman, 2021; Schläpfer et al., 2014; Tizzoni et al., 2015). For example, one study compared urban scaling structures in three cities and found that more centralized cities, where mobility gathers in a few hotspots, tend to experience larger epidemic size and faster spread rates (Aguilar et al., 2022). Similarly, two other studies found that cities with the higher degree of scaling can facilitate the overall disease spread (Schläpfer et al., 2014; Tizzoni et al., 2015).

### **2.2.3 Urban complex systems**

The concept of urban scaling structure is deeply rooted in the theory of urban complex systems. Cities are often viewed as complex systems that are constructed from the bottom up in a hierarchical way in which the basic components of cities and their interactions give rise to emergent properties (Batty, 2013). Urban scaling structure specifically describes how these basic components interact with each other, shaping the overall urban system.

The fundamental characteristic of complex systems is that the whole system is greater than the sum of its individual parts. Basic components in complex systems self-organize into patterns, leading to non-linear interactions that give rise to various levels

of organization and hierarchies (Holland, 2014). This complexity theory has been applied in Batty's new science of cities, where he elucidated the characteristics and origins of urban versions of complex systems (Batty, 2013).

In urban complex systems, the distribution of basic components, such as hubs or nodes in networks, often follows highly skewed distributions, reflecting the competitive processes that drive a city's functions and shape its form and structure. These distributions, also referred as scaling laws or power laws, usually describe large numbers of small objects and small numbers of large objects. Scaling laws highlight the self-similar nature of cities, indicating that cities are composed of hierarchically ordered subsystems (Batty, 2008).

According to Batty's theory, understanding urban complex systems necessitates focusing on flows and networks between places rather than just the intrinsic attributes of individual places (Batty, 2013). There is an inherent order, akin to a power-law distribution, in the number, size, and shape of properties within networks. This understanding helps us comprehend how urban characteristics are shaped by the networks that connect different places. This is why this thesis takes the urban scaling structure as a starting point to grasp the heterogeneity in disease spread patterns across places.

## **2.3 Disaster vulnerability and resilience**

As indicated last section, cities, as complex systems, exhibit dynamic interactions across social and physical systems (Batty, 2008, 2013; J. Liu et al., 2007). Disasters,

unfolding within this context, is intimately intertwined with a combination of socio-physical drivers and dynamic processes (Adger, 2000; Folke, 2006; Yabe et al., 2022). Disaster resilience, defined as the capacity to recover from and adapt to disruptions (Cutter et al., 2008; Folke, 2006; Tang et al., 2024), is now the focal point in disaster research. Prior to the shift within disaster communities towards resilience, attention predominately gravitated towards disaster vulnerability, a concept aimed at measuring potential losses (Adger, 2006; Cutter, 1996, 2003). Understanding vulnerability and fostering resilience under the context of urban complex systems are vital for effectively mitigating risks, minimize impacts, and facilitating recovery and adaptation after disaster strike.

For conceptualizing vulnerability and resilience, Cutter proposed the vulnerability of places model and the DROP model (Cutter, 1996; Cutter et al., 2008). The models delineate the impact of natural disasters as influenced by various factors, including the intrinsic vulnerability and resilience, event characteristics, and coping responses, all of which are moderated by absorptive and adaptive capacities of systems (Cutter, 1996; Cutter et al., 2008). While the models lay a solid foundation for assessing vulnerability and resilience, traditional assessment approaches often employ static measures, overlooking the dynamic nature of both vulnerability and resilience (Folke, 2006; Yabe et al., 2022). Such a static measurement is not suitable to capture the cumulative impact of disasters, the dynamic interplay of social and physical systems, and regime transitions (Yabe et al., 2022).

To solve this issue, modelling approaches, such as System Dynamics model and ABM, have emerged as promising tools. System Dynamics model can account for the macroscopic relationship between the functionality of physical systems and social systems. Sutley & Hamideh (2018) designed a System Dynamics model integrating engineering and social factors that interact to influence housing recovery process. Yabe et al. (2021) built interdependent socio-physical systems to examine their effects on disaster recovery and resilience during Hurricane. Zarghami & Dumrak (2021) projected socio-economic and demographic characteristics of populations to explore future social vulnerability.

In contrast, ABMs focus on modelling the interactions of individual behaviours and their impact on the emergent patterns of the whole system. Ghaffarian et al. (2021) developed an ABM that simulated individual behaviours and their interactions with socio-economic institutions to explore physical recovery patterns. Nejat & Damnjanovic (2012) proposed an ABM incorporating homeowners' reaction to neighbours' reconstruction and relocation behaviours to study housing recovery process. Haer et al. (2019) considered adaptive behaviours of governments and households in the face of river flooding.

### **2.3.1 COVID-19 research on disaster vulnerability and resilience**

As a special disaster, the COVID-19 pandemic presents distinctive complexities in terms of vulnerability and resilience within urban complex systems. Numerous studies

on COVID-19 have primarily focused on assessing infection risk or vulnerability (Franch-Pardo et al., 2020, 2021; Yao et al., 2023). Most of them perceive the risk as the proximity to the potential infected cases, which can effectively capture the spatial and temporal differences in risk under specific contexts (Coccia, 2020; Hong et al., 2021a; Huang & Kwan, 2021; H. Yang et al., 2023). However, in the face of changing contexts, for example, the invasion of new variants, this framing may not effectively predict new situations, as it overlooks the complex interactions among multiple risk factors (Yao et al., 2023).

Most COVID-19 studies on urban resilience have mainly focused on delineating recovery processes of diverse aspects of urban systems, such as mobility patterns, economic activities, and public health condition (Tang et al., 2024). For example, Li and Lasenby (2023) utilize various urban mobility data to analyse the impacts of restrictive policies on daily mobility and exhaust emissions in the post-pandemic period. Che, Lee, and Kim (2023) observed a notable transformation in the patterns of online and in-store sales, with retailers experiencing disparate recovery rates at both neighbourhood and district levels. Zhang & Wang (2023) thoroughly modelled changes in urban resilience under various control policies by incorporating subsystem resilience related to governance, infrastructure, socio-economy, and energy-material flow, using System Dynamics and epidemic simulation model.

Different from recovery capacity, only a few research has explored the adaptive capacity of urban complex systems, especially their ability to resist the emergence of new waves. Lloyd-Smith et al. (2005) and Goyal et al. (2022) identified key factors,

including individual infectiousness and social contact number, that influenced the emergence or distinction of new circulating variants, using mathematical models. However, they did not account for the impact of heterogeneous human mobility on this emergence. Considering that human mobility can cause large disparities in infections across places (Chang et al., 2021; Peng & Liu, 2024), different origin places of new variants may also be crucial for new wave emergence.

In summary, empirical research on dynamic resilience process modelling is still in its early stage, with most studies utilizing System Dynamics to consider the macro-level relationships of subsystems. There is a need for further exploration into spatial heterogeneity and dependency of dynamics that operate at smaller scales within cities. Specifically, in the context of COVID-19 resilience, a promising direction involves utilizing ABMs to explore how the interplay of initial invasion places and human mobility could influence dynamic resilience processes in response to new variants.

## **2.4 Summary**

Section 2.1 introduces four main types of disease dynamic modelling approaches: statistical models, mathematical models, complex network models, and agent-based models. Statistical models primarily fit historical case data, making them suitable for short-term projections. In contrast, the other three approaches consider mechanistic processes, making them potentially more suitable for relatively long-term projections and evaluations of intervention effectiveness (Holmdahl & Buckee, 2020). Mathematical models assume various forms of homogeneity, but local or individual

heterogeneity can play critical roles in disease transmission. Complex networks and agent-based models can incorporate this heterogeneity, with agent-based models being particularly flexible in including complex factors.

Most current infectious disease modelling focuses on projecting temporal dynamics, with spatial dimensions often considered at highly aggregated levels for cities, countries, or globally (Yao et al., 2023). These high-level predictions have limited capacity to inform targeted interventions, which is why this thesis concentrates on exploring fine-grained local spread dynamics.

In Section 2.2, a geographical perspective is highlighted as shedding new light on the complexity of local spread dynamics. From classic spatial diffusion theory to the latest urban complex system theory, these perspectives hold significant reference value for understanding the formation processes and mechanisms of complex urban phenomena. Spatial diffusion of diseases or other social phenomena is heavily influenced by the human landscape. The human landscape of mobility heavily depends on the underlying scaling structure. Therefore, it is promising to explore complex spatial diffusion processes of disease from the urban scaling structure perspective. This exploration provides a mesoscopic view to shed new lights in urban complex systems, aiding in better understanding how macro-level patterns emerge from micro-level individual interactions.

Section 2.3 introduces the conceptualizations of disaster vulnerability and resilience within urban complex systems. Disaster vulnerability and resilience, unfolding within urban complex systems, are influenced by both socio-physical drivers

and dynamic processes. Current static measures struggle to capture cumulative impacts and regime transitions, emphasizing the need to dynamically explore the factors driving vulnerability and resilience within urban complex systems.

## Chapter 3 Methodology

To reconstruct the case trajectories of the fifth and sixth waves, a spatially explicit ABM was developed. Initially, census data was utilized to generate demographic and household characteristics of synthetic individuals (Figure 3-1a) (Templ et al., 2017; Wong, 1992). A total of 727,796 agents, representing around 10% of the Hong Kong population, with attributes such as age, sex, and household structure, were generated.

Subsequently, the mobility and social contact behaviours of the synthetic individuals were generated. For mobility behaviours (Figure 3-1b), a complex network was constructed to capture the urban scaling structure, considering the hierarchical and spatial relationships of places (Jiang & Jia, 2010; D. Ma et al., 2020; Schläpfer et al., 2021). Based on the complex network, the scaling index was calculated using Google's PageRank algorithm (Brin & Page, 1998) to simulate mobility flows across places (Jiang et al., 2009; Jiang & Jia, 2010).

The model incorporated a two-layer contact structure (Figure 3-1c). On a daily basis, agents had contacts with their families at home, and with other individuals in shared locations during trips. Each contact entailed a specific probability for susceptible agents to contract the virus from infectious individuals, leading to the latency period and subsequently the infectious period.

Most of the parameters in the model were derived from empirical evidence (Table 3-1). However, two constant parameters for each wave, namely individual infectiousness and the initial proportion of latent cases, required calibration based on

observed city-level daily cases. The model’s predictive accuracy was evaluated by comparing the calibrated model’s predictions with empirical case data of both waves. After calibration and validation, this model was used to explore the influence of individual infectiousness heterogeneity on the vulnerability and resilience of urban complex systems (Figure 3-1d).

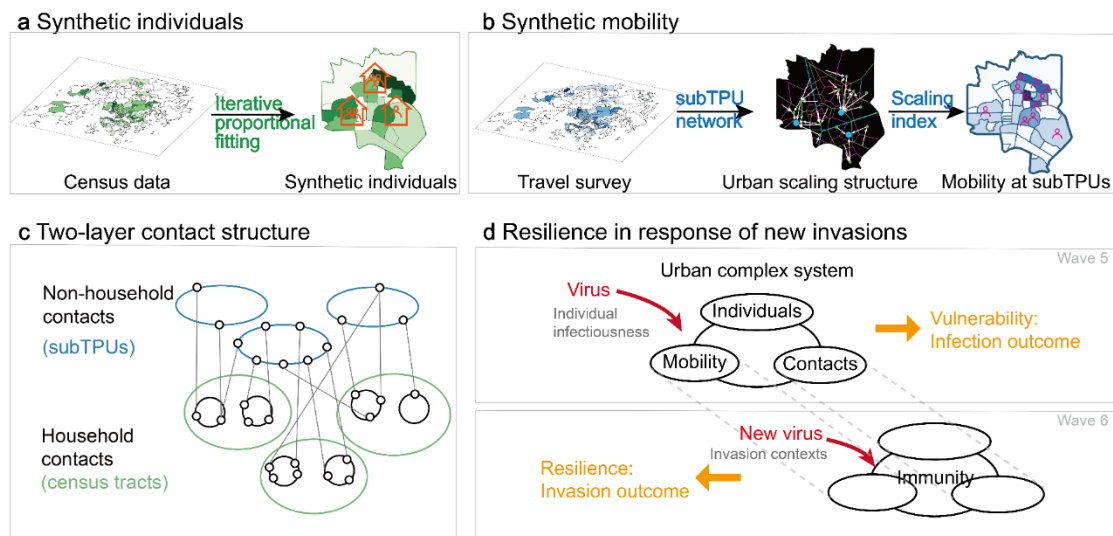


Figure 3-1 The spatially explicit agent-based model and simulation scenarios. **a**, synthetic population was generated through iterative proportional fitting based on census data. **b**, synthetic mobility was simulated at 4,863 subunits of tertiary planning units (subTPUs) using urban scaling structure built based on travel survey data. **c**, the two-layer contact structure consists of household contacts and non-household contacts during trips. The model simulated vulnerability to infections during fifth wave considering individual infectiousness heterogeneity, and then simulated the resilience to new variant invasions during sixth wave (**d**).

### 3.1 Study events and datasets

Our study focuses on Hong Kong, a global metropolitan city with a population of over 7.4 million. Due to the limited number of cases (in total 12,258 cases by Dec. 20, 2021) during the first four waves in Hong Kong, we chose the fifth and sixth waves as our study events, from 1 February to 30 March 2022, and from 1 May to 30 September

2022, respectively. The fifth wave was characterized by a significant spread of Omicron, with 1.19 million confirmed cases (B. Yang et al., 2024). Prior to this wave, only 0.2% of the population had been confirmed as cases, leading to limited infection-induced immunity (B. Yang et al., 2024). Combined with ineffective vaccine-induced immunity against Omicron and the presence of a relatively singular circulating strain (BA.2), the fifth wave presented a relatively straightforward and representative event to model (Andrews et al., 2022; Kirsebom et al., 2022). Therefore, we chose it as one of our study events to validate our model structure and also assess the community vulnerability.

To study the adaptive capacity gained from the fifth wave, we selected the sixth wave as our other study event. This wave had 0.56 million confirmed cases, with the major strain being BA.5 (B. Yang et al., 2024), which was about 1.4 times more infectious than BA.1 (Fan et al., 2022). It is important to note that BA.2 was also circulating in the early stages of this wave. However, as our study specifically focused on the adaptive capacity in response of the new variant, namely BA.5, we isolated the number of confirmed cases attributed to BA.5 according to the whole genome sequencing data from The Hong Kong Polytechnic University (Gilman, 2022). By doing this, we only modelled the spread of BA.5 during the sixth wave. To model and validate these two events, empirical data regarding four aspects are used, including case data, demographic data, mobility data, and vaccine data.

### **3.1.1 Case data**

For the fifth wave, empirical case data at three spatial scales were used to validate our

model (see *Section 3.4.3*). Firstly, at the city level, we directly used the number of daily confirmed cases. Secondly, at the tertiary planning units (TPU) level, we obtained the number of daily cases confirmed by Rapid Antigen Tests (RAT) from the RAT reporting platform. This platform, launched on 7 March 2022, contains data on over 460 thousand self-reporting cases and their respective home building locations (Hong Kong Government, 2022b). Finally, at the subunit of TPU (subTPU) level, we identified high-risk subTPUs based on contact tracing data. This data includes information on the buildings visited by cases during the period 1 to 14 days prior to the onset of symptoms, as of 6 February 2022 (Hong Kong Government, 2022a). The contact tracing data consists of 22,869 visitations made by 10,608 cases.

For the sixth wave, only the city-level case data was available and used to validate our model. To separate the BA.5 cases from all local cases, we used the proportion of BA.5 samples in the total sequenced samples of local cases from 1 May to 30 September 2022 (Gilman, 2022). As shown in Figure S1, sporadic cases of BA.5 were detected around May, but it was until July that BA.5 gradually gained dominance, increasing from an initial proportion of 2% to eventually occupying 80% of the confirmed local cases at the end of September. The dominance of BA.5 in July can be primarily attributed to the Hong Kong government's decision to reduce the quarantine period of inbound persons from overseas from 14 days to 7 days (Gilman, 2022).

### **3.1.2 Demographic data**

The 2016 census tables were utilized to create a synthetic population, comprising

population figures for 1,622 census tracts categorized by sex, age groups, and household sizes. Meanwhile, the 2011 household survey data from the Hong Kong Transport Department documents the compositions of household members in 35,401 households.

### **3.1.3 Mobility data**

The 2011 travel survey data collected by the Hong Kong Transport Department were employed to generate synthetic mobility behaviors, encompassing 121,204 one-day trips made by 58,843 residents across 4,863 subTPUs. Despite not covering the simulation period, Figure 7-1 demonstrates that the 2011 travel survey data exhibits a significant representativeness of mobility patterns, when comparing to the mobility structure depicted in the 2020 subway data (Zhang et al. 2021). Moreover, the Google mobility change index (Google LLC, 2022) was utilized to represent the overall mobility changes resulting from interventions during the simulation period. The index measures variations in mobility volume at the city level. By analysing anonymized and aggregated location data from users, Google calculates the percentage change relative to a baseline period (from 3 January to 6 February, 2020), facilitating temporal comparisons. Figure S2 illustrates that the fifth wave led to a substantial reduction in human mobility, while the sixth wave had a limited impact on mobility.

### **3.1.4 Vaccine data**

To address vaccine-acquired immunity, we obtained daily vaccination data categorized

by age group from the Hong Kong Health Bureau Department (DATA.GOV.HK, 2022). This dataset provides cumulative counts of COVID-19 vaccine uptake for BioNTech or Sinovac vaccines, categorized by vaccine type and order across different age groups on a daily basis, e.g., BioNTech-BioNTech, or BioNTech-Sinovac.

## **3.2 Simulating individuals**

### **3.2.1 Demographic and household characteristics**

Based on the aggregate census tables and individual-level household survey data, we employed iterative proportional fitting (IPF) to generate and calibrate a population of 727,796 agents and 263,609 households. The generated population exhibited age, sex, household structure characteristics consistent with the real population across 1,622 census (Templ et al., 2017; Wong, 1992). The simulation of household structure encompassed the composition of individuals within each household unit, considering household sizes as well as the age and sex distribution of household members.

We conducted the following workflows using the R package **simPop** (Templ et al., 2017): firstly, the individual-level household survey data is calibrated to match the true population numbers by age and sex, using IPF. IPF is a technic to fit an n-dimensional table with unknown entries to match a set of marginal distributions. This process unfolds iteratively, focusing on individual dimensions one after the other. Within each dimension, adjustments are made to the internal cells to align with the specified totals.

This iterative cycle continues until convergence is achieved, ensuring that the n-dimensional table aligns with all margins accurately.

To elaborate, the calibration involves fine-tuning sample weights based on known population totals across different demographics. Once estimates for the expected number of individuals in each group are established within the contingency table, individuals in the sample dataset are assigned probabilities of selection based on original sampling weights and the required number of similar individuals to supplement the synthetic population. Subsequently, individuals are randomly chosen from the sample until the targeted number of individuals per group is met. The **simPop** package streamlines this calibration process through the `calibSample()` function, facilitating a seamless execution of these intricate adjustments.

Secondly, the calibrated individual-level household survey data is extrapolated to create the realistic household structure of the synthetic population. Within the household structure, a predefined set of "basic variables" such as age, gender, and location of household members is incorporated. The data integrated into the synthetic population at this phase are sourced from real survey participants, ensuring the fidelity of household representations and averting the generation of unrealistic structures.

To expedite the sampling process for a substantial number of elements, alias sampling, as introduced by Walker (1977), proves to be exceptionally efficient for our objectives. Leveraging the `simStructure()` function within the **simPop** package facilitates the seamless implementation of this sampling technique. For a deeper

understanding of the methodology, please refer to the comprehensive mathematical exposition provided by (Walker, 1977).

Finally, synthetic individuals and households are randomly allocated to each census tract, with ongoing adjustments to the allocation process until the convergence is achieved and a good fit to the aggregate census tables is attained. In cases where the population is to be allocated into more localized geographic zones, such as districts in Austria, we utilize the `simInitSpatial()` function to simulate these smaller regions. Within the current configuration of **simPop**, this function necessitates the provision of one of two tables as input, each comprising precisely three columns. The first two columns within these tables designate the broader (first column) and more specific (second column) geographic areas. The third column contains the documented population figures corresponding to the smaller geographical units.

Table 3-1 Individual attributes, values, and sources

Attributes	Value	Source
<b><i>Demographics and households</i></b>		
Identify of individual	Agent ID	Simulated
Age	Twelve age groups	(2016 HK Census)
Sex	Male, female	(2016 HK Census)
Identify of household	Household ID	Simulated
Household location	Census tract ID	(2016 HK Census)
<b><i>Travel and contact behaviors</i></b>		
Trip destinations	subTPU IDs	Derived from HK travel survey data
The total number of total contacts	17.5 (the mean value)	Derived from HK contact survey data (Kucharski et al., 2014)
Number of contacts at home	Decided by household size	Simulated
Number of contacts outside home	Decided by the number of total contacts and household size	Simulated

<i>Infection attributes</i>	<i>Wave 5</i>	<i>Wave 6</i>	
Individual infectiousness	0.05	0.065	Estimated
Probability of being initial latent cases	$6 \times 10^{-5}$	$5 \times 10^{-4}$	Estimated
Latency period	1.20 (the mean value)	1.20 (the mean value)	(Cai et al., 2022; Xu et al., 2023)
Infectious period	5.64 (the mean value)	5.64 (the mean value)	(Cai et al., 2022; Manica et al., 2022; Xu et al., 2023)
Period from infectious to confirmed	5.05 (the mean value)	4.00 (the mean value)	(B. Yang et al., 2024)
Probability of being confirmed when being infected	8% (before 24 Feb), 30% (24 Feb. to 7 Mar.), 35% (after 7 Mar.)	20%	Estimated based on HKUMed (2022)
<b><i>Coping responses</i></b>			
Mobility reductions due to non-pharmaceutical interventions (NPI) during wave 5	Google mobility index		(Google LLC, 2022)
Social contact reductions due to NPI during wave 6	47%		(HKUMed, 2022)
Probability of cancelling all trips (stay at home) when being infected	50%		(HKUMed, 2022)
Vaccination information	Vaccine dose and type, inoculation date		Vaccine data (DATA.GOV.HK, 2022)
Vaccination effectiveness	Decided by vaccine information (see Table S3)		(HKUMed, 2022)
Infection-induced immunity	Decided by prior-infection time (see Table S4)		(Malato et al., 2023)

### 3.2.2 Urban scaling structure, the scaling index, and mobility behaviors

As shown in Figure 3-2, to account for spatial heterogeneity in mobility, the TPU-TPU

mobility flows were initially simulated using the departure-diffusion mobility model (Giles & Wesolowski, 2022). However, considering the trade-off between spatial resolution and prediction accuracy of traditional mobility models, a subTPU complex network was constructed to refine mobility at finer spatial scales. This network, characterized by nodes and links, captures the urban scaling structure, delineating the scaling properties of mobility towards different locations within a city. The scaling index, which encapsulate the scaling properties, was utilized to distribute the destinations of previously simulated TPU-TPU flows to the subTPU level. Consequently, this approach enables the simulation of mobility volumes across subTPUs that adhere to the scaling law.

In the simulation of TPU-TPU mobility flows, the departure-diffusion model was employed (Giles & Wesolowski, 2022). This model estimates travel probability within and outside the origin separately and combines them using conditional probability rules. The model first estimates the travel probability outside the origin location  $i$  (the departure process) and then the distribution of travel from the origin by normalizing connectivity values across all  $j$  destinations (the diffusion process). These two processes are then combined in the departure-diffusion model as  $\tau_i$  (the probability of leaving origin  $i$ ) and  $\pi_{ij}$  (the probability of going from  $i$  to  $j$ ). The probability of travel within the origin  $i$  is denoted as **Equation 1**, and the probability of travel outside the origin  $i$  is described as **Equation 2**. The expected mean number of trips for route  $i \rightarrow j$  is then as shown in **Equation 3**, where  $\theta$  is a proportionality

constant representing the overall number of trips per person in an origin population of size  $N_i$ .

$$Pr(-depart_i) = 1 - \tau_i \quad (1)$$

$$Pr(depart_i, diffuse_{i \rightarrow j}) = Pr(diffuse_{i \rightarrow j} | depart_i) Pr(depart_i) = \tau_i \pi_{ij} \quad (2)$$

$$\lambda_{ij} = \begin{cases} \theta N_i (1 - \tau_i) & \text{if } i = j \\ \theta N_i \tau_i \pi_{ij} & \text{if } i \neq j \end{cases} \quad (3)$$

As there is a trade-off between spatial resolution and prediction accuracy of traditional mobility models with limited number of travel survey data (**Table S6**), we then characterized urban scaling structure to further refine the mobility patterns across subTPUs. However, due to limited travel survey data and the trade-off between spatial resolution and prediction accuracy (Table S1), urban scaling structure was further employed to enhance the mobility patterns across subTPUs.

Urban scaling structure, here, refers to the scaling property of human mobility within cities, where the mobility volumes originating from or destined for different locations in a city follows the scaling law (Batty, 2008; Brockmann et al., 2006; Jiang et al., 2009). The scaling property is reflected in nodes (origin and destination of movement) and links (between nodes) of a network, which effectively inform mobility at finer spatial scales (Jiang & Jia, 2010; D. Ma et al., 2020; Schlöpfer et al., 2021). Jiang (2018) introduced a topological network representation that considers urban space as a living structure that differentiates from and adapts to each other, as intense local competition for space could be the major reason of the emergent scaling property of

cities (Batty, 2008). By classifying nodes into different hierarchies and creating links within and across hierarchies, the complex network portrays the scaling property of mobility within cities at fine spatial scales (Jiang, 2018; Jiang & Liu, 2012; D. Ma et al., 2020). Therefore, this topological complex network was utilized to characterize the urban scaling structure. Detailed steps are as follows:

Firstly, we took subTPUs as distinct nodes, and divided them into 5 hierarchies (see

Table S2) by mobility volume using head/tail breaks proposed by Jiang (2013). The head/tail breaks classification method is specifically designed for heavy-tailed data (e.g., the power-law scaling distributed data). This method involves iteratively partitioning all data values around the mean into two parts until the head part are no longer heavy-tailed distributed. Secondly, the nodes in the same hierarchy were then used to create Thiessen polygons, and one hierarchy leads to one way of segmentation of urban space. The hierarchies and the Thiessen polygons we partitioned demonstrate how urban areas differentiate from each other. Thirdly, based on the polygon-to-polygon relationships, we created edges among subTPUs, which show how urban areas adapt to each other. Specifically, in the same hierarchy, the small sized subTPU points to the adjacent large subTPUs, and across two consecutive hierarchies, the low-level subTPU points to the high-level subTPU which contains it. As a result, the subTPU complex network was created to characterize the scaling property of human mobility patterns across subTPUs.

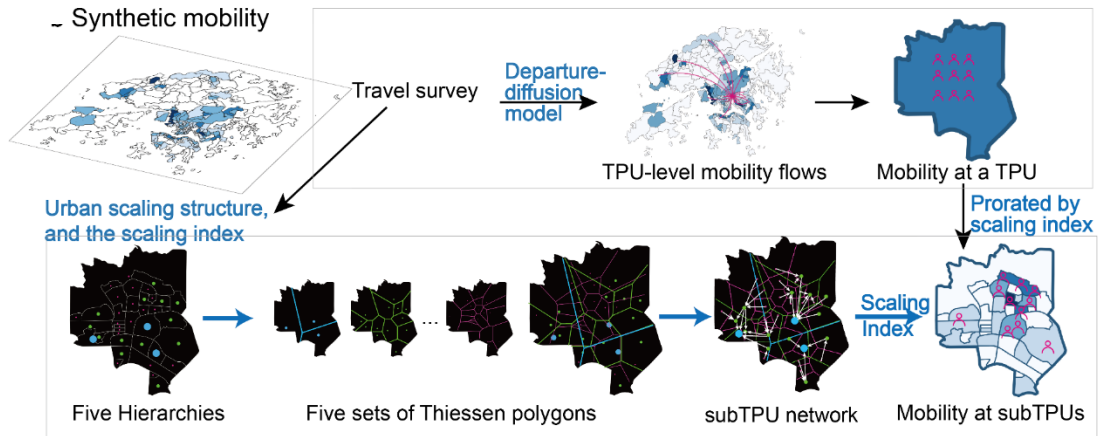


Figure 3-2 The workflow for simulating synthetic mobility behaviors across 4,863 subunits of tertiary planning units (subTPUs) utilizing the subTPU network.

The Weighted PageRank algorithm (Brin & Page, 1998) was applied to calculate the scaling index for each node based on the constructed subTPU network. This algorithm assesses the relative importance of nodes in scaling-characterized networks. It considers not only the mobility volume of the node itself but also the mobility volumes of its neighbours and their neighbours' neighbours through an iterative process (Xing and Ghorbani 2004). The “neighbours” of a node here is defined as the other nodes that directly point to it. The algorithm first assigns an initial index (the mobility volume) to each node. Then, through an iterative process, it adjusts these indices by considering the indices of linking nodes (**Equation 4**). This iterative nature of this algorithm ensures convergence to stable values, providing a measure of a node's relative importance within the complex network.

$$PR(i) = (1 - d) + d \sum_j PR(j)W_{i,j} \quad (4)$$

where  $d$  is a damping factor (usually set to 0.85), and  $j$  is the nodes that point to  $i$ ,  $W_{i,j}$  is the weight of  $link_{i,j}$  which is typically normalized to ensure that the sum of the

weights for outgoing links from each node is equal to 1. More mathematics details can be found in Xing and Ghorbani (2004).

As the calculated scaling index is a good indicator to predict the fine-grained aggregate mobility (Jiang et al., 2009; Jiang & Jia, 2010), it was used to prorated TPU-level mobility to subTPUs. Specifically, while the origins (i.e., home locations of synthetic individuals) remained at the TPU level due to limitations in available census tables, the destinations of the original TPU-TPU mobility flows were refined to the subTPU level. This refinement process allocated agents their TPU destinations based on their home TPUs. Subsequently, agents were assigned finer subTPU destinations based on the refinement of TPU destinations. Consequently, the visits of agents were differentiated across 4,863 subTPUs, which significantly influenced the social contact behaviours within these subTPUs.

### **3.2.3 Contact behaviors**

In the two-layer contact structure (Figure 3-1c), all agents initially had daily contacts with every other family member, which were categorized as household contacts. Contacts that occurred during trips, excluding those within households, were classified as non-household contacts. To model the impact of Non-pharmacological Interventions (NPI) on mobility, a certain percentage of agent trips were cancelled. For agents who still had trips, they visited various subTPUs and had the opportunity to contact a certain number of contactees within the same subTPU. The contactees were randomly selected on the first day of simulation and remained fixed thereafter, using the Monte Carlo

method. The number of contacts for each agent was sampled from age-dependent distributions (Figure S3) (Kucharski et al., 2014). Initially, the total number of contacts was sampled based on the age-dependent distribution. Then, it was assumed that the number of non-household contacts were evenly distributed among the subTPUs visited by the agent on a daily basis.

### **3.2.4 Infection attributes**

The Susceptible-Latent-Infectious-Removed model was used to represent the course of COVID-19 infection. In both waves of the simulation, a proportion of initial cases was introduced. These initial cases, through daily contacts, have a certain level of infectiousness to infect susceptible agents. Infected individuals would then enter the latency period and subsequently the infectious period. To sample the lengths of the latency period and the infectious period for each individual, we used the Gamma distribution with mean values of 1.20 and 5.64, respectively. The Gamma distribution is suitable to model right-skewed data, and this is why we choose it to model the right-skewed nature of the latency and infectious periods of the Omicron variants (Cai et al., 2022; Manica et al., 2022). For the BA.2 and BA.5 variants, which exhibit comparable key time-to-event periods, such as incubation periods of 4.06 and 3.81, respectively (Xu et al., 2023), we used the same Gamma distribution. The slight difference in key periods has negligible impact on the simulation results, given that our model is based on a rather coarse daily temporal scale. Moreover, we further used Gamma distributions to sample the confirmation delay from being infected to being confirmed. The mean

delay time was 5.05 days for the fifth wave and 4.00 days for the sixth wave (Manica et al., 2022; B. Yang et al., 2024).

### **3.3 Coping responses**

#### **3.3.1 Protection behaviors**

For the fifth wave, we assume that the effect of social distancing, school closure, and work from home can be reflected as mobility decline in Google mobility change data. The reduced mobility would result in decreased social contacts and thus disease control. However, for the sixth wave, Google mobility change data is not representative anymore. Figure S2 shows that the sixth wave had limited impact on mobility. This is mainly because people had a decreased level of worry about infection after experiencing the fifth wave (Yang et al. 2024). It is important to note that the limited decrease in mobility does not imply a lack of protective behaviours among individuals. The telephone survey data show that about 50% of individuals still avoided going out or touching shared objects during the sixth wave (B. Yang et al., 2024).

For the sixth wave, we assume that the effect of NPIs can be reflected as a 47% reduction in social contacts. Evidence from the fourth wave in Hong Kong shows that the implementation of Level 1 NPI reduced 47% of the effective reproductive number (HKUMed, 2022), which mathematically corresponds to a 47% decrease in contact rate. Considering that the Level 1 NPIs during the fourth wave were similar to those implemented during the sixth wave, such as restrictions on social gatherings in

restaurants and indoor leisure facilities, and closure of kindergartens, we assume NPIs during the sixth wave reduced contacts by 47%.

We make the assumption that half of infected individuals would undergo a 7-day isolation period at home during both waves of the simulation (HKUMed, 2022). The mobility changes resulting from isolation were incorporated into our daily mobility change index. This assumption aligns with real-world scenarios where individuals who develop symptoms or test positive are more likely to stay home (Bian et al., 2012; Cai et al., 2022; HKUMed, 2022). To implement this setting, we utilized probability sampling to determine which infected individuals would undergo isolations. Once an individual developed symptoms or received a positive test result (whichever occurred earlier), they would start their 7-day isolation period. After this, the remaining reduction in mobility was randomly assigned to other non-infected individuals using the Monte Carlo method.

### **3.3.2 Vaccine- and infection-acquired immunity**

For the fifth wave, this work only considered vaccine-acquired immunity, due to the limited number of prior infections (in total 12,258 cases by Dec. 20, 2021) during previous waves in Hong Kong. As there is no geographic information of vaccination data, we randomly assigned the vaccination status to agents by age group, using the Monte Carlo method. The vaccination status includes how many doses and which type of vaccine the agent had been taken. We assume that the vaccination can reduce individual infectiousness by certain percentages (

Table S3) that are determined by the inoculation time, the number of doses, and the vaccine type (Andrews et al., 2022; HKUMed, 2022; Kirsebom et al., 2022).

For the sixth wave, we employed the same setting to consider vaccine-acquired immunity, but we also took into account infection-acquired immunity from the fifth wave. As evidence shows that hybrid immunity, resulting from both vaccination and prior infection, can be highly effective, we assume that prior infection can reduce individual infectiousness by certain percentages, as indicated in

Table S4 (Malato et al., 2023). The effects of prior infection and vaccination are multiplied together to determine the overall reduction in individual infectiousness in our study.

### **3.3.3 Reporting behaviours**

In our simulation, the reporting behaviours during both waves were constantly changing. To estimate the number of reported cases during the fifth wave, we assume that 8% of the infections were reported before 24 February, 30% were reported between 24 February and 7 March, and afterward, 35% were reported, based on the changing reporting standard. On 24 February, the Hong Kong government officially acknowledged positive cases tested by commercial laboratories as confirmed cases, reporting them without double confirmation. Additionally, the RAT online reporting system, launched on 7 March, allowing citizens to report positive results tested since 26 February. The report rates used in our study were derived from research conducted by the Hong Kong University (HKUMed, 2022), assuming report rates were 8% before

and 20% after 24 February. However, these rates did not consider RAT-reported cases, as they were estimated before the system’s launch. To adjust the report rates to our current setting, we considered that RAT-reported cases accounted for 40% of the total reported cases during the fifth wave ( $20\% \div (1 - 40\%) \approx 33\%$ ).

For the sixth wave, the reporting rate was assumed to be 20%. The lower reporting rates can be attributed to several factors. First, milder symptoms may result from almost half of the population having been infected and developed immunity (HKUMed, 2022), leading to fewer people seeking testing and reporting their cases. Additionally, pandemic fatigue may contribute to a reduced willingness among individuals to report their symptoms (B. Yang et al., 2024).

### **3.4 Model initialization, calibration and validation**

#### **3.4.1 Model initialization**

The experiments span from 1 February to 30 September 2022. For the fifth wave, we assume that on 1 February, a proportion  $L_1$  of agents were infected and in the latency period. Similarly, for the sixth wave, on 1 July, a proportion  $L_2$  of agents were infected and in the latency period. The latent agents were randomly selected from the whole population, using the Monte Carlo method.

#### **3.4.2 Model calibration**

Most model parameters (Table 3-1) can be estimated from empirical data or studies.

Apart from this, two parameters for each wave need to be calibrated with data: (1) individual infectiousness  $p_i$ ; (2) the initial proportion of exposed cases  $L_i$ . For the fifth wave, we calibrated these parameters to the city-level number of confirmed cases from 1 February to 30 March 2022. Similarly, for the sixth wave, calibration was done using the city-level case numbers from 1 July and 30 September 2022. The calibration processes are as follows:

We initially identified plausible parameter ranges and selected multiple parameter combinations for evaluation. For the fifth wave, we assume that the basic reproduction number ( $R_0$ ) of BA.2 variant ranged from 6 to 10. This is a relatively wide range, as a previous study estimated the  $R_0$  of 8.2 (Y. Liu & Rocklöv, 2022). To determine the values of individual infectiousness ( $p_i$ ) that would result in the assumed  $R_0$  range, we created a well-mixed agent-based model. This choice was made because the definition of  $R_0$  requires a completely susceptible and fully mixed population. In the well-mixed model, there are no immunity and mobility settings, meaning that all agents were fully susceptible and they randomly choose their contacts in the whole population. Under this scenario, we initialized a proportion of index cases ( $L_i = 10^{-4}$ ) and recorded the number of secondary cases. Let  $N_0$  represent the number of index cases and  $N_s$  the number of secondary cases, which gives  $R_0 = \frac{N_s}{N_0}$ . We averaged these  $R_0$  values over 30 replicates for each  $p_i$  value, and the results showed that  $R_0$  is linear in  $p_i$  (Chang et al., 2021). To allow  $R_0$  in the plausible range,  $p_i$  for the fifth wave should range from 0.04 to 0.06. We used increments of 0.001 to obtain 20 unique values of  $p_i$ , which were then used in the model fitting. For the sixth wave, we assume the plausible

range  $p_i$  should range from 1 to 1.4 times the best-fit  $p_i$  for the fifth wave, considering that BA.5 was about 1.4 times more infectious than BA.1 (Fan et al., 2022).

For both waves, it is still not clear that how many infections existed at the beginning of simulations. We set  $L_{5th}$  with a range between  $10^{-5}$  to  $10^{-4}$  and  $L_{6th}$  with a range between  $10^{-4}$  to  $5 \times 10^{-4}$ , to account for the uncertainty of the real situation. This setting takes into account the strict control policies and entry restrictions during the initial stage of the fifth wave. However, during the sixth wave, the relaxation of entry policies results in a larger number of imported cases (B. Yang et al., 2024).

Each combination was tested by running 30 replicates of the simulation. The model's predictions were compared to the empirical data using the Root Mean Square Error (RMSE), which quantifies the difference between observed and simulated confirmed cases: for each replicate,

$$RMSE = \sqrt{\frac{1}{D} \sum_{d=1}^D (N_{confirmed}^d - \hat{N}_{confirmed}^d)^2} \quad (5)$$

where  $\hat{N}_{confirmed}^d$  is the observed confirmed cases (per 10,000 people) on day  $d$ , and  $N_{confirmed}^d$  is the corresponding value in the simulation. The average RMSEs across 30 replicates were used to evaluate each parameter combinations.

The best-fit parameter set was identified as the one with the lowest average RMSE. To account for parameter uncertainty, parameter sets with RMSE values within 20% of the lowest RMSE were selected (Chang et al., 2021). The model predictions were then obtained by aggregating the predictions from the selected parameter sets and replicates. The mean, as well as the 2.5<sup>th</sup>/97.5<sup>th</sup> percentiles, were calculated to provide estimates of the central tendency and uncertainty range, respectively.

### 3.4.3 Model validation

For the fifth wave, three empirical data was used to validate different aspects of the simulation outcomes. The first data includes the city-level number of confirmed cases, which allowed us to calculate the city-level RMSE. The second data is the observed high-risk subTPUs. We compared it with the simulated superspreading subTPUs that were identified by counting cumulative non-household infections that occurred in every subTPU. The third data consists of the TPU-level number of RAT-confirmed cases from 1<sup>st</sup> to 30 March 2022. We calculate the RMSEs of 214 TPUs and summed them to obtain the TPU-level RMSE. The number of cases confirmed by RAT at every TPU can be used to evaluate the TPU-level model accuracy. Different from the city-level data, this data only records partial confirmed cases (not including cases confirmed by the polymerase chain reaction test) and does not cover the whole period of simulation (starting from 26<sup>th</sup> February 2022). Due to its incompleteness, we do not use it to calibrate our model, but we directly use it to validate the model accuracy on the local scale. We sum the RMSEs of TPUs together to evaluate the TPU-level prediction,

$$RMSE_{TPU} = \sum_{tpu}^{TPU} \sqrt{\frac{1}{D} \sum_{d=1}^D (N_{RAT}^{d,tpu} - \hat{N}_{RAT}^{d,tpu})^2} \quad (6)$$

where  $\hat{N}_{RAT}^{d,tpu}$  is the observed RAT-confirmed cases in a  $tpu$  on a day  $d$ , and  $N_{RAT}^{d,tpu}$  is the corresponding value in our simulation. As our model predict on all confirmed cases, we assume that a  $p_{RAT} = 0.4$  proportion of cases are confirmed by RAT,  $N_{RAT}^{d,tpu} = p_{RAT} \times N_{confirmed}^{d,tpu}$ .  $p_{RAT}$  is determined by the proportion of the total number of RAT-

confirmed cases in the total number of observed confirmed cases. The time series of this validation also spans from 1<sup>st</sup> March to 30<sup>th</sup> March 2022.

For the sixth wave, we used the city-level BA.5 case numbers to calculate the RMSE. This study focuses on reconstructing the new virus invasion situations, specifically the spread of BA.5. However, as mentioned in *Case data*, the empirical case numbers included both BA.2 and BA.5 cases throughout the sixth wave. To separate the BA.5 cases from overall cases, we used the sequenced sample data (Gilman, 2022), which recorded the temporal changes in the proportion of BA.5 samples among all recorded samples from 1 May to 30 September 2022 (Figure S1).

# **Chapter 4 Local spread dynamics influenced by urban scaling structure**

Superspreading events underscore the uneven distribution of COVID-19 spread among individuals and locations. Chapter 4 aims to explore the underlying mechanism of heterogeneous local spread dynamics and its relationship with urban scaling structure. In this chapter, the spatially explicit ABM (see Chapter 3) is used to reconstruct local spread processes across 4,863 subTPUs. To validate our model, we compared the simulation outcomes with empirical case data from the fifth wave in Hong Kong across three spatial scales. Further statistical analyses of simulation data examined the relationship between the scaling index, representing a location's importance within the structure, and local spread risk as well as the likelihood of local visitors becoming superspreader. Additionally, we analysed the unevenly distributed stress on local hospitals resulting from heterogeneous spread patterns and provided suggestions for hospital emergency preparedness. This chapter thus enhances our understanding of how human mobility and its scaling structure influence local spread risks and superspreading events, which may inform precise and effective interventions to combat future pandemic.

## **4.1 Model Results**

### **4.1.1 Model fitting**

Our model fits empirical case data roughly well at both the city level and the TPU level (Figure 4-1). Noted that the TPU-level prediction is more difficult than the city-level prediction, as the former predicts 214 epidemic curves, and the latter only predicts one curve. At the city level, our model accurately predicts the number of cases during the peak period from 21 February to 10 March 2022, but underestimates the case numbers before 21 February. This underestimation can be attributed to the Chinese New Year celebrations (from 1 to 15 February 2022) that caused intense social contacts and thus large number of infections. The limitations of our model stem from its reliance on Google mobility change data, which may not accurately capture the nuances of social behaviour changes during holidays, despite its proven representativeness during regular periods in other studies (Chang et al., 2021; Cot et al., 2021; Yilmazkuday, 2021). To solve this issue, more detailed social contact data during holiday periods are needed in future studies.

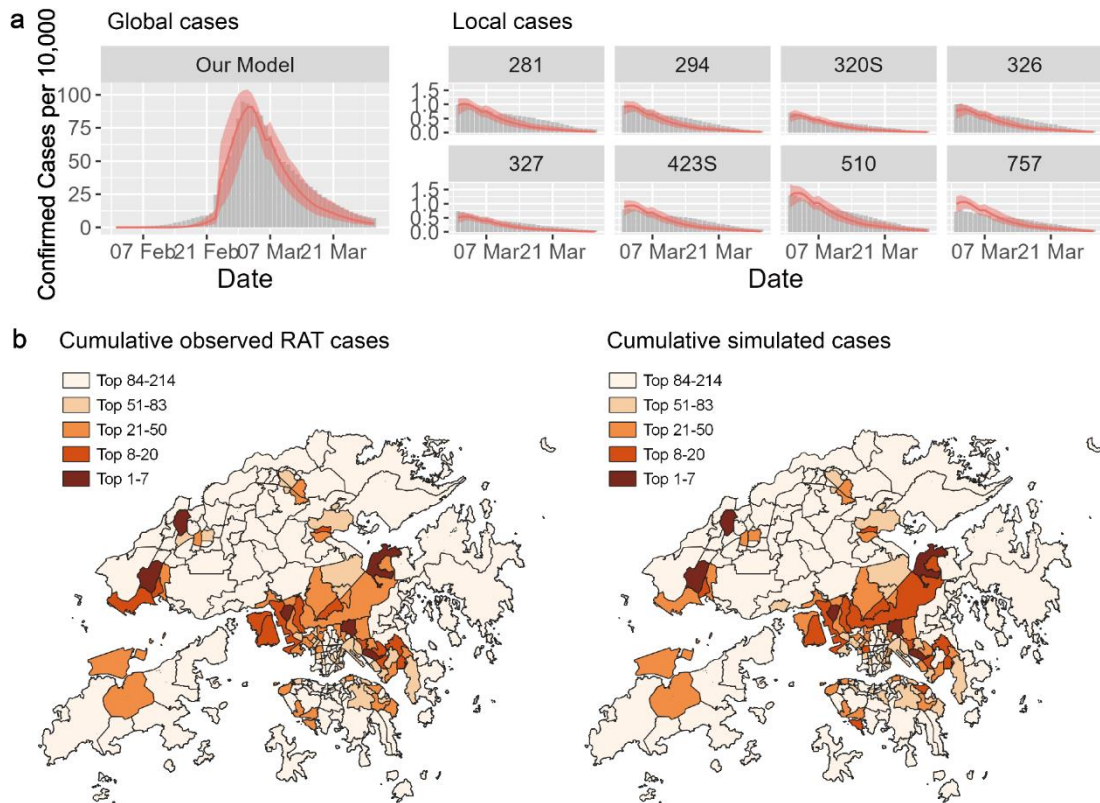


Figure 4-1 Model fitting results. **a**, epidemic curves. The left plot is the city-level prediction, and the right plot is the TPU-level prediction on the eight worst affected TPUs. The grey bar is the 7-day moving average of observed confirmed cases. Shaded regions denote the 2.5<sup>th</sup> and 97.5<sup>th</sup> percentiles across selected parameter sets and stochastic realizations. **b**, the spatial distribution of the total number of observed RAT cases (left) and simulated cases averaged across selected parameter sets and stochastic realizations (right).

At the TPU level, our model predicts well the peak period of the eight most serious TPUs, but underestimates the cases after 7 March. As the empirical case data has an unnatural increase after 7 March, which could be largely resulted from the increased reporting behaviours due to the RAT reporting system launched on 7 March 2022, we infer that our underestimates could be partly originated from this reason. Although our model considered the increased report rate after 7 March (increasing the report rate from 0.3 to 0.35), other potential factors could still play in a role. For example, the launch of RAT reporting system might change the time gaps between the test date and

the report date, and such change may significantly vary among individuals. Despite the underestimation, the analysis reveals a strong positive relationship between the cumulative observed RAT cases and simulated cases, as evidenced by a high Pearson correlation coefficient of 0.97 ( $p < 0.01$ ). Furthermore, both empirical data and simulated results exhibit similar spatial patterns (Figure 4-1b).

### **4.1.2 The superspreading subTPUs**

By calculating the average cumulative non-household infections (see *Section 3.2.3*) across 30 runs using the best-fit parameters, we identified the superspreading subTPUs: 20 percent of superspreading subTPUs account for 78 percent of non-household infections (Figure 4-2a). When comparing with the top 20 percent of the empirical high-risk subTPUs that were most frequently visited by cases (see *Section 3.1*), our results identified 46 percent of them (Figure 4-2b). The top 20 percent of observed subTPUs gathered 83 percent of the visits by cases, which shows a similar nonlinear relationship with our results (Figure 4-2c).

The spatial distribution of simulated superspreading subTPUs is similar to the observed patterns (Figure 4-2b, d). They both confirmed that the financial and commercial centers and the most densely residential areas were highly risky. The differences between the simulated and observed patterns are that the simulated results include more high-risk subTPUs around the populated areas but exclude some high-risk subTPUs in the financial and commercial centers. Notably, the observed patterns include all visits of cases, but only a minority of them would lead to infections.

Therefore, they may overestimate the risk degree of some subTPUs, especially subTPUs that gather a large volume of visits, such as some in the financial and commercial centers.

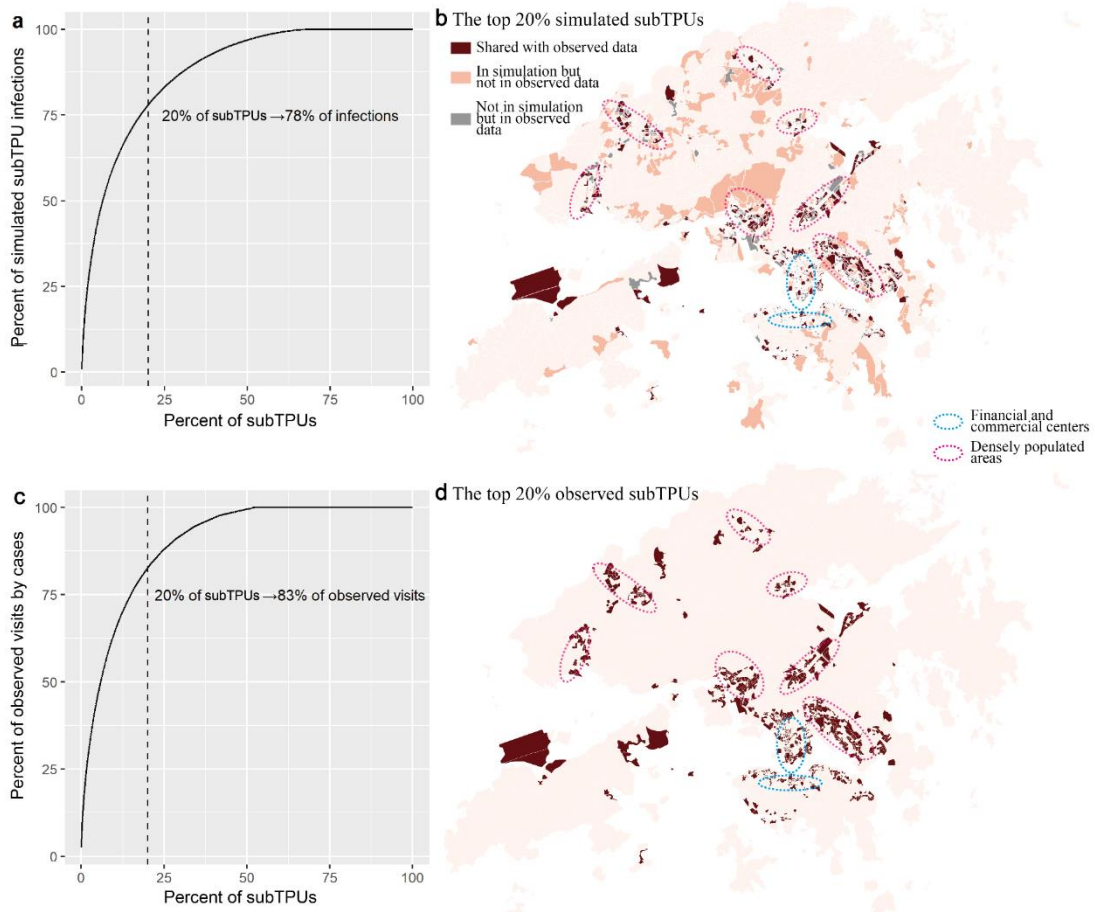


Figure 4-2 The simulated superspreading subTPUs and the observed high-risk subTPUs. a, the top 20% of simulated subTPUs (or superspreading subTPUs), ranked by the average number of infections occurred in subTPUs across 30 runs, accounts for 78% of the average number of simulated infections. b, the spatial distribution of simulated superspreading subTPUs. c, the top 20% of observed subTPUs, ranked by the total number of visits by infected cases occurred in subTPUs, account for 83% of visits. d, the spatial distribution of the observed high-risk subTPUs.

### 4.1.3 The effects of urban scaling structure on local transmission risks

To understand heterogenous transmission risks across subTPUs, multivariate linear regression was used to estimate the effects of key components, including spatial structure, mobility density, and the structure of social network for each subTPU. The transmission risk for subTPU was measured by the proportion of transmission contacts that successfully transmit the virus among all contacts. The mobility density refers to the number of visiting agents per unit of subTPU area. The social network is generated by the process described in *Section 3.2.3*. As the successful transmission is a chance event, we took 30-run average as the reported result to guarantee a more reliable estimation. After controlling mobility densities and clustering coefficients of social networks for 4,863 subTPUs, the scaling index still have an important effect on the transmission risk: a 1-percent-point increase in the scaling index leads to 2.54 percent increase in transmission risk on average (Table 4-1).

Table 4-1 The effect of the scaling index on the average transmission risk (the average proportion of transmission contacts across 30 runs with the best-fit parameters) for subTPUs through multivariate linear regression.

Variable	Coefficient
<b>The scaling index</b>	<b>2.54***</b>
Average mobility density	0.16***
Average clustering coefficient of social network	0.09***

\*\*\* Significant result with p-value < 0.001.

Table 4-2 The average effects of the scaling index on individual's probability of becoming a superspreader (the top 10% of individuals ranked by the number of secondary cases) through logistic regressions across 30 runs with the best-fit parameters.

Variable	The mean of coefficients	Exponential of (coefficients*1 unit)
<b>The average scaling index</b>	<b>3.94 * ^</b>	<b>104% (a 1-percent-point increase)</b>
The number of contacts	0.03 ***	103% (a 1-point increase)

\*\*\* Significant result with p-value < 0.001; \* ^ 60% of results are significant with p-value < 0.05.

#### **4.1.4 The effects of urban scaling structure on individual's probability of becoming a superspreader**

As subTPUs with larger scaling index have higher transmission risks, individuals who visits these subTPUs may have higher chance to infect more people and become superspreaders. The top 10 percent of agents, ranked by the number of secondary cases, were classified as superspreaders, and these superspreaders accounted for on average 77.3 percent (95% CI: 76.5%-78.6%) of infections across 30 simulations. Logistic regressions were used to quantify the average effect of spatial structure on individual's probability of becoming a superspreader. After controlling the number of daily contacts, the average scaling index has a large influence on the probability of being superspreaders: A 1-percent-point increase in the average scaling index enhances 3.94 percent of the log odds ratio for individual becoming a superspreader, suggesting that the probability of being a superspreader would be increased by 4 percent (Table 4-2).

#### **4.1.5 The unevenly distributed strain on local hospitals**

Because the infections are unevenly distributed, the consequent hospital strain also expected to vary across space. To evaluate the local strain, we calculated the ratios of

the simulated demands to available local capacities for ED visits and hospital beds (see *Section 3.3.1*). During the peak period of the pandemic (from 1 March to 15 March 2022), all hospitals were heavily hit, but the degree of hospital strain varies (Figure 4-3). In 17 hospitals with ED services, three of them experienced the most drastic surge in ED visits that exceeded 350 percent of their capacities, and the rest of the hospitals mainly required 150 percent to 300 percent of current capabilities to cope with local ED demands (Figure 4-3a). To show the hospital strain on space, we take the service area (TPUs) of each hospital as a group and show the average hospital strain on each group. TPUs in the central of the city experienced severe ED strain, and remote TPUs in the west and north were slightly better (Figure 4-3a).

The strain on hospital bed capacity was also unevenly distributed across seven COVID-19 designated hospitals (Figure 4-3b). Three in seven hospitals required over 300 percent of their current hospital bed capacities, but one hospital only used 18 percent of hospital beds, during the peak period. Remote TPUs in the west and east of the city experienced severe strain on hospital bed capacity, and the strain for the central TPUs was slightly relieved. The Island District in the southwest corner of the city was an exception, and the demand was much less than the local capacity.

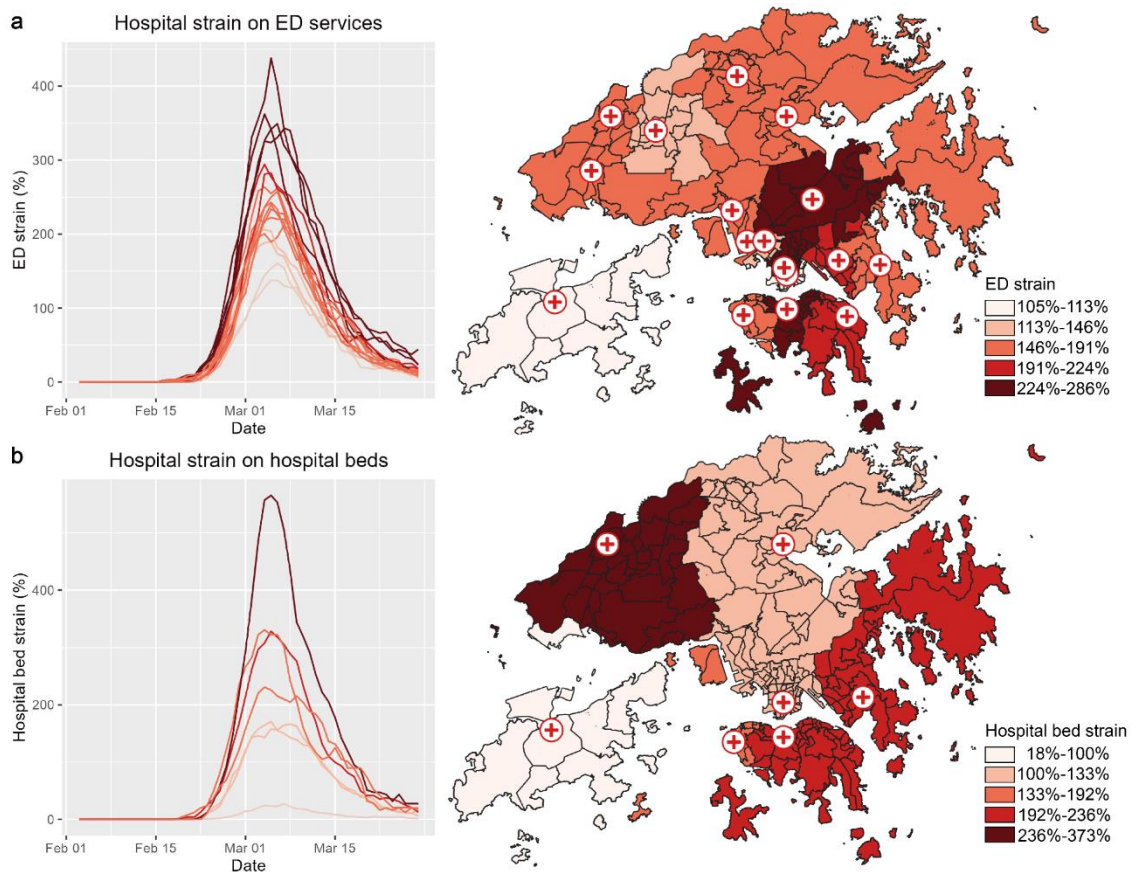


Figure 4-3 Simulated hospital strain on the Emergency Department (ED) services (a) and hospital beds (b). The strain on each hospital was estimated by the ratio of simulated local demand to available hospital capacity. In a and b, Left, the hospital strain varied by hospital and time. Right, the average hospital strain during the peak period (from 1 March to 15 March 2022) varied across TPUs.

## 4.2 Discussion

This study employed the spatially explicit ABM to reconstruct the spread processes at the fine spatial scale. After validating by city-level to subTPU-level empirical data, further statistical analyses of model results reveal that not only the quantity of mobility but also the scaling structure of mobility have important impacts on local transmission risk: areas with low scaling indices could be less likely to transmit virus, even when they have a rather large mobility density or a clustering social network; similarly,

individuals who tend to visit low-scaling-index areas could be less likely to transmit the virus to others, even when they have a large number of contacts. These findings suggest urban scaling structure may play an important role in the mechanisms driving the heterogeneity in local transmission risks among urban areas and individuals.

#### **4.2.1 How urban scaling structure influences local transmission risks**

It is widely acknowledged that high population or mobility density would increase the local transmission risk (Alessandretti, 2022; Damme et al., 2020; Hong et al., 2021a; Wong & Li, 2020). However, our findings suggest areas with a rather high mobility density may not necessarily be more likely to transmit virus, especially when they have low scaling indices. The scaling index measures the relative importance of different areas in the entire structure based on the links pointing to them and the links of those links through an iterative process (see *Section 3.2.2*). Due to the nature of the scaling law (Clauset et al., 2009; Jiang, 2009; Jiang et al., 2009), only a minority of areas are of great importance in this structure, and they would be more likely to rapidly import the virus from the initial infections occurred in elsewhere. In this case, the high-scaling-index areas take one step ahead to infect susceptible people first, leaving little chance for most low-scaling-index areas to transmit the virus, as most of their visitors would have already been infected elsewhere.

Therefore, the scaling index could be a potential risk factor for local transmission. Different from the local population or mobility density, it highlights the urban

structure's impact on local risk. Urban scaling structure offers a minority of areas the 'first-mover advantage', allowing them to initiate infections earlier and on a larger scale. In this regard, our study provides a deeper understanding of superspreading places or Points of Interests (POIs): while large population or mobility may be necessary, they are not sufficient conditions for superspreading places. The opportunity for early access to the virus brought by urban scaling structure also matters.

#### **4.2.2 How urban scaling structure contributes to superspreaders**

The heterogeneity in local transmission risk would further influence individuals' chance of having more infections and becoming superspreaders. In our model, we assumed that all individuals have an equal probability of successfully transmitting the virus per contact. Therefore, infected people with large number of contacts are more likely to infect more susceptible people and thus become superspreaders. However, our analyses found that where those infected people visited also matters. Individuals tends to visit locations with large scaling indices are more likely to become superspreaders. This suggests that when individuals are embedded in areas with low scaling indices, even those with large number of daily contacts may not necessarily become superspreaders. The reason could be that these individuals fail to infect their contactees when competing with others at high-scaling-index locations who also want to infect the same contacts. The high scaling index offers others an advantage in infecting the same contactee first, as the large value of scaling index increased the local transmission risk.

Therefore, individuals at low-scaling-index locations encounter fewer susceptible people to infect, reducing their likelihood of becoming superspreaders.

In contrast to our findings, some researchers posit that it is the high infectiousness of certain individuals that causes superspreaders (Sidik, 2023; Zhou et al., 2023). They think infectiousness is highly unequal distributed among infected cases. However, our results demonstrate that even with the same level of infectiousness, superspreaders are naturally emerged from the interaction of social contacts, in which the location also play an important role. Nevertheless, we conducted a sensitive analyse to consider the heterogeneity in infectiousness and found that the urban scaling structure is a still important risk factor for individuals becoming superspreaders (see *Section 7.4*). Therefore, superspreaders could be originated from a complex interplay of both individual, social, and environmental factors. To comprehensively quantify these intricate interactions, more individual-level viral and behaviour data is needed in future studies.

### **4.2.3 Practical suggestions on hospital emergency preparedness**

The uneven distribution of infections and medical resources gives rise to the heterogeneous strain on the existing healthcare systems (see *Section 3.3.1*). After considering the high spatial heterogeneity in hospital strain, we may provide some qualitative suggestions on hospital emergency preparedness to adequately staff local hospitals in advance and wisely share the existing resources. The specific suggestions

are as follows:

Firstly, to relieve the strain on local EDs, triage centers are needed in Sha Tin District in the middle of the city and Wan Chai District in Hong Kong Island. During the fifth wave in Hong Kong, many patients with mild symptoms occupied the ED resources that should have been used to treat those with severe symptoms (A. Ma & Parry, 2022). The triage centers in the most severe areas can efficiently filter out a large number of non-urgent patients and identify the critical patients for further ED services. Secondly, more hospital beds should be assigned for local COVID-19 patients in Tin Shui Wai and Tuen Mun New Towns in the west of the city. Thirdly, transferring the patients to the hospital in Island District is another practical suggestion as there would be relatively lower pressure even at the peak of the pandemic. The hospital in Island District (North Lantau Hospital Hong Kong Infection Control Centre) started the services special for COVID-19 patients in 2021 and has over 800 isolation beds, so it is capable to take patients from other hospitals and regions.

### **4.3 Summary**

To gain a deeper understanding of the underlying mechanisms by which urban scaling structure of human mobility contributes to local transmission risks of COVID-19 within cities, this chapter utilized the spatially explicit ABM which incorporated urban scaling structure to reconstruct fine-grained mobility patterns and spread processes. After validating by empirical data at various spatial scales, further statistical analyses of simulation outcome reveal that not only the quantity of mobility but also its scaling

structure have important impacts on local transmission risks among urban areas and individuals. For urban areas, a large volume of local mobility is only a prerequisite for high transmission risk, and their significance within the urban scaling structure also plays a crucial regulatory role in it. Consequently, the resulted heterogenous risks among urban areas would further influence the transmission potential of their visitors becoming superspreaders.

In summary, urban scaling structure may provide the ‘first-mover advantage’ to a small group of urban areas and individuals, enabling them to initiate infections earlier and on a more substantial scale. This chapter thus brings important insights for the spread dynamics of COVID-19 and similar diseases, highlighting the role of urban scaling structure in driving the heterogeneity in local transmission risks and superspreading events. These insights may serve as valuable guidance for the development of precise and effective interventions to mitigate future pandemics.

# **Chapter 5 Vulnerability and resilience to different virus characteristics**

Disaster vulnerability and resilience, unfolding within urban complex systems, are influenced by a combination of socio-physical drivers and dynamic processes. Chapter 5 aims to explore the vulnerability and resilience under the different contexts of virus characteristics. The aforementioned ABM (Chapter 3) was employed to reconstruct case trajectories of the fifth and the sixth waves in Hong Kong. After validating the model by empirical data at various spatial scales, we investigated how a small change in virus characteristics, specifically individual infectiousness heterogeneity, might influence community vulnerability and resilience. For community vulnerability, we assessed local spread risk and local risk for SSEs during the fifth wave. For resilience, we measured the successful probability of new virus invasions during the sixth wave. Additionally, we conducted a counterfactual simulation to evaluate the potential long-term implications of a lockdown policy. This study thus enhances our understanding of how virus characteristics would interact with urban complex systems, contributing to community vulnerability and resilience in the COVID-19 context. The unique urban complex system perspective can serve as a promising tool to understand vulnerability and resilience in various disaster contexts and inform future policy decisions.

## **5.1 Analyzing vulnerability and resilience under individual infectiousness heterogeneity scenarios**

### **5.1.1 Vulnerability under individual infectiousness heterogeneity scenarios**

During the calibration stage, we assume uniform infectiousness among individuals. This common simplification allows us to identify the best-fit average value for the entire population. However, in reality, infectiousness can vary by individuals (Sidik, 2023), but the exact degree of heterogeneity remains unclear. The individual infectiousness heterogeneity can potentially impact the spread dynamics. To investigate its effects on vulnerability patterns during the fifth wave, we conducted simulations with varying heterogeneity degrees using the Beta distribution. We chose the Beta distribution to model individual infectiousness because it allows us to constrain values between 0 and 1. It also enables us to control the mean value and heterogeneity of this distribution through its parameters. We controlled the heterogeneity degree using the alpha parameter, which was set to 0.01, 0.1, 0.5, 1, and 10 (Figure 5-2a). Additionally, we controlled the mean value of the distribution using the beta parameter, which was determined by  $\left(\frac{1}{mean} - 1\right) \times alpha$ . The mean value was set to be the best-fit infectiousness value in Table 3-1.

### **5.1.2 Resilience to new virus invasions under individual infectiousness heterogeneity scenarios**

During the calibration stage for the sixth wave, we simplified the scenario by assuming that the initial cases of new variants were introduced on July 1, 2022. However, in reality, the first local case of the BA.5 variant were detected around late April in Hong Kong, which did not lead to an observable wave. Our simplification avoids the high uncertainty associated with spread dynamics before July, considering the low number and high randomness of early infections. However, in this stage, we modified this assumption to align with reality by introducing three cases to the city centre (high-scaling-index places) on May 1, 2022. By doing so, we thoroughly explored the probability of successful invasions under various scenarios of individual infectiousness heterogeneity. Similar to the section of *Vulnerability under various heterogeneity degrees in individual infectiousness*, we used Beta distributions to control the heterogeneity degree with varying alpha parameters, set to 0.01, 0.1, 0.5, 1, 10, and 10000.

### **5.1.3 The counterfactual simulation of the lockdown scenario**

During the Hong Kong COVID-19 pandemic, the fifth wave was the most severe period of infection. To control the outbreak, the Hong Kong government had considered implementing a lockdown policy, but this option was ultimately abandoned due to various considerations. To evaluate the potential short-term and long-term outcomes,

we conducted a counterfactual simulation of implementing a lockdown policy during the early stages of the fifth wave. Specifically, we assume that the lockdown policy would begin on February 1, 2022, reducing contacts by 85% estimated from the regional lockdowns implemented in mainland Chinese cities in response to outbreaks of Delta (HKUMed, 2022).

## **5.2 Model results**

### **5.2.1 Model fitting**

For both the fifth and sixth waves, our model fits empirical case data roughly well. For the fifth wave, we used three empirical data at different spatial scales to validate our model (see Section 4.1.1). For the validation of the sixth wave, we used the city-level BA.5 case number. Note that the model fitting for the sixth wave faces a higher level of difficulty compared to that of the fifth wave. This is due to the more complex spread context, which involved prior infection-acquire immunity and the relatively low number of cases. Despite the challenges, our model was still able to effectively capture the general trend of the sixth wave (Figure 5-1a). This further verifies the validity of our model structure and provides a solid foundation for subsequent resilience analyses on different contexts of new virus invasions.

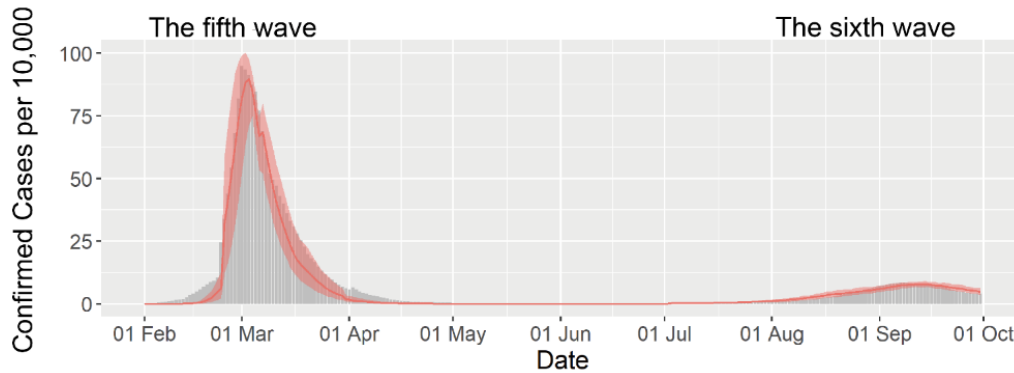


Figure 5-1 Model fitting of the city-level epidemic curves for the fifth and sixth waves. The grey bar is the 7-day moving average of observed confirmed cases. Shaded regions denote the 2.5th and 97.5th percentiles across selected parameter sets and stochastic realizations.

## 5.2.2 The effects of individual infectiousness heterogeneity on community vulnerability

After validation, we utilized Beta distributions with varying alpha parameters to sample individual infectiousness, to investigate community vulnerability patterns (see *Section 5.1.1*). Figure 5-2a shows that a smaller alpha parameter corresponds to a higher degree of individual infectiousness heterogeneity.

To assess community vulnerability, we introduced two variables. The first variable is local transmission risk, measured by the proportion of transmission contacts that successfully transmit the virus among all local contacts, averaged across 30 runs. To compare the heterogeneity scenarios, we conducted the Kruskal-Wallis test, a non-parametric statistical test used to compare the medians of two or more groups (Kruskal & Wallis, 1952). The test results revealed a significant impact of individual infectiousness heterogeneity on local transmission risk, with a high chi-squared value of 11,670 ( $p\text{-value} < 0.001$ ). A higher chi-squared value indicates larger differences

among the groups. Figure 5-2**b** shows significant differences in the distributions of local transmission risks among five scenarios, where a decrease in heterogeneity corresponds to an increase in the average value of local transmission risks.

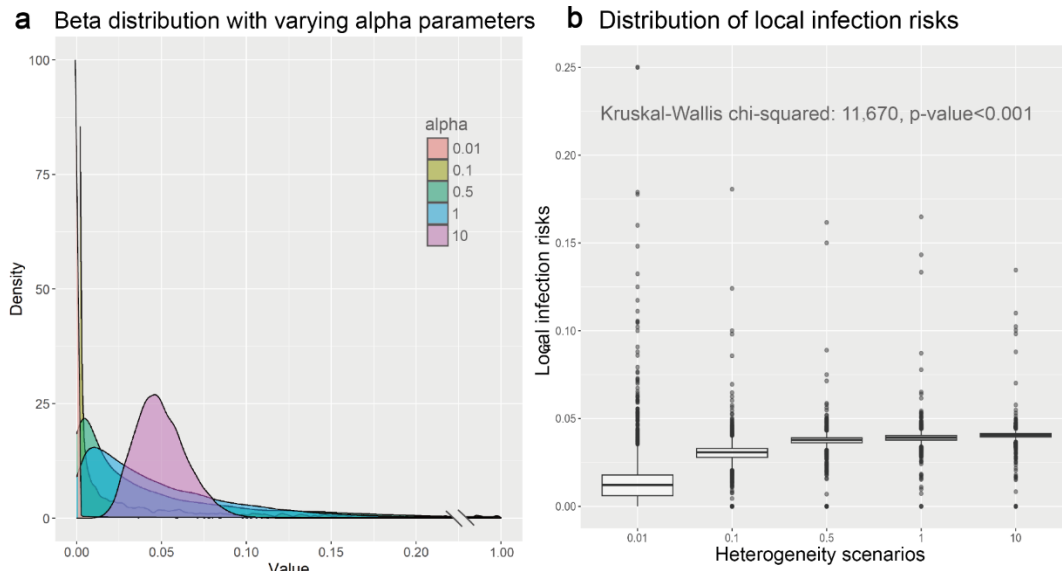


Figure 5-2 The individual infectiousness heterogeneity and community vulnerability in local infection risks. **a**, Beta distribution with varying alpha parameters ranging from 0.01, 0.1, 0.5, 1, 10, and a fixed mean value of 0.05 (the best-fit infectiousness), used to sample individual infectiousness. **b**, distribution of infection risks for subTPUs under different scenarios of heterogeneity degree. Kruskal-Wallis results show significant differences among scenarios, with the chi-squared coefficient of 11,670 ( $p$ -value < 0.001).

In addition to analysing the average value of local risk, we also examined the extreme value, namely the local risk for SSEs. Local SSE risk was measured by the proportion of SSEs among all local spreading events, averaged across 30 runs. Here, SSEs were determined by the top 20 percent of spreading events, ranked by the number of secondary cases. A spreading event is defined as an agent’s infectious contacts within a specific place. As the occurrence of SSEs is influenced by both individual and place characteristics (Chang et al., 2021; Peng & Liu, 2024), we used multivariate linear

regression to estimate the interaction effect of individual infectiousness heterogeneity and the scaling index.

Table 5-1 shows that the scaling index have a positive effect on local SSE risk: a 0.1 increase in the scaling index leads to a 1.91 percent increase in local SSE risk. However, a decrease in the heterogeneity degree has a slightly negative impact on local SSE risk. When comparing to the most heterogeneous scenario (scenario 0.01), other scenarios are associated with a negligible decrease in local SSE risk. Although the different heterogeneity scenarios exhibit limited direct effects on local SSE risk, they significantly modify the positive relationship between the scaling index and local SSE risk. Specifically, when comparing to the scenario 0.01, all other scenarios exhibit negative coefficients. In other words, individual infectiousness heterogeneity significantly amplifies the positive effect of the scaling index, when the heterogeneity degree increases.

Table 5-1 The effect of individual infectiousness heterogeneity on local SSE (superspreading event) risks through multivariate linear regression, including the interaction term with the scaling index

Variable	Coefficient
The scaling index	0.191***
Heterogeneity scenario 0.01	ref
Heterogeneity scenario 0.1	-0.00006***
Heterogeneity scenario 0.5	-0.00006***
Heterogeneity scenario 1	-0.00006***
Heterogeneity scenario 10	-0.00007***
The scaling index* Heterogeneity scenario 0.01	ref
The scaling index* Heterogeneity scenario 0.1	-0.116***

The scaling index* Heterogeneity scenario 0.5	-0.127***
The scaling index* Heterogeneity scenario 1	-0.125***
The scaling index* Heterogeneity scenario 10	-0.119***

---

\*\*\* Significant result with p-value < 0.001.

### 5.2.3 The effects of individual infectiousness heterogeneity on resilience to new virus invasions

After analysing the community vulnerability during the fifth wave, we conducted experiments to assess resilience to new virus invasions during the sixth wave. Specifically, three BA.5 cases were introduced to high-scaling-index places on May 1, 2022, under different heterogeneity scenarios (see *Section 5.1.2*). The resilience was evaluated by calculating the probability of successful invasions across 30 runs. A successful invasion is defined as the presences of infections for at least 75% of the period from May 1 to September 30. Figure 5-3a shows that when the heterogeneity degree decreases, the probability of successful invasions increases. Notably, in the most heterogenous scenario (scenario 0.01), there were no successful invasions across 30 runs. Conversely, in the least heterogenous scenario (scenario 10000), over 30% of the invasions successfully initiated a new wave.

To further explore the underlying reasons behind the successful invasions, we analysed the early infection situations within the first seven day after the importation. We calculated the proportion of SSEs (spreading events with five or more cases) among all spreading events. Figure 5-3b shows that the successful invasions exhibited higher

average infection numbers and larger SSE proportions. Furthermore, as the heterogeneity degree increased, invasions required a higher proportion of SSEs to successfully break through. Specifically, under scenario 0.1, about 9.4% of the spreading events were classified as SSEs, which was significantly higher than in other scenarios with lower heterogeneity.

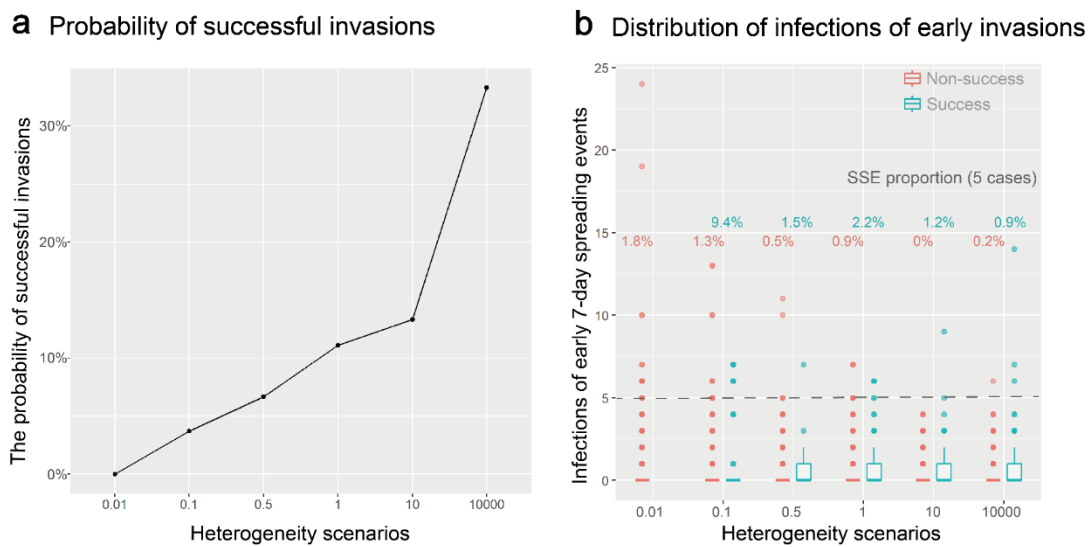


Figure 5-3 Individual infectiousness heterogeneity and resilience to new virus invasions. **a**, probability of successful invasions across heterogeneity scenarios (0.01, 0.1, 0.5, 1, 10, and 10,000). **b**, distribution of early infections during the first 7-day spreading events across heterogeneity scenarios. Each scenario is represented by red and blue boxplots, indicating the infection numbers of non-successful and successful invasions, respectively. The proportion of superspreading events ( $\geq 5$  cases) is displayed above each boxplot.

## 5.2.4 The counterfactual outcomes of the lockdown scenario

To evaluate the potential outcomes of the lockdown policy, we conducted a counterfactual simulation where the lockdown was implemented on February 1, 2022 (see *Section 5.1.3*). Figure 5-4a shows that the lockdown policy effectively prevented the fifth wave, but inadvertently resulted in a more severe sixth wave, compared to the

empirical situation. When comparing the total infection numbers, both the lockdown scenario and the empirical situation exhibited comparable figures. The lockdown scenario yielded slightly fewer total infections (about 475,000) compared to the empirical situation (about 515,000). Moreover, we compared the variations in local transmission risk between the lockdown scenario and the empirical situation. To ensure comparability, we standardized the local transmission risk by setting the mean to 0 and the standard deviation to 1. Figure 5-4b shows that the lockdown scenario displayed a wider dispersion for extreme values in local transmission risks.

To compare the change in variation status for each subTPU, we calculated the differences in standardized local transmission risks between the empirical situation and the lockdown scenario. Figure 5-4c shows the spatial distribution of the status change across subTPUs. Positive values indicate an elevation in risk status under the lockdown scenario compared to the empirical situation, while negative values signify a decrease in risk status. To contextualize the change in risk status, we conducted Spearman correlations with the scaling index, mobility density, and clustering coefficient of the social network. Spearman correlation evaluates the similarity in the ranks of the variables rather than the specific values. The results show that the scaling index (Spearman coefficients: -0.26, p-value<0.001) and mobility density (Spearman coefficients: -0.22, p-value<0.001) are negatively associated with the change in risk status. Conversely, the clustering coefficient of the social network shows a positive association with the change in risk status (Spearman coefficients: 0.15, p-value<0.001).

Finally, Figure 5-4**d, e** show that the risk status of low-value places either significantly increases or decreases, but overall, the status leans towards an increase. Most high-value places maintain a relatively stable risk status, although their status may be slightly reduced due to competition from a few low-value places with an increased status.

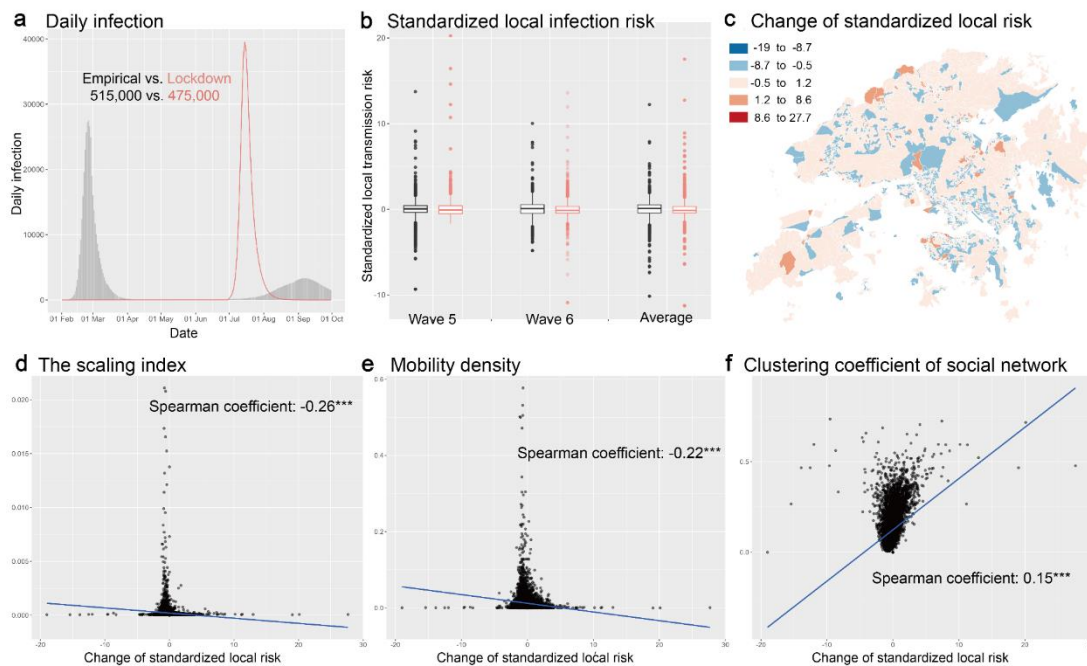


Figure 5-4 Counterfactual simulation of the lockdown scenario. **a**, daily infection comparison with the lockdown scenario (**red**) and the empirical situation (**grey**). **b**, Relative heterogeneity in local infection risks for subTPUs in the lockdown scenario (**red**) and the empirical situation (**black**). The relative heterogeneity status for each subTPU is represented by the standardized standard deviation of local infection risk. **c**, Change of relative heterogeneity status from the empirical situation to the lockdown scenario across subTPUs. **d-f**, Contextualizing the change in relative heterogeneity status within the scaling index (**d**), mobility density (**e**), and clustering coefficient of social networks (**f**) by using Spearman correlation.

### 5.3 Discussion

This study developed a spatially explicit ABM to reconstruct the spread dynamics of two consecutive waves at a fine spatial scale. After validating by three empirical data

from different spatial scales, this model was employed to investigate how a small change in individual infectiousness heterogeneity influence community vulnerability and resilience. The findings reveal that individual infectiousness heterogeneity has opposing effects on two different vulnerability characteristics: local transmission risk and local SSE risk. Moreover, the study reveals that increased heterogeneity amplifies the positive effects of the scaling index on local SSE risk. Resilience analyses further highlight the importance of early SSEs in determining the resilience to new virus invasions across different individual infectiousness scenarios. Successful invasions were associated with a higher proportion of SSEs, especially in scenarios with greater individual infectiousness heterogeneity. Additionally, a counterfactual simulation on the lockdown scenario demonstrates a numerically comparable but spatially more uneven infection outcome to the empirical situation, despite a significant cost.

### **5.3.1 The opposing effects of individual infectiousness heterogeneity on two community vulnerability patterns**

Our findings demonstrate that individual infectiousness heterogeneity has opposing effects on two community vulnerability characteristics. Specifically, an increase in individual infectiousness heterogeneity leads to a decrease in local transmission risk but an increase in local SSE risk increases. The local transmission risk measures the average transmission risk in a local place, while the local SSE risk quantifies the extreme high-value risk. The observed opposing effects can be attributed to the fact that a higher degree of heterogeneity means only a minority of individuals exhibit high

infectiousness, while the majority of individuals have low infectiousness. This creates favourable conditions for the incubation of SSEs. When these highly infectious individuals visit high-scaling-index places, they are more likely to contribute SSEs, thereby increasing the local SSE risk. However, the majority of individuals with low infectiousness tend to cause limited infections, resulting a decrease in the overall local transmission risk.

Our linear regression analysis reveals that the scaling index has a positive effect on local SSE risk. This aligns with prior research that reported a positive association between the scaling index and the individual risk of becoming a superspreader (Peng & Liu, 2024). Expanding upon this finding, our study refines the concept of superspreading by shifting the focus from individual-centred superspreaders to individual- and place-centred SSEs. By doing this, we find consistent positive effects of the scaling index on local SSE risk. Moreover, our study highlights that increased individual infectiousness heterogeneity amplifies the positive effect of the scaling index on local SSE risk, although individual heterogeneity alone has a negligible effect. This implies that individual infectiousness characteristics may not play as decisive a role in SSE occurrences as previously speculated in existing literature (Goyal et al., 2021, 2022; Sidik, 2023). Instead, places act as the dominant mechanism by constraining individuals' ability to fully realize their infectious potential.

### **5.3.2 The critical role of early SSEs in the resilience to new virus invasions**

Our findings highlight the critical role of early SSEs in successful new virus invasions. Compared to non-successful invasions, those successful were associated with a higher proportion of SSEs during the early infection stage, especially for those scenarios with higher individual infectiousness heterogeneity. This aligns with prior research that demonstrates the importance of early SSEs in determining variant predominance when multiple variants compete with each other (Goyal et al., 2022; Lloyd-Smith et al., 2005). However, it is important to note that the prior study primarily focused on individual characteristics, such as viral loads and numbers of contacts, without fully considering the restrictive role of places (Goyal et al., 2022; Lloyd-Smith et al., 2005). In contrast, our vulnerability findings emphasize the importance of policies that diminish SSEs in high-scaling index places. Implementing such policies can make a crucial difference between the emergence or the prevention of a new wave. It is crucial not to become complacent based on a low average transmission risk during the early stages, as the potential for high SSE risk remains and could still increase the likelihood of a new wave emerging.

### **5.3.3 Long-term implications of the lockdown policy**

This study demonstrates that implementing a lockdown policy yield limited long-term benefits with high costs. Similar findings have been shown in previous research

(O’Sullivan et al., 2020), which emphasizes the real challenge of effectively managing large metropolitan areas that cannot be easily divided into separately controlled regions. Furthermore, this study highlights the phenomenon of temporal risk transfer, where immediate risks are shifted to the future (Cutter, 2003), leading to more concentrated outbreaks, particularly during recurring waves. This study also reveals a more pronounced degree of heterogeneity in local transmission risks, indicating a potential increase in spatial inequality. Based on these findings, our research emphasizes the importance of policy design that considers comprehensive consequences over longer time scales and addresses potential spatial inequalities (Axhausen, 2021; Cutter, 2019; Tian, 2017). In situations characterized by increasingly infectious and recurring waves, it may be more suitable to adopt more flexible policies that aim to manage infections within the capacity of healthcare systems. Such an approach can help strike a balance between mitigating the spread of the virus and minimizing the societal and economic costs.

## **5.4 Summary**

To gain a deeper understanding of community vulnerability and resilience in the COVID-19 context, this chapter utilized a spatially explicit ABM to represent urban complex systems where individuals and urban scaling structure dynamically interact. This model enabled us to reconstruct fine-grained spread processes across two consecutive Omicron waves in Hong Kong. By examining the influence of individual infectiousness heterogeneity, we found the opposing effects on two vulnerability

characteristics: local transmission risk from an average perspective and local SSE risk from an extreme perspective. Moreover, we found that while individual infectiousness heterogeneity alone has a small effect on local SSE risk, it amplifies the positive effects of urban scaling structure on local SSE risk when the degree of heterogeneity increases. This implies that individual characteristics may not play as decisive a role in spread dynamics as expected. Instead, places could play a dominant role by constraining individuals' ability to fully realize their transmission potential.

The resilience analyses revealed that early SSEs, as a vulnerability characteristic, also play a crucial role in determining the success of new virus invasions. Additionally, a counterfactual simulation of the lockdown scenario demonstrated that implementing lockdown measures, despite the significant cost, would not yield substantial long-term benefits and could potentially exacerbate spatial inequalities. These findings highlight the importance of future policy decisions that considers the specific complexities of the context and comprehensively evaluating the consequences in both long-term temporal scales and spatial dimensions. This chapter thus underscores the importance of adopting an urban complex system perspective to understand vulnerability and resilience in the contexts of COVID-19 and other disasters and inform future policy decisions.

# **Chapter 6 Resilience to different invasion contexts**

Path dependency characterizes urban complex systems, suggesting initial invasion events may have a large impact on subsequent resilience outcomes. This chapter aims to explore urban resilience under different contexts of initial invasion places. The aforementioned ABM (Chapter 3) was employed to reconstruct case trajectories of the fifth and the sixth waves in Hong Kong. After validating the model by empirical data at various spatial scales, we used this model to compare the resilience outcomes of the high and low scenarios, considering the initial cases of new variants originating from places with high or low scaling indices. These indices reflect the importance of places within the urban scaling structure. In terms of resilience outcomes, we analysed the success probability of invasions and the subsequent spatiotemporal spread dynamics in both scenarios. This study thus enhances our understanding of how invasion contexts would interact with urban complex systems, contributing to resilience in the face of recurring new waves. The unique urban complex system perspective can serve as a promising tool to understand resilience in various disaster contexts and inform future policy decisions.

## **6.1 Modelling the high and low scenarios of invasion contexts**

### **6.1.1 The high and low scenarios**

To examine the influence of the initial conditions on the spread of viruses, this study considers the importance of the invasion places of initial cases. The validated model (see Section 4.1.1 and 5.2.1) was used to explore two distinct scenarios within the context of the sixth wave: the high scenario and the low scenario. In the high scenario, initial cases originate from the top 30 places with high scaling indices, while in the low scenario, initial cases originate from the bottom 30 places with low scaling indices. These places are considered structurally important in the urban scaling structure, indicating high density and connectivity. On the other hand, the low scenario involves initial cases originating from the bottom 30 places with low scaling indices. This selection allows for a comparison that highlights the influence of the initial invasion contexts on the subsequent spread. In both scenarios, three initial cases with an identical number of contacts (18, the average contact number of Hong Kong population (Kucharski et al., 2014)) are introduced on May 1<sup>st</sup>, 2022. For each scenario, we run 100 replicates from February 1<sup>st</sup>, 2022 to January 15<sup>th</sup>, 2023.

### **6.1.2 Analyzing spatial characteristics of spread**

We utilized three measures from social media studies to analyse spatial diffusion: *infection focus*, *infection entropy*, and *infection spread* (Kamath et al., 2013). *Infection focus* ( $F$ ) represents the maximum probability of transmitting new cases at a single

location over time. It is determined by identifying the location with the highest probability of transmitting new cases ( $P_i$ ) among all locations ( $i \in I$ ), where  $F = \max_{i \in I} P_i$ ,  $P_i = \frac{O_i}{\sum_{i \in I} O_i}$ , and  $O_i$  is the number of infections in  $i$ . Initially, there are a few focal points with a high focus degree, which is expected to decrease as the virus spreads to more locations. *Infection entropy* ( $E$ ) quantifies the randomness in spatial distribution of infections. It is measured by  $E = -\sum_{i \in I} P_i \log_2 P_i$ . A value of 0.0 indicates infections occurring in a single location, while higher values reflect greater randomness in the distribution and require more information to represent the spread. To consider the distance travelled by the virus, we introduced *Infection spread* ( $S$ ). It calculates the mean distance of all occurrences from the geographic midpoint. The formula is as follows:  $S = \frac{1}{O} \sum_{o \in O} D(o, G(O))$ , where  $G(O)$  is the geographic midpoint for all occurrences and  $D$  is the measurement of the distances between the occurrence to the midpoint.

## 6.2 Model results

### 6.2.1 Success probability of new invasions in the high and low scenarios

We compared the high and low scenarios, and observed differences in success probability of new invasions. The high scenario exhibited a higher success probability (19%) in initiating a new wave compared to the low scenario (15%). In this study, successful invasions were defined as runs resulting in an observable peak in the daily

infection curves. Specifically, runs that did not produce any new infections after August 1<sup>st</sup>, 2022, were classified as failed invasions, as almost all unsuccessful invasion had ceased to produce new infections around July 1<sup>st</sup>, 2022.

Figure 6-1 illustrates the differences in daily infections and peak dates for successful runs. The curves in the low scenario show greater dispersion, while those in the high scenario are relatively more concentrated. Both scenarios have a comparable average number of total infections, around 178 thousand. However, when comparing the average number of daily infections, we observed slightly higher numbers in the early stage for the low scenario, while the high scenario exhibited slightly higher numbers in the later stage (Figure 6-1**b**). Additionally, both scenarios reached their peak on September 11<sup>th</sup>, 2022. However, when examining the peak date distributions across runs, Figure 6-1**c** shows that the high scenario had a greater proportion of late peaks, while the low scenario tended to have more early peaks.

Based on these characteristics, we categorized the spread dynamics into three stages: the accumulation stage from May to July 2022, where successful or failed invasions were determined; the rapid growth stage from August to October 2022, where successful invasions reached their peak; and the decline stage from November 2022 to January 2023, where invasions slowed down.

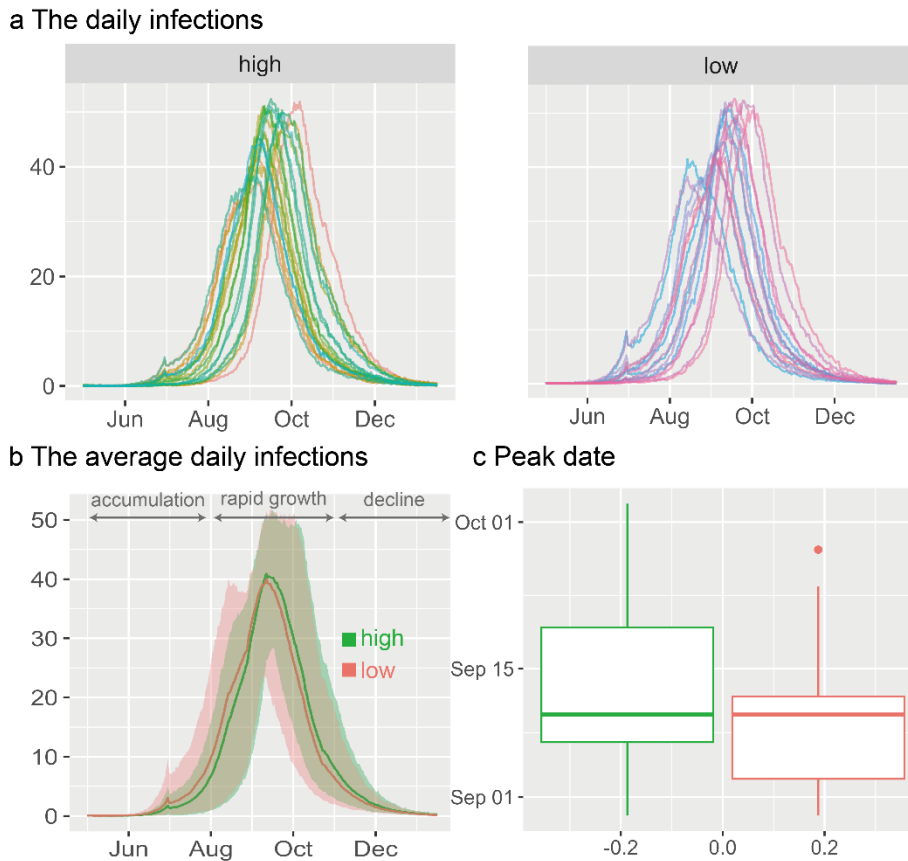


Figure 6-1 Daily infections of successful invasions across high and low scenarios. **a**, daily infection curves for successful invasions in the high (left) and low scenarios (right). **b**, the average daily infections in the high (in green) and low scenarios (in red). **c**, the peak date distributions of successful invasions in high (in green) and low scenarios (in red).

## 6.2.2 Early spread characteristics critical for successful invasions

### 6.2.2.1 The first seven-day spread characteristics

After comparing the difference in success probabilities between the high and low scenarios, we further analysed the potential influencing factors. Given the importance of early SSEs (Goyal et al., 2022; Lewis, 2021; Lloyd-Smith et al., 2005), we first calculated the proportions of successful invasions that included SSEs during the first

seven-day spread. We defined SSE as a spreading event where an infected individual transmitted to at least three individuals in a single place. The results, in Table 6-1, show that a majority of successful runs, all successful invasions in the low scenario and 63% in the high scenario involved SSEs. This indicates the critical role of SSEs in the success of invasions, particularly in the low scenario. Interestingly, some invasions in the high scenario were able to break through even without SSEs.

Furthermore, when comparing the average infection numbers during the first seven-day spread, a large disparity emerged between the low and high scenarios. The low scenario exhibited notably higher average infection numbers (9.00) compared to the high scenario (6.79). However, for failed runs, the low scenario exhibited slightly lower values (4.54) than the high scenario (4.81). Namely, in most cases, the high scenario tends to lead to a greater number of infections compared to the low scenario.

Table 6-1 Comparison of the first seven-day spread characteristics of the high and low scenarios.

Scenario	Success probability	The proportion of successful runs that involved SSE	The average infection number of successful runs	The average infection number of failed runs
The high scenario	19%	63%	6.79	4.81
The low scenario	15%	100%	9.00	4.54

### 6.2.2.2 The first month spread characteristics

Apart from the first seven-day situation, we investigated the spread characteristics of the first month (May, 2022). Three spatial characteristics were calculated: infection focus, infection entropy, and infection spread (see *Section 5.1.2*). We compared the

cumulative distribution function (CDF) of these characteristics among successful and failed runs in the high and low scenarios. Figure 6-2 shows significant gaps between successful runs and failed runs, regardless of the high and low scenarios. Successful runs exhibited a higher proportion of small focus values, large entropy values, and large spread values, indicating more dispersed and distant spread patterns.

Further comparisons between successful runs in the high and low scenarios revealed that the low scenario had a relatively higher proportion of small focus values, large entropy values, and large spread values (Figure 6-2), indicating more dispersed and distant spread patterns. About 75% of successful runs in the low scenario HAD focus values below 0.28, compared to about 0.33 in the high scenario (Figure 6-2a). For entropy, about 55% of successful runs in the low scenario had values above 2.5, whereas less than 50% had values above 2.5 in the high scenario (Figure 6-2b). As for spread, around 65% of successful runs in the low scenarios travelled distances exceeding 7.5 thousand meters, while only 37.5% achieved the same in the high scenario (Figure 6-2c).

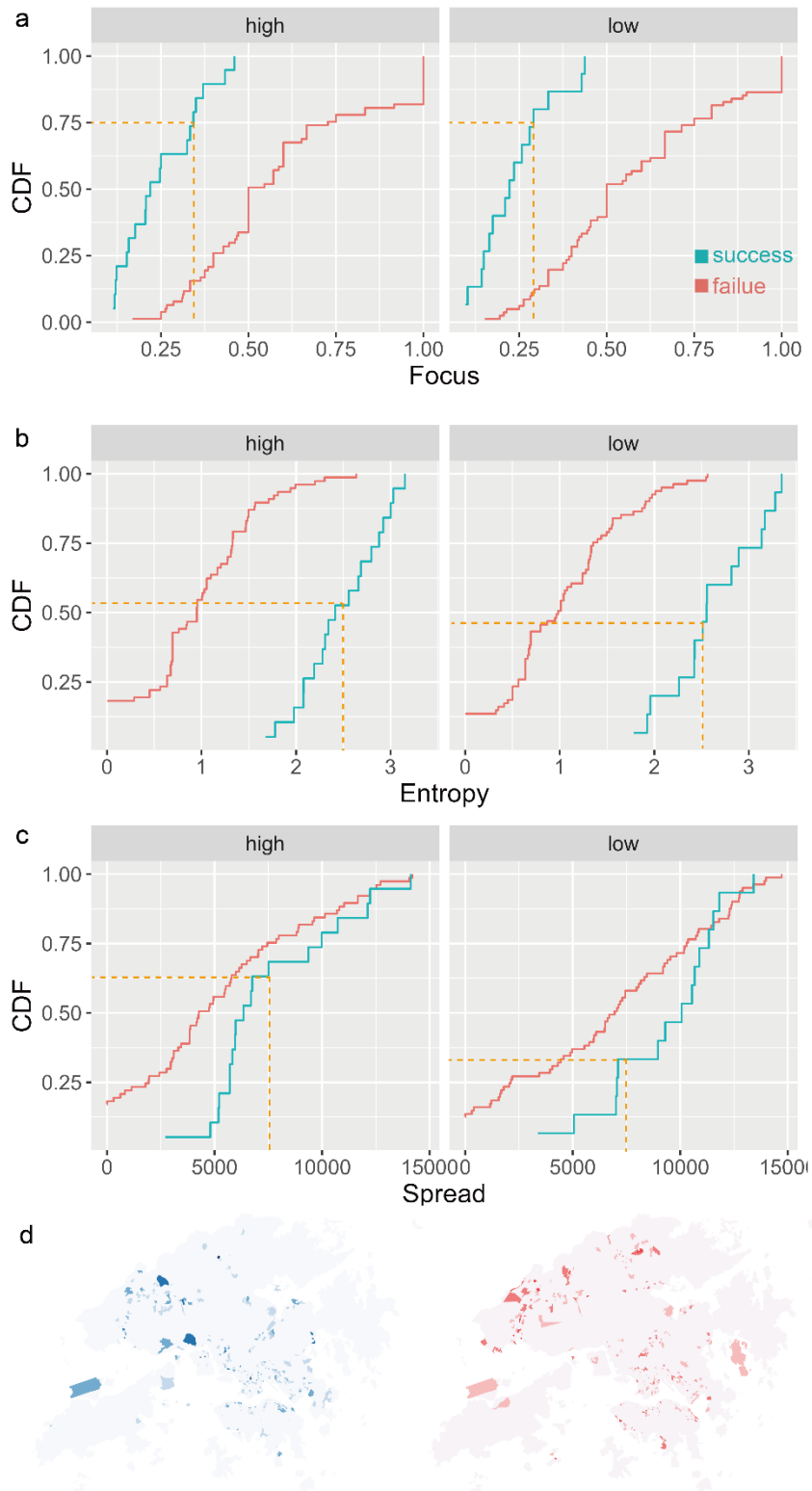


Figure 6-2 The spatial characteristics of the first month spread among successful and failed runs in the high and low scenarios. **a**, the cumulative distribution functions (CDF) of infection focus. **b**, the CDF of infection entropy. **c**, the CDF of infection spread. **d**, the spatial distributions of infections.

Additionally, Figure 6-2d illustrates a large difference in the spatial distribution of early spread between the high and low scenarios. The high scenario demonstrates a relatively concentrated spatial distribution, primarily in the lower and middle regions. Conversely, the low scenario displays a more dispersed distribution, encompassing areas such as the remote northern, western, and eastern regions. The Pearson correlation coefficient between local infection numbers and the scaling indices across subTPUs also verifies this spatial difference. The low scenario had a negative correlation with the scaling index (-0.04, P-value: 0.46), indicating a tendency to spread in areas with low scaling indices. In contrast, the high scenario exhibited a positive correlation with the scaling index (0.07, P-value: 0.26), suggesting an initial spread in areas with high scaling indices.

### **6.2.3 Spatiotemporal spread characteristics for successful invasions**

After analysing the early spread characteristics, we expanded our analysis to subsequent months. Figure 6-3 shows the monthly changes in focus and entropy characteristics for successful runs in the high and low scenarios. Overall, the focus values of all runs initially converged towards smaller values and then expanded towards larger values. In contrast, the entropy values exhibited the opposite trend, initially converging towards larger values and then contracting towards smaller values. Initially, the distribution of focus values ranged from 0.1 to 0.5, gradually contracting until the infection peak in September 2022, when the focus value approached the minimum of 0. Afterwards, the

focus values gradually expanded until January 2023, stabilizing around 0 to 0.2. In contrast, the distribution of entropy values started from 0 and ranged up to 3.5, gradually increasing until reaching a peak of approximately 6. Subsequently, the entropy values gradually decreased, dispersing between 3 and 5.

Comparing the high and low scenarios, we observed that the low scenario exhibited a slightly more extreme and rapid convergence towards the upper left corner. It displayed relatively higher entropy values and smaller focus values, suggesting a more widespread early spread. Additionally, after the peak month, the low scenario had a stronger and faster dispersion towards the lower right corner. This suggests a more rapid transition to a more localized spread in the low scenario.

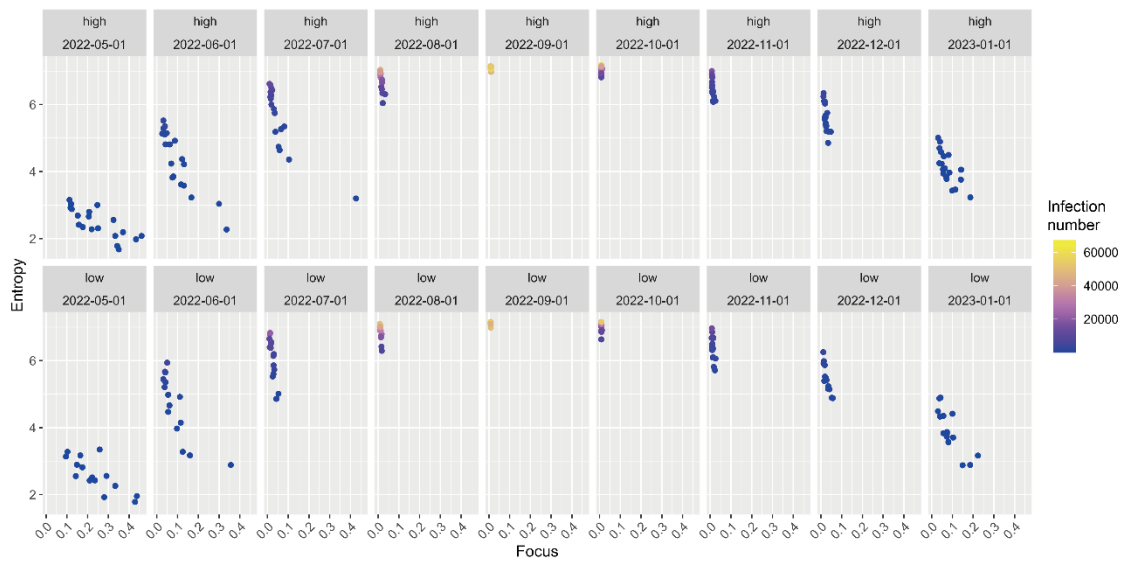


Figure 6-3 The monthly changes in spread characteristics for successful runs in the high and low scenarios.

## 6.2.4 Local spread dynamics for successful invasions

After analysing global spread characteristics, we examined local spread dynamics

across subTPUs and their potential influencing factor: the scaling index, which evaluates the importance of places in the overall structure (Jiang & Jia, 2011; Xing & Ghorbani, 2004). We measured the correlation between monthly average number of local infections and the scaling index using Pearson's correlation coefficient. To satisfy Pearson's assumption of normality, we logarithmically transformed the scaling indices due to their long-tailed distribution.

Figure 6-4 shows that during the accumulation stage, both the high and low scenarios exhibited an increasing correlation with the scaling indices. Notably, the low scenario exhibited a more significant increase, ranging from -0.04 to 0.62, while the high scenario increased from 0.07 to 0.57. Throughout the rapid growth stage, the positive correlations continued to rise for both scenarios until reaching a peak. The correlation strength of the high scenario gradually caught up with that of the low scenario. In the decline stage, the correlations between both scenarios and the scaling index experienced a consistent decrease, with the decline being more pronounced for the low scenario.

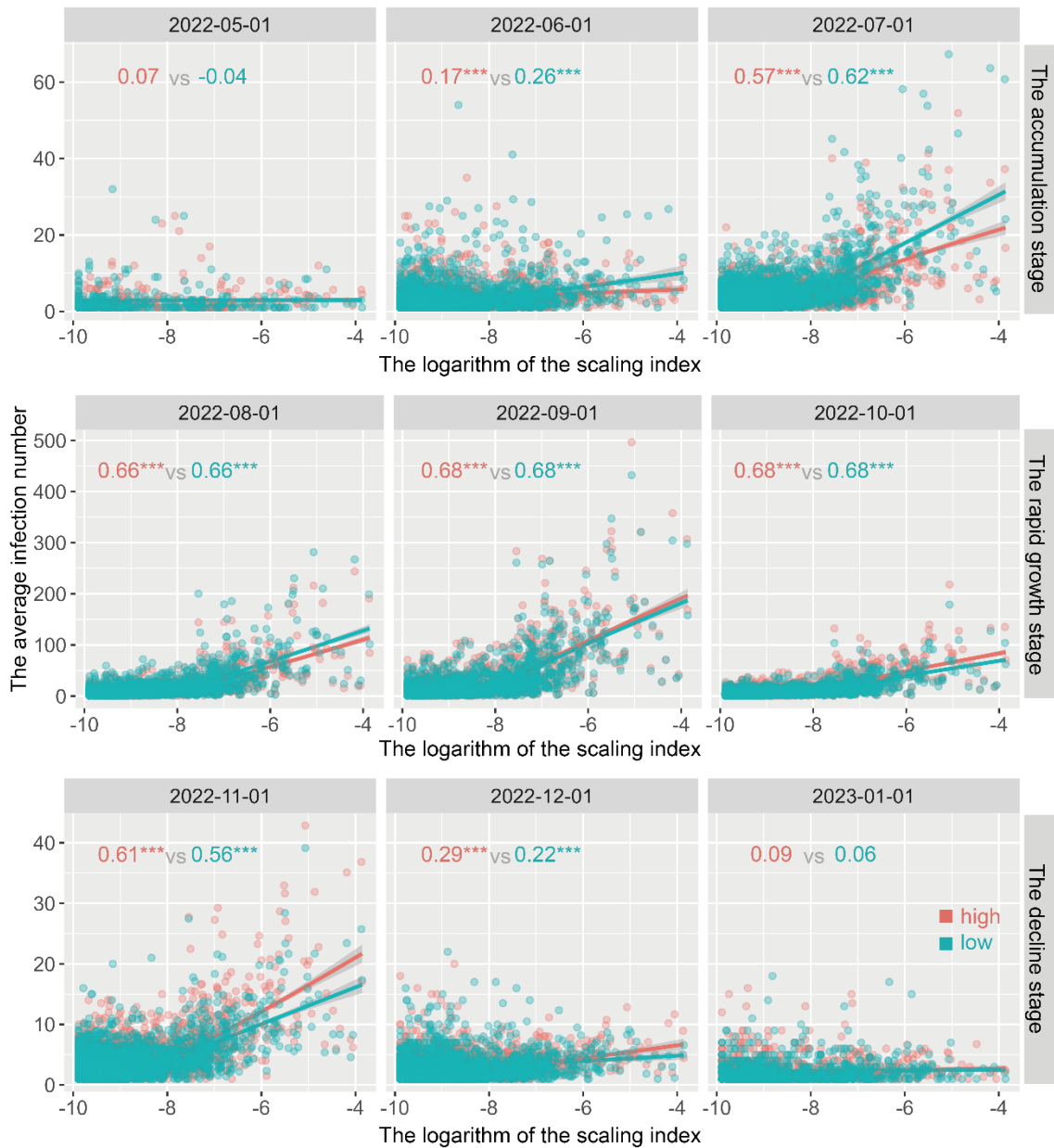


Figure 6-4 Correlation between monthly mean of local infections and log-transformed scaling index for successful runs in the high (red) and low (low) scenarios across subTPUs.

In addition to analysing the mean of local infections, we also examined the variance across successful runs. To facilitate comparability, we calculated the coefficient of variation (CV) by dividing the variance by the mean for each subTPUs. The CV

signifies the diversity of spread possibilities at a location. A higher CV indicates greater variability and a wider range of possibilities.

Figure 6-5 illustrates that during the accumulation stage, the CV increased with the rising scaling index, indicating a diverse range of spread possibilities for both scenarios. Notably, in May, there was a significant difference between the high and low scenarios. The low scenario had higher CV values in low-scaling-index places, while the high scenario had higher values in high-scaling-index places. From June to July, the low scenario exhibited higher variability in high-scaling-index places, compared to the high scenario. During the rapid growth stage, the CV decreased with the increasing scaling index, indicating a decline in spread possibilities for both scenarios. In the decline stage, the CV increased again with the rising scaling index. The high scenario exhibited slightly stronger variability, suggesting more spread possibilities compared to the low scenario.

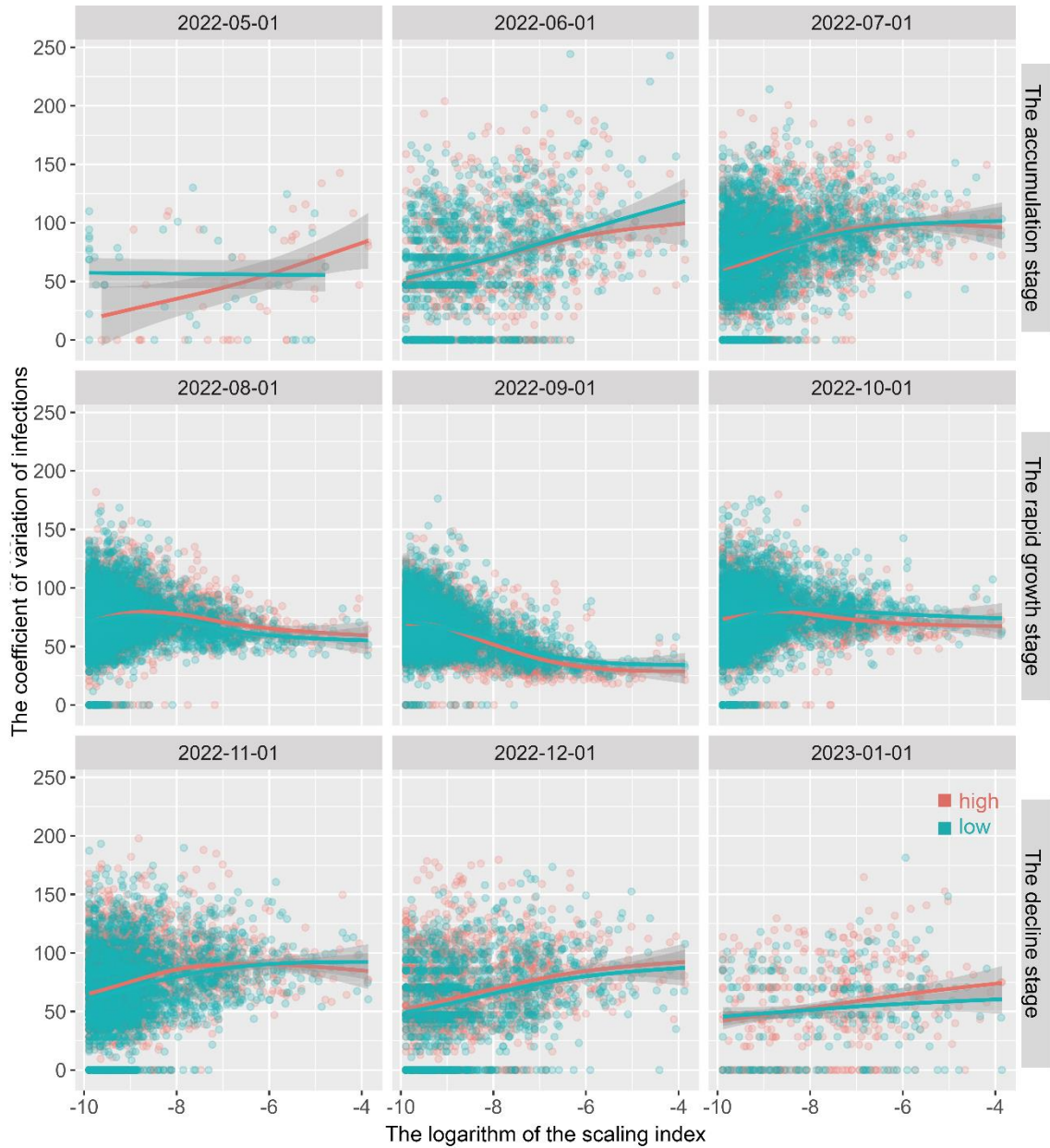


Figure 6-5 Correlation between monthly coefficient of variation of local infections and log-transformed scaling index for successful runs in the high (red) and low (low) scenarios across subTPUs.

## 6.3 Discussions

This study developed a spatially explicit ABM to reconstruct spread trajectories of two consecutive waves at a fine spatial scale. After validating the model using three empirical data from different spatial scales, it was employed to investigate how a small

change in invasion places influences urban resilience, namely, the success probability of new invasions and the subsequent spatiotemporal spread dynamics. The results reveal that the high scenario, where initial cases originated from the top 30 places with high scaling indices, had a higher success probability than the low scenario with the bottom 30 places. Further analyses on spatiotemporal dynamics of successful invasions show that the low scenario initially had a spread advantage, but this advantage later shifted to the high scenario. Moreover, local spread dynamics of the high and low scenarios exhibited varying degrees of correlations with the underlying scaling structure at different spatial and temporal scales.

### **6.3.1 The influence of invasion places on the success probability of new invasions**

This study revealed that the early spread of successful invasions exhibited a higher proportion of SSEs, compared to failed invasions. SSE demonstrates an intense concentration and strength of spreading in a short time. Our finding emphasizes the importance of early SSEs in facilitate invasions to break through (Goyal et al., 2022; Lewis, 2021; Lloyd-Smith et al., 2005). This ‘explosion-and-spread’ pattern has also been observed in outbreaks of online phenomena, such as the spread of Twitter hashtags or YouTube video (Brodersen et al., 2012; Kamath et al., 2013). Moreover, some invasions in the high scenario succeeded without early SSEs. This suggests that a more favourable spread environment can support relatively ordinary invasions in gradually breaking through. However, in the low scenario, an explosive early spread becomes

almost a crucial prerequisite for successful invasions due to less favourable environments.

The more important role of early SSEs in further partly explains the counterintuitive finding of the low scenario having more intense initial spread shortly after the importation, compared to the high scenario. Previous studies have found that places with high population density or structural importance were associated with higher risk of spread (Hamidi et al., 2020; Hong et al., 2021b; Peng & Liu, 2024). Indeed, our study verifies this point based on the slightly higher average numbers of infection among failed invasions in the high scenario. Therefore, the more explosive and intense early spreading of successful invasions in the low scenario may be attributed to the survivorship bias, as invasions selected from the less favourable environments had to be more vigorous to guarantee successful breakthrough.

### **6.3.2 The underlying reasons for the shifting spread advantage between the low and high scenarios**

As discussed previously, the low scenario initially had a spread advantage, which continued until the peak. However, the high scenario later reversed this advantage after the peak. This shift in advantage may be attributed to the path dependency effect of the varying spread power in the early stage. Firstly, shortly after the importation, the low scenario exhibited a relatively stronger degree of spread power, due to the survivorship bias. This allowed it to effectively leverage the urban scaling structure for rapid and extensive spread from June to August. This observation is supported by the stronger

positive correlations between the low scenario and the scaling index (Figure 6-4).

Secondly, the spatial distributions of early spread differed between the high and low scenarios. In the low scenario, the early spread dispersed around less important periphery of urban space, whereas in the high scenario, it primarily concentrated in structurally more important places (Figure 6-2d). The limited spread potential in less important places caused the spread to be quickly inhibited once saturation was reached (R. Morrill et al., 1988). As a result, the low scenario tended to expand more rapidly towards higher-scaling-index places. Overall, these difference in the degree and spatiotemporal scales of early spread power contributed to the low scenario maintaining its initial advantage and yielding a larger number of infections before the peak period.

However, the prior spread advantage in the low scenario did not guarantee higher infection peaks. In fact, the high scenario reversed the early disadvantage and ultimately led to comparable total infections. This transition can be attributed to the dispersed nature of the early spread waves in the low scenario. The early spread in the low scenario was more dispersed than the high scenario (Figure 6-3), spreading around less important periphery of urban space (Figure 6-2d). The dispersed waves of spread in multiple directions could weaken their overall impact. It is akin to throwing several scattered pebbles into a pond, where the ripples generated from different directions meet and result in energy loss during the spread process. This phenomenon aligns with the wave theory of spatial diffusion, which explains that the meeting of dissimilar waves of spread reduces the probability of further spread due to energy dissipation (R. L. Morrill, 1968).

Contrastingly, the high scenario, although having slightly lower early spread power, had relatively more concentrated waves of spread, resulting in fewer contradictions and less energy loss during subsequent spread. Consequently, the high scenario eventually reversed the spread advantage previously held by the low scenario.

### **6.3.3 The significance and challenges of early detection in proactive policy design**

Our study underscores the critical role of early detection in designing proactive policy actions to effectively control and mitigate risks. By analysing the spatial patterns of initial spread, policymakers can effectively differentiate between the high and low scenarios, enabling them to anticipate and manage future risks based on different spatiotemporal characteristics of each scenario. For example, the low scenario, despite having a relatively lower success probability, exhibits a more explosive early spread. This highlights the need for policymakers to pay closer attention to the low-scaling-index places. These areas are often underestimated in terms of their risk, yet their sheer quantity poses significant governance challenges. In contrast, the high scenario may be relatively easier to control due to its less intense early spread. Implementing early interventions in the high scenario can yield greater long-term benefits. However, it is crucial to note that the window of opportunity for making such differentiation is limited. Once early spread patterns are missed, the subsequent spread dynamics of the high and low scenarios become increasingly similar. Therefore, this study underscores the importance as well as the challenges associated with early detection.

## 6.4 Summary

To understand the impact of different invasion contexts on urban resilience, this chapter built a spatially explicit ABM to represent urban complex systems where individuals and urban scaling structure dynamically interact. After model validation, we compared the influence of invasion places, and found that the high scenario, where initial cases originated from structurally important places (namely, those with high scaling indices), had a higher success probability, compared to the low scenario. The success of invasions is significantly influenced by the early ‘explosion-and-spread’ pattern, with the low scenario being more heavily influenced. Furthermore, this chapter revealed a counterintuitive finding that successful invasions in the low scenario exhibited the early spread advantage, even though the high scenario later reversed this advantage. This can possibly be attributed to the overly dispersed and distant waves of early spread in the low scenario, which were akin to overlapping ripples from scattered pebbles thrown into a pond, may lead to greater energy loss in subsequent spread progression.

Overall, we uncover intriguing findings regarding the impact of invasion contexts on urban resilience. Despite the high and low scenarios sharing the same underlying urban scaling structure, differences in historical conditions trigger varying degrees of spread forces across different spatial scales and temporal scales. Consequently, these differences give rise to distinct probabilities of regime shift and spatiotemporal spread dynamics. These insights can inform more effective intervention strategies. By identifying different invasion contexts and anticipating the potential trajectories, policymakers can

devise targeted interventions at appropriate time points and implement necessary control measures. This study underscores the importance of adopting an urban complex system perspective to understand resilience in the contexts of COVID-19 and other disasters, ultimately informing more effective policy decisions.

# Chapter 7 Sensitivity analysis

## 7.1 Comparison of 2011 travel survey data with 2020 mobility data

To verify the representativeness of 2011 travel survey data, we compared the mobility structure of 2011 travel survey data with that of 2020 subway data in Hong Kong as presented in Zhang et al. (2021), the most recent figure available. Using the Louvain heuristics algorithm, as employed in Zhang et al. (2021), to detect communities in complex networks, we found consistent community structures in both 2011 travel survey and the latest 2020 data (Figure 7-1). This indicates a high degree of temporal and spatial regularity in human mobility patterns (Gonzalez et al., 2008; Song et al., 2010). Therefore, even though the 2011 data do not cover the simulation period, it is still acceptable to apply the 2011 data for modelling human travel behaviours.

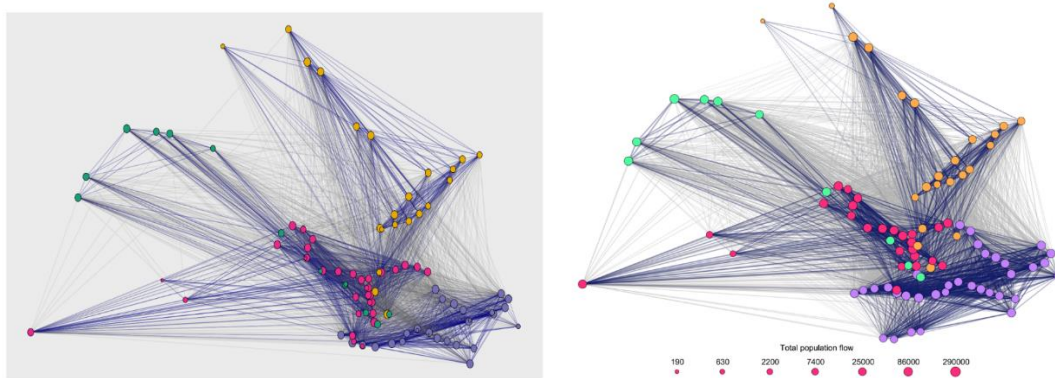


Figure 7-1 The comparison of the mobility structure of 2011 travel survey data (**Left**) and 2020 MTR (Mass Transit Railway) card data (**Right**) from Zhang et al. (2021), both using Louvain heuristics. **Left**, 45,960 trips involved MTR stations in 2011 travel survey data were used, and four groups of communities were found. **Right**, MTR card data on a typical day between 1 January to 31 March 2020 were used, and also four groups of communities were found. In **Left** and **Right**, the

edges in grey and dark blue represent population flows between and within communities, respectively. The vertex size is proportional to the total population flow after log transformation.

## 7.2 Sensitivity analyses on report rates

To account for the uncertainty of report rate values, sensitivity analyses were conducted on three additional parameter sets (Table 7-1). As mentioned in *Infection attributes* in **Method** section, the report rates referenced from Hong Kong University was 0.08 and 0.20 before and after 24 February (HKUMed, 2022). These values did not consider the RAT online reporting platform, which accepts RAT positive results tested since 26 February. Therefore, the actual values are more likely larger than those values. To address this, we increased the report rate between 24 February and 7 March from 0.20 to 0.25 or 0.30, and the report rate after 7 March from 0.20 to 0.30 or 0.35. What's more, report rate before 24 February was increased from 0.08 to 0.10 to account for the potential bias in referenced value.

After replicating the model calibration process for three scenarios (see *Section 3.4.2*), Table 7-2 and Figure 7-2 show that compared to our model, scenario S2 yielded comparable model fits, and scenario S1 and S3 generated slightly worse results. In other words, larger values in post-February 24 report rates fit better. Given that the report rate is a global index, and changes in report rates equally affect local case numbers, the relative differences in local-scale spread are likely to remain consistent across scenarios. Thus, although there are uncertainties in report rates in our model, these uncertainties are expected to exert limited influence on our conclusions.

Table 7-1 Scenarios of report rates

Scenarios	Report rate before 24 February	Report rate between 24 February and 7 March	Report rate after 7 March
<i>Our model</i>	0.08	0.30	0.35
S1	0.08	0.25	0.30
S2	0.10	0.30	0.35
S3	0.10	0.25	0.30

Table 7-2 The comparison of the city-level and TPU-level RMSE of the best-fit models across scenarios

Scenarios	City-level RMSE	TPU-level RMSE
<b>Our model</b>	<b>7.486</b>	<b>9.257</b>
S1	10.976	9.287
S2	7.668	9.558
S3	10.509	9.472

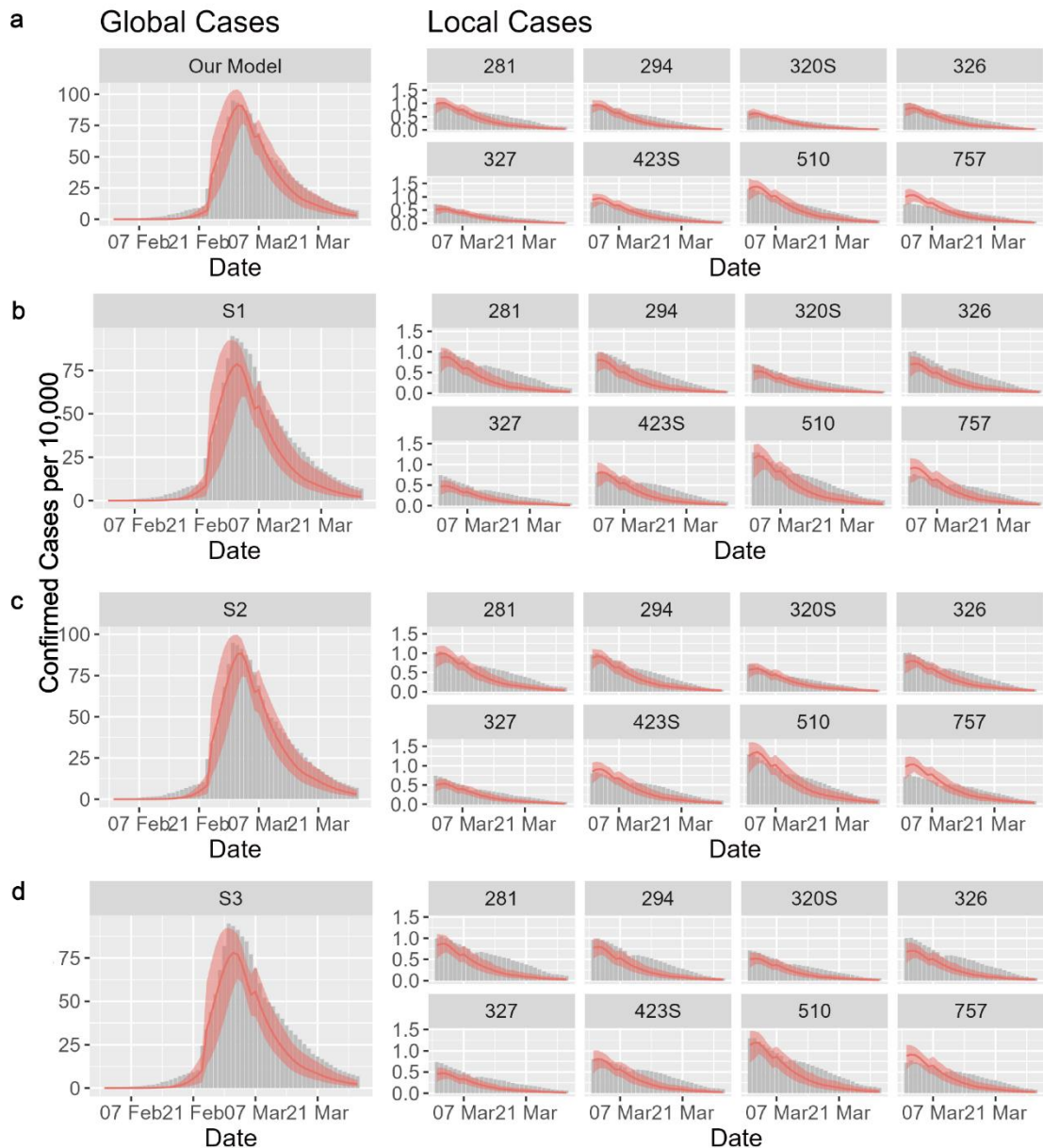


Figure 7-2 Model fittings under different report rate settings. The report rates for our model (a) were 0.08 before 24 February, 0.30 between 24 February and 7 March, and 0.35 after 7 March. Similarly, the report rates for S1 (b) are 0.08, 0.25, and 0.30; for S2 (c) were 0.10, 0.30, and 0.35; for S3 (d) were 0.10, 0.25, and 0.30.

### 7.3 Sensitivity analyses on partially-fixed contactees

Instead of assuming that all contacts remain the same, we assume that 70% of contacts are fixed, and 30% of contacts are updated daily. On the first simulation day, agents were randomly connected to a certain number of contactees in the same subTPU. After

the initial setup, the planned links in each subTPU were partitioned into two parts: 70% of them were classified as fixed contacts, and 30% of them were classified as random contacts. The random contacts were then rearranged, meaning 30% of links in each subTPU were rewired on a daily basis. All other dynamics remains the same with the original model. After 30 runs using the best-fit parameters, we repeated the multivariate linear regression (see Table 4-1) and logistic regression (see Table 4-2) used in the main manuscript.

The regression results demonstrate that our conclusion holds true for the partially-fixed contactee scenario. As shown in Table 7-3 and Table 7-4, the scaling index still play an important role in influencing the local transmission risk and individual’s probability of becoming a superspreader. These results echo with the main findings of Smieszek, Fiebig, and Scholz (2009), who compared two types of epidemic models—one assuming no repetition of contacts, the other assuming the same contacts repeat day-by-day. The study found that when the transmission probability is very high (e.g., for Measles and Chickenpox), both models exhibit similar outcomes. Given Omicron’s notably high transmission probability ( $R_0$  is comparable to that of Measles and Chickenpox), it is acceptable to assume fully fixed contactees in our study.

Table 7-3 For partially-fixed contactee scenario, the effect of the scaling index on the average transmission risk (the average proportion of transmission contacts across 30 runs with best-fit parameters) for subTPUs through multivariate linear regression.

Variable	Coefficient
<b>The scaling index</b>	<b>2.61<sup>***</sup></b>
Average mobility density	0.17 <sup>***</sup>

Average clustering coefficient of social network 0.09<sup>\*\*\*</sup>

---

\*\*\* Significant result with p-value < 0.001.

Table 7-4 For partially-fixed contactee scenario, the average effects of the scaling index on individual’s probability of becoming a superspreader (the top 10% of individuals ranked by the number of secondary cases) through logistic regressions across 30 runs with best-fit parameters.

Variable	The mean of coefficients	Exponential of (coefficients*1 unit)
<b>The average scaling index</b>	<b>4.80<sup>* ^</sup></b>	<b>105%</b>
		<b>(a 1-percent-point increase)</b>
The number of contacts	0.03 <sup>***</sup>	103%
		(a 1-point increase)

\*\*\* Significant result with p-value < 0.001; \* ^ 73% of results are significant with p-value < 0.05.

## 7.4 Sensitivity analyses on the effect of heterogeneous infectiousness on superspreader results

In this scenario, instead of assuming equal infection probabilities for all agents, we assume that the infection probabilities of agents follow the lognormal distribution with  $\mu = \log(0.05)$  and  $\sigma = 0.5$ . As shown in Figure 7-3, the lognormal distribution can guarantee that most of samples would be low values (around 0.05) and a small proportion of samples would be large values (the maximum can reach 0.5 that is 10 times of the original infection probabilities 0.05 (Table 3-1)). What’s more, the mean value of sampled infection probabilities would be comparable to the original infection probabilities 0.05 (Table 3-1). We randomly sampled the infection probabilities from

the lognormal distribution to account for the heterogeneous infectiousness across individuals, and all other dynamics remains the same with the original model. After 30 runs, we repeated the multivariate linear regression used in the main manuscript (see *Section 4.1.4*).

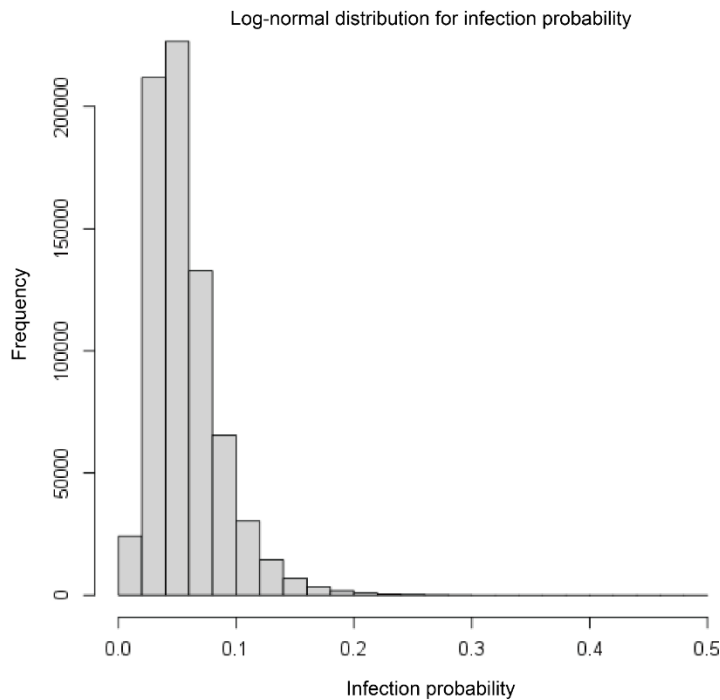


Figure 7-3 The log-normal distribution for sampling the infection probability.

The results of this scenario did not show much difference. Firstly, superspreaders (the top 10% agents with the large number of secondary cases) still accounted for a large proportion (76.6%, 95% CI: 76.4%-76.7%) of infections. Secondly, conditioning on the infection probability does not substantially change the magnitude and the direction of the coefficients of the average scaling index (Table 7-5). The results suggest the infection probability could be one of the important reasons that influence the individual's risk of becoming superspreaders, but similar to the number of contacts, individuals with high infection probability need to be embedded in areas with high

scaling indices, so that they can reach full potential in infecting more people and becoming superspreaders.

Table 7-5 When the infection probabilities are heterogeneously distributed among agents, the average effects of the scaling index on individual's risk of becoming superspreaders (the top 10% of individuals ranked by the number of secondary cases) through logistic regressions across 30 simulations.

Variable	The mean of coefficients	Exponential of (coefficients*1 unit)
<b>The average scaling index</b>	<b>3.42 <sup>* ^</sup></b>	<b>104%</b> <b>(a 1-percent-point increase)</b>
The infection probability	6.82 <sup>***</sup>	107% (a 1-percent-point increase)
The number of contacts	0.03 <sup>***</sup>	103% (a 1-point increase)

<sup>\*\*\*</sup> Significant result with p-value < 0.001; <sup>\* ^</sup> 46% of results are significant with p-value < 0.05.

## Chapter 8 Conclusion

To gain a deeper understanding of the underlying mechanisms of local spread dynamics, this thesis employs a spatially explicit ABM which incorporates urban scaling structure to simulate fine-grained mobility patterns and local spread processes across places. The findings indicate that places with a large volume of local mobility are only a prerequisite for high spread risks within those places, and their significance within the urban scaling structure also plays a crucial regulatory role in it. The urban scaling structure may provide the ‘first-mover advantage’ to a small group of places and their local visitors, enabling them to initiate infections earlier and on a more substantial scale.

To further explore the impact of urban scaling structure on community vulnerability and resilience under different COVID-19 scenarios, the aforementioned ABM was utilized to simulate local spread dynamics across two consecutive Omicron waves in Hong Kong. By comparing the influence of varying degrees of individual heterogeneity in infectiousness on local vulnerability to SSEs, this study indicates that individual characteristics, may not be as significant as expected in driving local SSEs. Instead, places could play a dominant role by constraining individuals’ ability to fully realize their transmission potential.

By comparing the influence of initial invasion places on urban resilience, this study reveals that despite the same underlying urban scaling structure, differences in historical conditions can trigger varying degrees of spread forces across different spatial and temporal scales, consequently giving rise to distinct probabilities of regime shift

and spatiotemporal spread dynamics.

The study sheds new light in the role of urban scaling structure in driving the heterogeneity in local spread dynamics and local SSEs. It further explores local vulnerability patterns and urban resilience in diverse COVID-19 contexts. These insights could offer valuable guidance for developing precise and effective interventions to enhance urban resilience in response to future pandemics. The research framework presented here holds potential for broader applications in wider spatial contexts (e.g., Great Bay Areas) and various disaster contexts.

## **8.1 Contributions**

### **8.1.1 Theoretical implications**

From the perspective of urban complex systems, a place is a synthesis of interactions, and it is the networks between places, rather than just intrinsic attributes, that shape our understanding of cities (Batty, 2013). Therefore, our study constructed a complex network to represent interactions between places. This network provides a dynamic and structural view to show how places, mobility, and disease spread that depend on the network that may change and evolve in time by adapting to and differentiating from other places (Jiang, 2018). During local competitions among places and visitors, the scaling properties of superspreading places and superspreaders were emerged. In a broader sense, many other scaling relationships of urban quantities also reflects the way competition determines the sizes (values) of different places within cities (Batty, 2008,

2013). Therefore, the way of thinking and modelling from the bottom up in our study could also be applicable to understand many other urban phenomena.

The place-to-place network not only provides mesoscopic view shedding new light in complex emergent behaviours from individual interactions to macro patterns, but also enables us to consider the dynamic interactions between individuals and places. During the spread processes of disease or other social phenomena, individual interactions gradually alter the landscape, and the landscape further alters the subsequent spread. While existing COVID-19 studies using agent-based framework emphasize the importance of individual-level mechanisms in understanding SSEs, our study indicates that sometimes place-level mechanisms may exert even greater structural influence.

Beyond focusing solely on the spatial dimension, our study underscores the significance of the time dimension within urban complex systems. Given that the behaviour of a complex system is path-dependent (Holland, 2014), it is important to explore how differences in historical conditions might impact subsequent outcomes. Understanding these characteristics can aid in policymaking in appropriate timing to break existent patterns and promote desired trends.

In addition to short-term perspectives, considering long-term views is vital since problem structure often undergo changes over extended periods (Hale, 2024). When studying individual wave, internal features of urban complex systems such as the structure of human mobility are the predominant factors to consider. However, when studying consecutive waves, it becomes essential to incorporate the distinct

characteristics of each wave event, like variant characteristics and initial invasion places.

### **8.1.2 Methodological implications**

This thesis adopts a spatially-explicit ABM framework to explore the underlying mechanisms of local spread processes. While classic ABM focuses on the emergent behaviours from individual interactions at the micro-level directly to macro-level patterns, this study introduces a meso-level analysis perspective based on place-to-place relations to shed new light in complex emergent processes. This analytical approach may aid in developing mid-range theories concerning the underlying mechanisms of phenomena of interest. Yeung (2023) and O’Sullivan (2024) advocate for the geographic field to develop mid-range theory to ensure that geographic theories strike a balance between breadth and specificity, making them more transferable to other social fields. ABM, in this regard, could potentially contribute to this endeavour.

ABM is a highly flexible framework capable of analysing the development of urban phenomena across various spatial and temporal scales. It can serve as a useful tool to analyse the dynamic processes of vulnerability and resilience in disaster contexts. Unlike traditional static measurements, which may overlook changes occurring in different contexts, this dynamic analytical perspective and modelling approach offer a deeper understanding of the nature of vulnerability and resilience.

### **8.1.3 Practical implications for policymaking**

Urban complex systems have the capacity to evolve in many directions. Therefore, the main goal of policymaking should not be solely to produce the best outcomes under specific scenarios, but rather to generate satisfactory outcomes across multiple possible scenarios (Tian, 2017). To achieve this goal, ABM emerges as an essential tool for examine the potential behaviors of urban complex systems. Based on this, this study offers insights to inform policymaking at finer spatial scales and over relatively longer temporal scales.

Targeted interventions within urban complex systems can have widespread effects, requiring a comprehensive consideration of their connections with other places. Moreover, the temporal scale plays a critical role in these interventions. For instance, while a short-term perspective on governance during a single wave may suggest that a lockdown is the optimal intervention. In the context of recurring waves, lockdowns may not represent a sustainable strategy for long-term benefits. Thus, this thesis highlights the importance of future policy decisions that considers the specific complexities of the context and comprehensively evaluating the consequences in both long-term temporal scales and spatial dimensions.

## **8.2 Limitations**

This study has several limitations from two aspects. The first aspect is the study design. The study solely focused on the fifth and the sixth waves of the pandemic in Hong Kong

to validate the proposed model. To bolster the robustness of the model, future studies could encompass diverse periods and cities, if more data can be collected. The first four waves in Hong Kong were excluded because these waves had limited infections (in total 12,258 cases by Dec. 20, 2021), and such a small number of infections might cover up the local-level findings.

The second aspect is the model structure. Firstly, the 2011 travel survey data used to simulate human mobility may not be representative of recent years. Despite evidence demonstrating a high degree of spatial and temporal regularities in human mobility patterns (Gonzalez, Hidalgo, and Barabasi 2008; Song et al. 2010), and considering Hong Kong's status as a developed city, significant structural changes might not have occurred. A comparison of 2020 subway data reveals substantial similarities (Figure 7-1), further supporting the representativeness of 2011 data.

Secondly, the study mainly focused on city-level mobility changes during the pandemic, overlooking finer spatial-scale changes. Nonetheless, the local-scale validation demonstrated our model's capacity to effectively replicate local situations. It is plausible that the spatial structure of mobility remain relatively stable, as suggested by Tang et al. (2023) in the context of urban floods. Future research with mobility behaviour change data should delve deeper into this aspect.

Thirdly, we assume that all contacts have an equal probability of successfully transmitting the virus irrespective of the contact duration and the contact intensity, which is a simplification of reality. If more biological data is available, further study can be conducted to thoroughly examine how the infectiousness per contact may

influence the local-scale transmission. Another simplification is the number of contacts at different places. For an agent, the total number of contacts is evenly distributed across its travel destinations regardless of the activity type. In reality, certain types of activities may lead to more contacts than others. If such kind of data is available in the future, we can further determine how the social contact characteristics may influence local transmission.

Fourthly, we did not explicitly consider the spatial heterogeneity in the vaccine-acquired immunity, but our model considered the vaccination by different age groups and the age groups were spatially heterogeneous distributed, through which our model may to some extent accounted for the spatial heterogeneity in vaccination. What's more, only a small proportion (12 percent) of population had taken the booster vaccination by Jan. 31<sup>st</sup>, 2021 (DATA.GOV.HK, 2022), and most of population that took the primary vaccination had limited protective effect for the Omicron (Andrews et al., 2022). Therefore, we infer that the spatial heterogeneity in vaccine may have limited effects on our results. If we can gather related empirical data, more realistic situations can be considered in the future study.

## **8.3 Future directions**

### **8.3.1 Building a scalable network of health systems to enhance urban resilience**

In rapidly changing world, the future development of societal challenges such as climate change remains profoundly uncertain. Therefore, devising robust policies to

enhance urban resilience in the face of this uncertain future stands as a crucial governance issue. Drawing lessons from the three-year-long pandemic, a flexible and scalable network of essential infrastructures (e.g., health systems) emerges as a viable solution. By ensuring that infrastructure capacity increases at a rate surpassing the rate of crisis development, challenges could be efficiently managed.

In the context of COVID-19, it is evident that different regions bear varying disease burdens. An intriguing question arises regarding the potential for local medical resources, including local hospitals, clinics, or community health centers, to collaboratively interact and share the load of treating mild and severe cases. This exploration can extend beyond the intra-city level, encompassing inter-city level, such as a Greater Bay Area network for cities to collectively address challenges.

### **8.3.2 The role of cyberspace in spatial diffusion phenomena**

The study of disease spread in this research represents a fundamental form of spatial diffusion phenomena. Similarly, the spatial diffusion of innovations, ideas, or behavior involve individual contacts, but the emergence of Information and Communication Technology has rendered the pathways of dissemination increasingly complex. While traditional methods typically focus solely on the physical space pathways of spread, cyberspace can also play a significant role in shaping human behavior as well (Liao, Kwan, et al., 2024; Liao, Wang, et al., 2024; X. Liu et al., 2022).

Exploring how virtual relationships in cyberspace affect individual adoption behaviors and consequently spatial diffusion of phenomena of interest holds practical significance. Leveraging cyberspace to establish incentives that guide individual

decisions toward desired outcomes is a promising avenue (Tian, 2017).

# Reference

- Adam, D. C., Wu, P., Wong, J. Y., Lau, E. H. Y., Tsang, T. K., Cauchemez, S., Leung, G. M., & Cowling, B. J. (2020). Clustering and superspreading potential of SARS-CoV-2 infections in Hong Kong. *Nature Medicine*, 26(11), 1714–1719. <https://doi.org/10.1038/s41591-020-1092-0>
- Adger, W. N. (2000). Social and ecological resilience: Are they related? *Progress in Human Geography*, 24(3), 347–364. <https://doi.org/10.1191/030913200701540465>
- Adger, W. N. (2006). Vulnerability. *Global Environmental Change*, 16(3), 268–281. <https://doi.org/10.1016/j.gloenvcha.2006.02.006>
- Aguilar, J., Bassolas, A., Ghoshal, G., Hazarie, S., Kirkley, A., Mazzoli, M., Meloni, S., Mimar, S., Nicosia, V., Ramasco, J. J., & Sadilek, A. (2022). Impact of urban structure on infectious disease spreading. *Scientific Reports*, 12(1), Article 1. <https://doi.org/10.1038/s41598-022-06720-8>
- Ahmed, F., Ahmed, N., Pissarides, C., & Stiglitz, J. (2020). Why inequality could spread COVID-19. *The Lancet Public Health*, 5(5), e240. [https://doi.org/10.1016/S2468-2667\(20\)30085-2](https://doi.org/10.1016/S2468-2667(20)30085-2)
- Alessandretti, L. (2022). What human mobility data tell us about COVID-19 spread. *Nature Reviews Physics*, 4(1), Article 1. <https://doi.org/10.1038/s42254-021-00407-1>
- Andrews, N., Stowe, J., Kirsebom, F., Toffa, S., Rickeard, T., Gallagher, E., Gower, C., Kall, M., Groves, N., O’Connell, A.-M., Simons, D., Blomquist, P. B., Zaidi, A., Nash, S., Iwani Binti Abdul Aziz, N., Thelwall, S., Dabrera, G., Myers, R., Amirthalingam, G., ... Lopez Bernal, J. (2022). Covid-19 Vaccine Effectiveness against the Omicron (B.1.1.529) Variant. *New England Journal of Medicine*, 386(16), 1532–1546. <https://doi.org/10.1056/NEJMoa2119451>
- Axhausen, K. W. (2021). COVID-19 and the dilemma of transport policy making. *Arbeitsberichte Verkehrs- Und Raumplanung*, 1596. <https://doi.org/10.3929/ethz-b-000470952>
- Badr, H. S., Du, H., Marshall, M., Dong, E., Squire, M. M., & Gardner, L. M. (2020). Association between mobility patterns and COVID-19 transmission in the USA: A mathematical modelling study. *The Lancet Infectious Diseases*, 20(11), Article 11. [https://doi.org/10.1016/S1473-3099\(20\)30553-3](https://doi.org/10.1016/S1473-3099(20)30553-3)
- Batty, M. (2008). The Size, Scale, and Shape of Cities. *Science*, 319(5864), 769–771. <https://doi.org/10.1126/science.1151419>

- Batty, M. (2013). *The New Science of Cities*. MIT Press.
- Bettencourt, L. M. A. (2013). The Origins of Scaling in Cities. *Science*, *340*(6139), 1438–1441. <https://doi.org/10.1126/science.1235823>
- Bian, L., Huang, Y., Mao, L., Lim, E., Lee, G., Yang, Y., Cohen, M., & Wilson, D. (2012). Modeling Individual Vulnerability to Communicable Diseases: A Framework and Design. *Annals of the Association of American Geographers*, *102*(5), 1016–1025. <https://doi.org/10.1080/00045608.2012.674844>
- Bian, L., & Liebner, D. (2007). A network model for dispersion of communicable diseases. *Transactions in GIS*, *11*(2), 155–173.
- Blundell, R., Costa Dias, M., Cribb, J., Joyce, R., Waters, T., Wernham, T., & Xu, X. (2022). Inequality and the COVID-19 Crisis in the United Kingdom. *Annual Review of Economics*, *14*(1), 607–636. <https://doi.org/10.1146/annurev-economics-051520-030252>
- Brin, S., & Page, L. (1998). The anatomy of a large-scale hypertextual web search engine. *Computer Networks and ISDN Systems*, *30*(1–7), 107–117. [https://doi.org/10.1016/S0169-7552\(98\)00110-X](https://doi.org/10.1016/S0169-7552(98)00110-X)
- Brockmann, D., Hufnagel, L., & Geisel, T. (2006). The scaling laws of human travel. *Nature*, *439*(7075), Article 7075. <https://doi.org/10.1038/nature04292>
- Brodersen, A., Scellato, S., & Wattenhofer, M. (2012). YouTube around the world: Geographic popularity of videos. *Proceedings of the 21st International Conference on World Wide Web*, 241–250. <https://doi.org/10.1145/2187836.2187870>
- Cai, J., Deng, X., Yang, J., Sun, K., Liu, H., Chen, Z., Peng, C., Chen, X., Wu, Q., Zou, J., Sun, R., Zheng, W., Zhao, Z., Lu, W., Liang, Y., Zhou, X., Ajelli, M., & Yu, H. (2022). Modeling transmission of SARS-CoV-2 Omicron in China. *Nature Medicine*, 1–8. <https://doi.org/10.1038/s41591-022-01855-7>
- Chang, S., Pierson, E., Koh, P. W., Gerardin, J., Redbird, B., Grusky, D., & Leskovec, J. (2021). Mobility network models of COVID-19 explain inequities and inform reopening. *Nature*, *589*(7840), 82–87. <https://doi.org/10.1038/s41586-020-2923-3>
- Che, J., Lee, J. S., & Kim, S. (2023). How has COVID-19 impacted the economic resilience of retail clusters?: Examining the difference between neighborhood-level and district-level retail clusters. *Cities*, *140*, 104457. <https://doi.org/10.1016/j.cities.2023.104457>
- Chen, D., Moulin, B., & Wu, J. (2014). *Analyzing and modeling spatial and temporal dynamics of infectious diseases*. John Wiley & Sons.

- Chinazzi, M., Davis, J. T., Ajelli, M., Gioannini, C., Litvinova, M., Merler, S., Pastore y Piontti, A., Mu, K., Rossi, L., Sun, K., Viboud, C., Xiong, X., Yu, H., Halloran, M. E., Longini, I. M., & Vespignani, A. (2020). The effect of travel restrictions on the spread of the 2019 novel coronavirus (COVID-19) outbreak. *Science*, *368*(6489), 395–400. <https://doi.org/10.1126/science.aba9757>
- Chowkwanyun, M., & Reed, A. L. (2020). Racial Health Disparities and Covid-19—Caution and Context. *New England Journal of Medicine*, *383*(3), 201–203. <https://doi.org/10.1056/NEJMp2012910>
- Clauset, A., Shalizi, C. R., & Newman, M. E. J. (2009). Power-Law Distributions in Empirical Data. *SIAM Review*, *51*(4), 661–703. <https://doi.org/10.1137/070710111>
- Cliff, A. D., Haggett, P., & Graham, R. (1983). Reconstruction of diffusion processes at different geographical scales: The 1904 measles epidemic in northwest Iceland. *Journal of Historical Geography*, *9*(1), 29–46. [https://doi.org/10.1016/0305-7488\(83\)90140-8](https://doi.org/10.1016/0305-7488(83)90140-8)
- Coccia, M. (2020). An index to quantify environmental risk of exposure to future epidemics of the COVID-19 and similar viral agents: Theory and practice. *Environmental Research*, *191*, 110155. <https://doi.org/10.1016/j.envres.2020.110155>
- Cot, C., Cacciapaglia, G., & Sannino, F. (2021). Mining Google and Apple mobility data: Temporal anatomy for COVID-19 social distancing. *Scientific Reports*, *11*(1), Article 1. <https://doi.org/10.1038/s41598-021-83441-4>
- Cutter, S. L. (1996). Vulnerability to environmental hazards. *Progress in Human Geography*, *20*(4), 529–539. <https://doi.org/10.1177/030913259602000407>
- Cutter, S. L. (2003). The Vulnerability of Science and the Science of Vulnerability. *Annals of the Association of American Geographers*, *93*(1), 1–12. <https://doi.org/10.1111/1467-8306.93101>
- Cutter, S. L. (2019). Tipping Points in Policy and Practice. In *U.S. Emergency Management in the 21st Century*. Routledge.
- Cutter, S. L., Barnes, L., Berry, M., Burton, C., Evans, E., Tate, E., & Webb, J. (2008). A place-based model for understanding community resilience to natural disasters. *Global Environmental Change*, *18*(4), 598–606. <https://doi.org/10.1016/j.gloenvcha.2008.07.013>
- Damme, W. V., Dahake, R., Delamou, A., Ingelbeen, B., Wouters, E., Vanham, G., Pas, R. van de, Dossou, J.-P., Ir, P., Abimbola, S., Borght, S. V. der, Narayanan, D., Bloom, G., Engelgem, I. V., Ahmed, M. A. A., Kiendrébéogo, J. A., Verdonck, K., Brouwere, V. D., Bello, K., ... Assefa, Y. (2020). The COVID-

- 19 pandemic: Diverse contexts; different epidemics—how and why? *BMJ Global Health*, 5(7), e003098. <https://doi.org/10.1136/bmjgh-2020-003098>
- DATA.GOV.HK. (2022). *Daily count of vaccination by age groups*. <https://data.gov.hk/en-data/dataset/hk-hhb-hhbcovid19-vaccination-rates-over-time-by-age>
- Fan, Y., Li, X., Zhang, L., Wan, S., Zhang, L., & Zhou, F. (2022). SARS-CoV-2 Omicron variant: Recent progress and future perspectives. *Signal Transduction and Targeted Therapy*, 7(1), 1–11. <https://doi.org/10.1038/s41392-022-00997-x>
- Folke, C. (2006). Resilience: The emergence of a perspective for social–ecological systems analyses. *Global Environmental Change*, 16(3), 253–267. <https://doi.org/10.1016/j.gloenvcha.2006.04.002>
- Franch-Pardo, I., Desjardins, M. R., Barea-Navarro, I., & Cerdà, A. (2021). A review of GIS methodologies to analyze the dynamics of COVID-19 in the second half of 2020. *Transactions in GIS*, 25(5), 2191–2239. <https://doi.org/10.1111/tgis.12792>
- Franch-Pardo, I., Napoletano, B. M., Rosete-Verges, F., & Billa, L. (2020). Spatial analysis and GIS in the study of COVID-19. A review. *Science of The Total Environment*, 739, 140033. <https://doi.org/10.1016/j.scitotenv.2020.140033>
- Ghaffarian, S., Roy, D., Filatova, T., & Kerle, N. (2021). Agent-based modelling of post-disaster recovery with remote sensing data. *International Journal of Disaster Risk Reduction*, 60, 102285. <https://doi.org/10.1016/j.ijdrr.2021.102285>
- Giles, J., & Wesolowski, A. (2022). *Mobility: An R package for modeling human mobility patterns*. <https://covid-19-mobility-data-network.github.io/mobility/index.html>
- Gilman, S. (2022). *Application of Whole Genome Sequencing*. Hong Kong Hospital Authority. <https://icidportal.ha.org.hk/Home/File?path=/Training%20Calendar/177/Application%20of%20Whole%20Genome%20Sequencing%20%E2%80%93%20COVID-19%20and%20beyond.pdf>
- Gonzalez, M. C., Hidalgo, C. A., & Barabasi, A.-L. (2008). Understanding individual human mobility patterns. *Nature*, 453(7196), 779–782. <https://doi.org/10.1038/nature06958>
- Google LLC. (2022). *Google COVID-19 Community Mobility Reports*. [https://www.google.com/covid19/mobility/data\\_documentation.html?hl=en](https://www.google.com/covid19/mobility/data_documentation.html?hl=en)

- Goyal, A., Reeves, D. B., Cardozo-Ojeda, E. F., Schiffer, J. T., & Mayer, B. T. (2021). Viral load and contact heterogeneity predict SARS-CoV-2 transmission and super-spreading events. *eLife*, *10*, e63537. <https://doi.org/10.7554/eLife.63537>
- Goyal, A., Reeves, D. B., & Schiffer, J. T. (2022). Multi-scale modelling reveals that early super-spreader events are a likely contributor to novel variant predominance. *Journal of The Royal Society Interface*, *19*(189), 20210811. <https://doi.org/10.1098/rsif.2021.0811>
- Haer, T., Botzen, W. J. W., & Aerts, J. C. J. H. (2019). Advancing disaster policies by integrating dynamic adaptive behaviour in risk assessments using an agent-based modelling approach. *Environmental Research Letters*, *14*(4), 044022. <https://doi.org/10.1088/1748-9326/ab0770>
- Hägerstrand, T. (1973). *Innovation Diffusion as a Spatial Process*. University of Chicago Press.
- Hale, T. (2024). *Long Problems: Climate Change and the Challenge of Governing across Time*. Princeton University Press.
- Hamidi, S., Sabouri, S., & Ewing, R. (2020). Does density aggravate the COVID-19 pandemic? Early findings and lessons for planners. *Journal of the American Planning Association*, *86*(4), 495–509. <https://doi.org/10.1080/01944363.2020.1777891>
- Heesterbeek, H., Anderson, R. M., Andreasen, V., Bansal, S., De Angelis, D., Dye, C., Eames, K. T. D., Edmunds, W. J., Frost, S. D. W., Funk, S., Hollingsworth, T. D., House, T., Isham, V., Klepac, P., Lessler, J., Lloyd-Smith, J. O., Metcalf, C. J. E., Mollison, D., Pellis, L., ... Isaac Newton Institute IDD Collaboration. (2015). Modeling infectious disease dynamics in the complex landscape of global health. *Science (New York, N.Y.)*, *347*(6227), Article 6227. <https://doi.org/10.1126/science.aaa4339>
- HKUMed. (2022, March 21). *HKUMed proposes forward planning after Hong Kong's fifth wave of Omicron BA.2*. <https://sph.hku.hk/en/News-And-Events/Press-Releases/2022/HKUMed-proposes-forward-planning-after-Hong-Kong>
- Holland, J. H. (2014). *Complexity: A very short introduction*. OUP Oxford. <https://books.google.com/books?hl=en&lr=&id=xL-iAwAAQBAJ&oi=fnd&pg=PP1&dq=complexity+holland&ots=ltkC3pCvO1&sig=YFd-JmUsY1QZAjmO6SE7VJ9gpBM>
- Holmdahl, I., & Buckee, C. (2020). Wrong but Useful—What Covid-19 Epidemiologic Models Can and Cannot Tell Us. *New England Journal of Medicine*, *383*(4), 303–305. <https://doi.org/10.1056/NEJMp2016822>

- Hong, B., Bonczak, B. J., Gupta, A., Thorpe, L. E., & Kontokosta, C. E. (2021a). Exposure density and neighborhood disparities in COVID-19 infection risk. *Proceedings of the National Academy of Sciences*, *118*(13), e2021258118. <https://doi.org/10.1073/pnas.2021258118>
- Hong, B., Bonczak, B. J., Gupta, A., Thorpe, L. E., & Kontokosta, C. E. (2021b). Exposure density and neighborhood disparities in COVID-19 infection risk. *Proceedings of the National Academy of Sciences*, *118*(13), e2021258118. <https://doi.org/10.1073/pnas.2021258118>
- Hong Kong Government. (2022a). *Archives of List of buildings with confirmed / probable cases of COVID-19*. <https://www.chp.gov.hk/en/features/102991.html>
- Hong Kong Government. (2022b). *Declaration System for Individuals Tested Positive for COVID-19 Using Rapid Antigen Test launched*. <https://www.info.gov.hk/gia/general/202203/07/P2022030700768.htm>
- Huang, J., & Kwan, M.-P. (2021). Uncertainties in the Assessment of COVID-19 Risk: A Study of People's Exposure to High-Risk Environments Using Individual-Level Activity Data. *Annals of the American Association of Geographers*, *0*(0), 1–20. <https://doi.org/10.1080/24694452.2021.1943301>
- Jiang, B. (2009). Street hierarchies: A minority of streets account for a majority of traffic flow. *International Journal of Geographical Information Science*, *23*(8), 1033–1048. <https://doi.org/10.1080/13658810802004648>
- Jiang, B. (2013). Head/Tail Breaks: A New Classification Scheme for Data with a Heavy-Tailed Distribution. *The Professional Geographer*, *65*(3), 482–494. <https://doi.org/10.1080/00330124.2012.700499>
- Jiang, B. (2015). Wholeness as a hierarchical graph to capture the nature of space. *International Journal of Geographical Information Science*, *29*(9), 1632–1648. <https://doi.org/10.1080/13658816.2015.1038542>
- Jiang, B. (2018). A Topological Representation for Taking Cities as a Coherent Whole. *Geographical Analysis*, *50*(3), 298–313. <https://doi.org/10.1111/gean.12145>
- Jiang, B. (2023). Chapter 3—A new kind of GeoInformatics built on living structure and on the organic view of space. In N. Stathopoulos, A. Tsatsaris, & K. Kalogeropoulos (Eds.), *Geoinformatics for Geosciences* (pp. 45–61). Elsevier. <https://doi.org/10.1016/B978-0-323-98983-1.00004-1>
- Jiang, B., & Jia, T. (2010). Agent-based Simulation of Human Movement Shaped by the Underlying Street Structure. *arXiv:0910.3055 [Physics]*. <http://arxiv.org/abs/0910.3055>

- Jiang, B., & Jia, T. (2011). Agent-based simulation of human movement shaped by the underlying street structure. *International Journal of Geographical Information Science*, 25(1), 51–64. <https://doi.org/10.1080/13658811003712864>
- Jiang, B., & Liu, X. (2012). Scaling of geographic space from the perspective of city and field blocks and using volunteered geographic information. *International Journal of Geographical Information Science*, 26(2), 215–229. <https://doi.org/10.1080/13658816.2011.575074>
- Jiang, B., Yin, J., & Zhao, S. (2009). Characterizing the human mobility pattern in a large street network. *Physical Review E*, 80(2), 021136. <https://doi.org/10.1103/PhysRevE.80.021136>
- Kamath, K. Y., Caverlee, J., Lee, K., & Cheng, Z. (2013). Spatio-temporal dynamics of online memes: A study of geo-tagged tweets. *Proceedings of the 22nd International Conference on World Wide Web*, 667–678. <https://doi.org/10.1145/2488388.2488447>
- Keni, R., Alexander, A., Nayak, P. G., Mudgal, J., & Nandakumar, K. (2020). COVID-19: Emergence, Spread, Possible Treatments, and Global Burden. *Frontiers in Public Health*, 8. <https://doi.org/10.3389/fpubh.2020.00216>
- Kermack, W. O., & McKendrick, A. G. (1927). A contribution to the mathematical theory of epidemics. *Proceedings of the Royal Society of London. Series A, Containing Papers of a Mathematical and Physical Character*, 115(772), 700–721.
- Kirsebom, F. C. M., Andrews, N., Stowe, J., Toffa, S., Sachdeva, R., Gallagher, E., Groves, N., O’Connell, A.-M., Chand, M., Ramsay, M., & Bernal, J. L. (2022). COVID-19 vaccine effectiveness against the omicron (BA.2) variant in England. *The Lancet Infectious Diseases*, 22(7), 931–933. [https://doi.org/10.1016/S1473-3099\(22\)00309-7](https://doi.org/10.1016/S1473-3099(22)00309-7)
- Kogan, N. E., Clemente, L., Liautaud, P., Kaashoek, J., Link, N. B., Nguyen, A. T., Lu, F. S., Huybers, P., Resch, B., Havas, C., Petutschnig, A., Davis, J., Chinazzi, M., Mustafa, B., Hanage, W. P., Vespignani, A., & Santillana, M. (2021). An early warning approach to monitor COVID-19 activity with multiple digital traces in near real time. *Science Advances*, 7(10), eabd6989. <https://doi.org/10.1126/sciadv.abd6989>
- Koks, S., Williams, R. W., Quinn, J., Farzaneh, F., Conran, N., Tsai, S.-J., Awandare, G., & Goodman, S. R. (2020). COVID-19: Time for precision epidemiology. *Experimental Biology and Medicine*, 245(8), 677–679. <https://doi.org/10.1177/1535370220919349>

- Kruskal, W. H., & Wallis, W. A. (1952). Use of Ranks in One-Criterion Variance Analysis. *Journal of the American Statistical Association*, 47(260), 583–621. <https://doi.org/10.1080/01621459.1952.10483441>
- Kucharski, A. J., Kwok, K. O., Wei, V. W. I., Cowling, B. J., Read, J. M., Lessler, J., Cummings, D. A., & Riley, S. (2014). The Contribution of Social Behaviour to the Transmission of Influenza A in a Human Population. *PLOS Pathogens*, 10(6), e1004206. <https://doi.org/10.1371/journal.ppat.1004206>
- Lau, M. S. Y., Grenfell, B., Thomas, M., Bryan, M., Nelson, K., & Lopman, B. (2020). Characterizing superspreading events and age-specific infectiousness of SARS-CoV-2 transmission in Georgia, USA. *Proceedings of the National Academy of Sciences*, 117(36), 22430–22435. <https://doi.org/10.1073/pnas.2011802117>
- Levin, A. T., Owusu-Boaitey, N., Pugh, S., Fosdick, B. K., Zwi, A. B., Malani, A., Soman, S., Besançon, L., Kashnitsky, I., Ganesh, S., McLaughlin, A., Song, G., Uhm, R., Herrera-Espósito, D., Campos, G. de los, Antonio, A. C. P., Tadese, E. B., & Meyerowitz-Katz, G. (2022). Assessing the burden of COVID-19 in developing countries: Systematic review, meta-analysis and public policy implications. *BMJ Global Health*, 7(5), e008477. <https://doi.org/10.1136/bmjgh-2022-008477>
- Levin, R., Chao, D. L., Wenger, E. A., & Proctor, J. L. (2021). Insights into population behavior during the COVID-19 pandemic from cell phone mobility data and manifold learning. *Nature Computational Science*, 1(9), 588–597. <https://doi.org/10.1038/s43588-021-00125-9>
- Lewis, D. (2021). Superspreading drives the COVID pandemic—And could help to tame it. *Nature*, 590(7847), 544–546. <https://doi.org/10.1038/d41586-021-00460-x>
- Li, D., & Lasenby, J. (2023). Investigating impacts of COVID-19 on urban mobility and emissions. *Cities*, 135, 104246. <https://doi.org/10.1016/j.cities.2023.104246>
- Li, M., Shi, X., Li, X., Ma, W., He, J., & Liu, T. (2019). Epidemic Forest: A Spatiotemporal Model for Communicable Diseases. *Annals of the American Association of Geographers*, 109(3), 812–836. <https://doi.org/10.1080/24694452.2018.1511413>
- Liao, M., Kwan, M.-P., & Liu, X. (2024). Exploration of human activity fragmentation in cyber and physical spaces using massive mobile phone data. *Annals of GIS*, 0(0), 1–18. <https://doi.org/10.1080/19475683.2024.2341704>
- Liao, M., Wang, H., & Liu, X. (2024). Digitalization era: Investigating the spatial interplay between cyber human activity and economy with a hierarchical

- framework. *Applied Geography*, 167, 103284.  
<https://doi.org/10.1016/j.apgeog.2024.103284>
- Lima, L. L., & Atman, A. P. F. (2021). Impact of mobility restriction in COVID-19 superspreading events using agent-based model. *PLOS ONE*, 16(3), e0248708.  
<https://doi.org/10.1371/journal.pone.0248708>
- Liu, J., Dietz, T., Carpenter, S. R., Alberti, M., Folke, C., Moran, E., Pell, A. N., Deadman, P., Kratz, T., Lubchenco, J., Ostrom, E., Ouyang, Z., Provencher, W., Redman, C. L., Schneider, S. H., & Taylor, W. W. (2007). Complexity of Coupled Human and Natural Systems. *Science*, 317(5844), 1513–1516.  
<https://doi.org/10.1126/science.1144004>
- Liu, X., Chen, M., Claramunt, C., Batty, M., Kwan, M.-P., Senousi, A. M., Cheng, T., Strobl, J., Cöltekin, A., Wilson, J., Bandrova, T., Konecny, M., Torrens, P. M., Zhang, F., He, L., Wang, J., Ratti, C., Kolditz, O., Klippel, A., ... Lü, G. (2022). Geographic information science in the era of geospatial big data: A cyberspace perspective. *The Innovation*, 3(5), 100279.  
<https://doi.org/10.1016/j.xinn.2022.100279>
- Liu, Y., & Rocklöv, J. (2022). The effective reproductive number of the Omicron variant of SARS-CoV-2 is several times relative to Delta. *Journal of Travel Medicine*, 29(3), taac037. <https://doi.org/10.1093/jtm/taac037>
- Lloyd-Smith, J. O., Schreiber, S. J., Kopp, P. E., & Getz, W. M. (2005). Superspreading and the effect of individual variation on disease emergence. *Nature*, 438(7066), Article 7066. <https://doi.org/10.1038/nature04153>
- Lorig, F., Johansson, E., & Davidsson, P. (2021). Agent-based Social Simulation of the Covid-19 Pandemic: A Systematic Review. *JASSS: Journal of Artificial Societies and Social Simulation*, 24(3).  
<http://urn.kb.se/resolve?urn=urn:nbn:se:mau:diva-44859>
- Ma, A., & Parry, J. (2022). When Hong Kong’s “dynamic zero” covid-19 strategy met omicron, low vaccination rates sent deaths soaring. *BMJ*, 377, o980.  
<https://doi.org/10.1136/bmj.o980>
- Ma, D., Osaragi, T., Oki, T., & Jiang, B. (2020). Exploring the heterogeneity of human urban movements using geo-tagged tweets. *International Journal of Geographical Information Science*, 34(12), 2475–2496.  
<https://doi.org/10.1080/13658816.2020.1718153>
- Majra, D., Benson, J., Pitts, J., & Stebbing, J. (2021). SARS-CoV-2 (COVID-19) superspreader events. *Journal of Infection*, 82(1), 36–40.  
<https://doi.org/10.1016/j.jinf.2020.11.021>

- Malato, J., Ribeiro, R. M., Fernandes, E., Leite, P. P., Casaca, P., Antunes, C., Fonseca, V. R., Gomes, M. C., & Graca, L. (2023). Stability of hybrid versus vaccine immunity against BA.5 infection over 8 months. *The Lancet Infectious Diseases*, 23(2), 148–150. [https://doi.org/10.1016/S1473-3099\(22\)00833-7](https://doi.org/10.1016/S1473-3099(22)00833-7)
- Manica, M., Bellis, A. D., Guzzetta, G., Mancuso, P., Vicentini, M., Venturelli, F., Zerbini, A., Bisaccia, E., Litvinova, M., Menegale, F., Grané, C. M., Poletti, P., Marziano, V., Zardini, A., d'Andrea, V., Trentini, F., Bella, A., Riccardo, F., Pezzotti, P., ... Merler, S. (2022). Intrinsic generation time of the SARS-CoV-2 Omicron variant: An observational study of household transmission. *The Lancet Regional Health – Europe*, 19. <https://doi.org/10.1016/j.lanepe.2022.100446>
- Metcalf, S. (2007). *Simulating the Social Dynamics of Spatial Disparity through Neighborhood Network Evolution*.
- Morrill, R., Gaile, G. L., & Thrall, G. I. (1988). *Spatial Diffusion*.
- Morrill, R. L. (1968). WAVES OF SPATIAL DIFFUSION. *Journal of Regional Science*, 8(1), 1–18. <https://doi.org/10.1111/j.1467-9787.1968.tb01281.x>
- Morrill, R. L. (1970). The Shape of Diffusion in Space and Time. *Economic Geography*, 46, 259. <https://doi.org/10.2307/143143>
- Nejat, A., & Damnjanovic, I. (2012). Agent-Based Modeling of Behavioral Housing Recovery Following Disasters. *Computer-Aided Civil and Infrastructure Engineering*, 27(10), 748–763. <https://doi.org/10.1111/j.1467-8667.2012.00787.x>
- Nouvellet, P., Bhatia, S., Cori, A., Ainslie, K. E. C., Baguelin, M., Bhatt, S., Boonyasiri, A., Brazeau, N. F., Cattarino, L., Cooper, L. V., Coupland, H., Cucunuba, Z. M., Cuomo-Dannenburg, G., Dighe, A., Djaafara, B. A., Dorigatti, I., Eales, O. D., van Elsland, S. L., Nascimento, F. F., ... Donnelly, C. A. (2021). Reduction in mobility and COVID-19 transmission. *Nature Communications*, 12(1), 1090. <https://doi.org/10.1038/s41467-021-21358-2>
- O'Sullivan, D. (2024). *Computing geographically: Bridging giscience and geography*. The Guilford Press.
- O'Sullivan, D., Gahegan, M., Exeter, D. J., & Adams, B. (2020). Spatially explicit models for exploring COVID-19 lockdown strategies. *Transactions in Gis*, 24(4), 967–1000. <https://doi.org/10.1111/tgis.12660>
- Pastor-Satorras, R., Castellano, C., Van Mieghem, P., & Vespignani, A. (2015). Epidemic processes in complex networks. *Reviews of Modern Physics*, 87(3), Article 3. <https://doi.org/10.1103/RevModPhys.87.925>

- Paul, E., Brown, G. W., & Ridde, V. (2020). COVID-19: Time for paradigm shift in the nexus between local, national and global health. *BMJ Global Health*, 5(4), e002622. <https://doi.org/10.1136/bmjgh-2020-002622>
- Peng, N., & Liu, X. (2024). The Impact of Urban Scaling Structure on the Local-Scale Transmission of COVID-19: A Case Study of the Omicron Wave in Hong Kong Using Agent-Based Modeling. *Annals of the American Association of Geographers*. <https://doi.org/10.1080/24694452.2024.2313517>
- Railsback, S. F. (2019). *Agent-based and individual-based modeling: A practical introduction* (2nd edition). Princeton University Press.
- Rasmussen, S. A., Khoury, M. J., & del Rio, C. (2020). Precision Public Health as a Key Tool in the COVID-19 Response. *JAMA*, 324(10), 933–934. <https://doi.org/10.1001/jama.2020.14992>
- Schläpfer, M., Bettencourt, L. M. A., Grauwin, S., Raschke, M., Claxton, R., Smoreda, Z., West, G. B., & Ratti, C. (2014). The scaling of human interactions with city size. *Journal of The Royal Society Interface*, 11(98), 20130789. <https://doi.org/10.1098/rsif.2013.0789>
- Schläpfer, M., Dong, L., O’Keeffe, K., Santi, P., Szell, M., Salat, H., Anklesaria, S., Vazifeh, M., Ratti, C., & West, G. B. (2021). The universal visitation law of human mobility. *Nature*, 593(7860), 522–527. <https://doi.org/10.1038/s41586-021-03480-9>
- Sidik, S. (2023). What makes a COVID superspreader? Scientists learn more after deliberately infecting volunteers. *Nature*. <https://doi.org/10.1038/d41586-023-01961-7>
- Smieszek, T., Fiebig, L., & Scholz, R. W. (2009). Models of epidemics: When contact repetition and clustering should be included. *Theoretical Biology and Medical Modelling*, 6(1), 11. <https://doi.org/10.1186/1742-4682-6-11>
- Song, C., Qu, Z., Blumm, N., & Barabási, A.-L. (2010). Limits of Predictability in Human Mobility. *Science*. <https://doi.org/10.1126/science.1177170>
- Sutley, E. J., & Hamideh, S. (2018). An interdisciplinary system dynamics model for post-disaster housing recovery. *Sustainable and Resilient Infrastructure*, 3(3), 109–127. <https://doi.org/10.1080/23789689.2017.1364561>
- Tang, J., Lu, Q., Batty, M., & Yang, C. (2024). Re-thinking ‘bounce back better’ in post-pandemic era: Building urban resilience into the new normal. *Cities*, 148, 104872. <https://doi.org/10.1016/j.cities.2024.104872>
- Tang, J., Zhao, P., Gong, Z., Zhao, H., Huang, F., Li, J., Chen, Z., Yu, L., & Chen, J. (2023). Resilience patterns of human mobility in response to extreme urban

- floods. *National Science Review*, 10(8), nwad097. <https://doi.org/10.1093/nsr/nwad097>
- Templ, M., Meindl, B., Kowarik, A., & Dupriez, O. (2017). Simulation of Synthetic Complex Data: The R Package simPop. *Journal of Statistical Software*, 79, 1–38. <https://doi.org/10.18637/jss.v079.i10>
- Tian, Q. (2017). *Chapter 7 The Complex Systems Approach to Policy Analysis*.
- Tizzoni, M., Sun, K., Benusiglio, D., Karsai, M., & Perra, N. (2015). The Scaling of Human Contacts and Epidemic Processes in Metapopulation Networks. *Scientific Reports*, 5(1), Article 1. <https://doi.org/10.1038/srep15111>
- Tracy, M., Cerdá, M., & Keyes, K. M. (2018). Agent-Based Modeling in Public Health: Current Applications and Future Directions. *Annual Review of Public Health*, 39(1), Article 1. <https://doi.org/10.1146/annurev-publhealth-040617-014317>
- Van den Broeck, W., Gioannini, C., Gonçalves, B., Quaggiotto, M., Colizza, V., & Vespignani, A. (2011). The GLEaMviz computational tool, a publicly available software to explore realistic epidemic spreading scenarios at the global scale. *BMC Infectious Diseases*, 11(1), 1–14.
- Walker, A. J. (1977). An Efficient Method for Generating Discrete Random Variables with General Distributions. *ACM Trans. Math. Softw.*, 3(3), 253–256. <https://doi.org/10.1145/355744.355749>
- Wong, D. W. S. (1992). The Reliability of Using the Iterative Proportional Fitting Procedure\*. *The Professional Geographer*, 44(3), 340–348. <https://doi.org/10.1111/j.0033-0124.1992.00340.x>
- Wong, D. W. S., & Li, Y. (2020). Spreading of COVID-19: Density matters. *PLOS ONE*, 15(12), e0242398. <https://doi.org/10.1371/journal.pone.0242398>
- Xing, W., & Ghorbani, A. (2004). Weighted PageRank algorithm. *Proceedings. Second Annual Conference on Communication Networks and Services Research, 2004.*, 305–314. <https://doi.org/10.1109/DNSR.2004.1344743>
- Xu, X., Wu, Y., Kummer, A. G., Zhao, Y., Hu, Z., Wang, Y., Liu, H., Ajelli, M., & Yu, H. (2023). Assessing changes in incubation period, serial interval, and generation time of SARS-CoV-2 variants of concern: A systematic review and meta-analysis. *BMC Medicine*, 21(1), 374. <https://doi.org/10.1186/s12916-023-03070-8>
- Yabe, T., Rao, P. S. C., & Ukkusuri, S. V. (2021). Resilience of Interdependent Urban Socio-Physical Systems using Large-Scale Mobility Data: Modeling Recovery Dynamics. *Sustainable Cities and Society*, 75, 103237. <https://doi.org/10.1016/j.scs.2021.103237>

- Yabe, T., Rao, P. S. C., Ukkusuri, S. V., & Cutter, S. L. (2022). Toward data-driven, dynamical complex systems approaches to disaster resilience. *Proceedings of the National Academy of Sciences*, *119*(8), e2111997119. <https://doi.org/10.1073/pnas.2111997119>
- Yancy, C. W. (2020). COVID-19 and African Americans. *JAMA*, *323*(19), 1891–1892. <https://doi.org/10.1001/jama.2020.6548>
- Yang, B., Lin, Y., Xiong, W., Liu, C., Gao, H., Ho, F., Zhou, J., Zhang, R., Wong, J. Y., Cheung, J. K., Lau, E. H. Y., Tsang, T. K., Xiao, J., Wong, I. O. L., Martín-Sánchez, M., Leung, G. M., Cowling, B. J., & Wu, P. (2024). Comparison of control and transmission of COVID-19 across epidemic waves in Hong Kong: An observational study. *The Lancet Regional Health – Western Pacific*, *43*. <https://doi.org/10.1016/j.lanwpc.2023.100969>
- Yang, H., Yao, X. A., Liu, R., & Whalen, C. C. (2023). Developing a Place–Time-Specific Transmissibility Index to Measure and Examine the Spatiotemporally Varying Transmissibility of COVID-19. *Annals of the American Association of Geographers*, *113*(6), 1419–1443. <https://doi.org/10.1080/24694452.2023.2182758>
- Yao, X. A., Crooks, A., Jiang, B., Krisp, J., Liu, X., & Huang, H. (2023). An overview of urban analytical approaches to combating the Covid-19 pandemic. *Environment and Planning B: Urban Analytics and City Science*, *50*(5), 1133–1143. <https://doi.org/10.1177/23998083231174748>
- Yeung, H. (Ed.). (2023). *Theory and explanation in geography* (1st ed.). Wiley. <https://doi.org/10.1002/9781119845515.fmatter>
- Yilmazkuday, H. (2021). Stay-at-home works to fight against COVID-19: International evidence from Google mobility data. *Journal of Human Behavior in the Social Environment*, *31*(1–4), 210–220. <https://doi.org/10.1080/10911359.2020.1845903>
- Zarghami, S. A., & Dumrak, J. (2021). A system dynamics model for social vulnerability to natural disasters: Disaster risk assessment of an Australian city. *International Journal of Disaster Risk Reduction*, *60*, 102258. <https://doi.org/10.1016/j.ijdrr.2021.102258>
- Zhang, J., & Wang, T. (2023). Urban resilience under the COVID-19 pandemic: A quantitative assessment framework based on system dynamics. *Cities*, *136*, 104265. <https://doi.org/10.1016/j.cities.2023.104265>
- Zhang, N., Jack Chan, P.-T., Jia, W., Dung, C.-H., Zhao, P., Lei, H., Su, B., Xue, P., Zhang, W., Xie, J., & Li, Y. (2021). Analysis of efficacy of intervention strategies for COVID-19 transmission: A case study of Hong Kong.

*Environment International*, 156, 106723.

<https://doi.org/10.1016/j.envint.2021.106723>

Zhang, N., Jia, W., Wang, P., Dung, C.-H., Zhao, P., Leung, K., Su, B., Cheng, R., & Li, Y. (2021). Changes in local travel behaviour before and during the COVID-19 pandemic in Hong Kong. *Cities*, 112, 103139. <https://doi.org/10.1016/j.cities.2021.103139>

Zhou, J., Singanayagam, A., Goonawardane, N., Moshe, M., Sweeney, F. P., Sukhova, K., Killingley, B., Kalinova, M., Mann, A. J., Catchpole, A. P., Barer, M. R., Ferguson, N. M., Chiu, C., & Barclay, W. S. (2023). Viral emissions into the air and environment after SARS-CoV-2 human challenge: A phase 1, open label, first-in-human study. *The Lancet Microbe*, 0(0). [https://doi.org/10.1016/S2666-5247\(23\)00101-5](https://doi.org/10.1016/S2666-5247(23)00101-5)

# Appendices

Table S1 Model fit statistics for the mobility models at the Tertiary Planning Unit (TPU) and sub-TPU scales

The mobility model	DIC	RMSE	R <sup>2</sup>	Mean trips (per person)
<i>Spatial scale: 214 TPUs</i>				
The gravity model	10071869	1812.46	0.93	-
The radiation model	NA	4550.83	0.73	-
The departure-diffusion model	<b>8652189</b>	<b>1936.98</b>	<b>0.90</b>	<b>2.17</b>
<i>Spatial scale: 1622 LSBGs*</i>				
The gravity model	13369799	742.45	0.71	-
The radiation model	NA	595.97	0.79	-
The departure-diffusion model	13259806	732.64	0.70	20.2

\* LSBG refers to Large Street Block Groups, which is a set of subunits of TPUs used by the Census and Statistics Department in Hong Kong.

Table S2 Head/tail breaks of 4,863 subTPUs (subunits of Tertiary Planning Units) by mobility volume

Hierarchy	Range	subTPU count
1	(0, 15.0)	3,780
2	(15.0, 56.2)	772
3	(56.2, 122.2)	222
4	(122.2, 227.8)	58
5	(227.8, 703)	31

Table S3 Vaccine effectiveness in reducing susceptibility to Omicron by time since the second or third dose, the estimates from HKU Li Ka Shing Faculty of Medicine (HKUMed, 2022)

Vaccine effectiveness	Time since 2 <sup>nd</sup> and 3 <sup>rd</sup> dose		
	<i>14 days</i>	<i>90 days</i>	<i>180 days</i>
<i>Vaccine</i>			
BioNTech × 1	0	0	0
Sinovac × 1	0	0	0
BioNTech × 2	0.20	0.05	0.01
Sinovac × 2	0.03	0.01	0.01
BioNTech × 3	0.89	0.86	0.77
BioNTech × 2 +Sinovac	0.81	0.67	0.44
Sinovac × 2 +BioNTech	0.64	0.47	0.29
Sinovac × 3	0.36	0.19	0.08

Table S4 Prior-infection induced immunity in reducing susceptibility to Omicron by time since the prior infection (Malato et al., 2023)

Time until reinfection in the sixth wave	Relative risk (compared with individuals without prior infections)
Below 90 days	0.06
90-120 days	0.14
120-150 days	0.26
150-180 days	0.30
180-210 days	0.32
210-240 days	0.35
Beyond 240 days	0.37

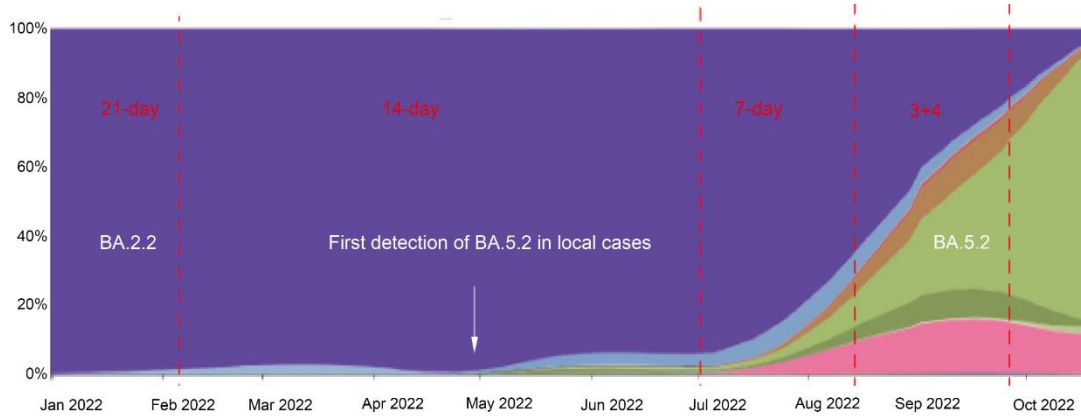


Figure S1 The proportion of BA.5 samples in the total sequenced samples of local cases from 1 May to 30 September 2022 in Hong Kong (Gilman, 2022).

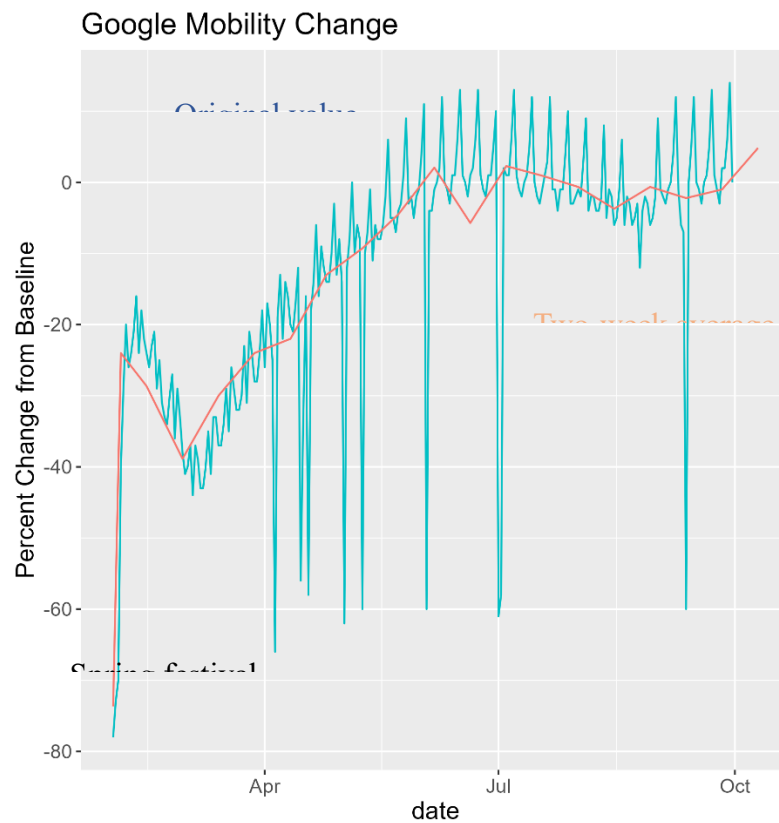


Figure S2 Google mobility change index in workplaces during Feb.1<sup>st</sup> to Sep. 30<sup>th</sup>, 2022. We took the two-week average of the original data to avoid weekly fluctuation due to noise or other bias. To better account for the large decline during Spring festival (Feb. 1<sup>st</sup> to 3<sup>rd</sup>), three-day average was calculated and taken as the mobility change index for the three special days.

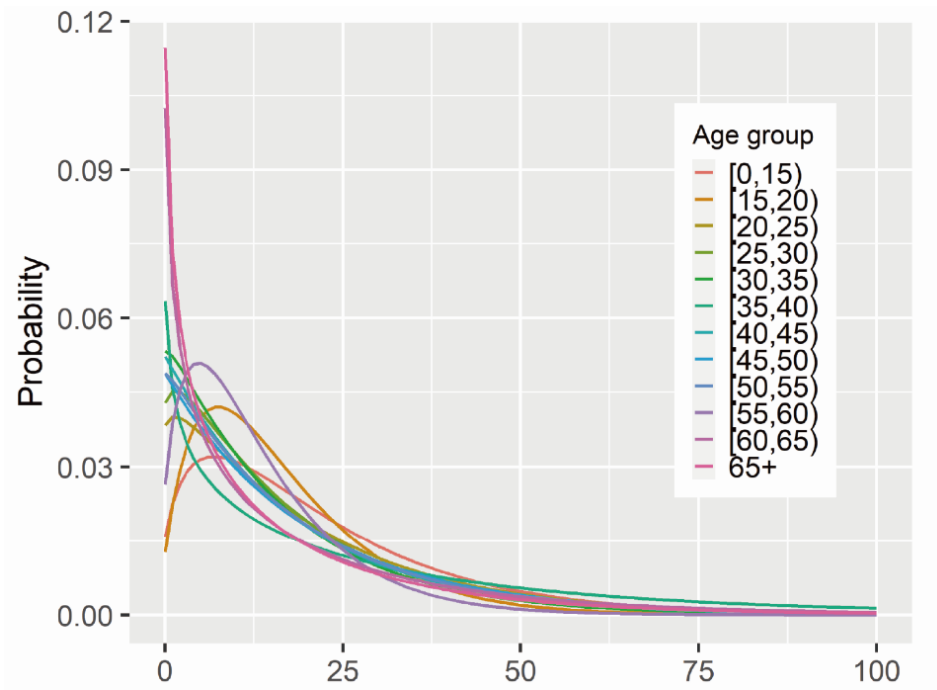


Figure S3 The age-dependent contact distributions for Hong Kong population (Kucharski et al., 2014).